MiWEBA

Millimetre-**W**ave **E**volution for **B**ackhaul and **A**ccess

EU Contract No. FP7-ICT-608637

WP4: Radio Resource Management for mm-wave Overlay HetNets

D4.5: Overall system performance evaluation results

Contractual date:	M30
Actual date:	M30
Authors:	See list
Work package:	4: Radio Resource Management for mm-Wave Overlay HetNets
Security:	Public
Nature:	Report
Version:	3.2
Number of pages:	86

Abstract

This report provides overall performance evaluation results of the proposed mm-wave overlay HetNet (MiWEBA architecture). The system level simulators with the mm-wave channel model, massive MIMO antenna model, space-time traffic model, and BS power consumption model are used for performance evaluation. It is clarified that the MiWEBA architecture with novel resource management algorithms in realistic scenarios can achieve more than 1000 times gain in system rate by installing 15 mm-wave smallcell BSs per macro cell area. This 1000x system rate is achieved with only 2x power consumption compared to the traditional homogenous network. Finally the analysis is extended to whole mm-wave frequency band to prioritize the spectrum for 5G systems by considering unified channel model for above 6GHz and current regulations in different continents.

Keywords

mm-wave access, system level simulator, Q-D channel model, massive MIMO, space-time traffic model, BS power consumption model, short term resource management, long term resource management, performance analysis, spectrum band evaluation for 5G

Authors

IMC	Maltsev Alexander	alexander.maltsev@intel.com
	Bolotin Ilya	ilya.bolotin@intel.com
	Lomayev Artyom	artyom.lomayev@intel.com
	Pudeyev Andrey	andrey.pudeyev@intel.com
	Ingolf Karls	ingolf.karls@intel.com
CEA	Domenico Antonio	antonio.de-domenico@cea.fr
POLIMI	Ilario Filippini	ilario.filippini@polimi.it
Osaka Univ	Kei Sakaguchi	sakaguchi@comm.eng.osaka-u.ac.jp
Tokyo Tech	Gia Khanh Tran	khanhtg@mobile.ee.titech.ac.jp
	Hidekazu Shimodaira	shimodaira@mobile.ee.titech.ac.jp
	Ebrahim Rezagah Roya	roya@mobile.ee.titech.ac.jp

Table of contents

Abbreviations **5**

Executive Summary **9**

0 Introduction **10**

0.1 Background for overall system performance evaluation 10

0.2 Relation to other work packages 10

0.3 Structure of the document 10

1 Use cases and simulation scenarios **10**

1.1 MiWEBA use cases 10

1.1.1 Outdoor environment 11

1.1.2 Indoor environment 12

1.2 Simulation scenarios 13

1.2.1 Open area 13

1.2.2 Street canyon 14

1.2.3 Hotel lobby (large indoor public area) 15

1.2.4 HetNet LTE + mmWave scenario 16

2 System level simulator **18**

2.1 Simulation parameters 18

2.1.1 Q-D Channel model 18

2.1.2 HetNet evaluation parameters 19

2.2 Full buffer scenarios 20

2.2.1 Isolated and dense hexagonal deployments of mmWave APs 20

2.2.2 Frequency reuse 21

2.3 Non-full buffer scenario 22

2.3.1 Space-time traffic model 23

2.3.2 BS power consumption model 24

3 Short term resource management **25**

3.1 Full buffer scenario 25

3.1.1 Basic assumptions 25

3.1.2 Basic simulation results 26

3.1.3 Coordinated resource management in Hotspot deployments 34
3.1.4 Analysis with partially adaptive antenna arrays 38
3.1.5 LTE+mmWave HetNet system performance 42
3.2 Non-full buffer scenario 47
3.2.1 Context based user association optimization problem 47
3.2.2 User association algorithm 47
3.2.3 Simulation results 50

4 Long term resource management 51
4.1 Dynamic cell search & beam training protocol 51
4.1.1 Location-based cell/beam discovery/selection protocol 51
4.1.2 Performance evaluation 53
4.2 Dynamic smallcell BS ON/OFF for energy efficiency 56
4.2.1 Energy efficient mm-wave smallcell activation and beam control for delay-constrained services 56
4.2.2 On-demand smallcell BS ON/OFF to maximize system rate over consumed power 62
4.3 Dynamic cell structuring for CoMP Joint Transmission 69
4.3.1 Algorithm for dynamic cell structuring for CoMP JT 70
4.3.2 Performance evaluation 70

5 Indications for 5G system design 76
5.1 Frequency bands for 5G 76
5.2 mmWave interpolated channel model 78
5.3 System level analysis 81

Conclusion 82

References 83

Abbreviations

Acronym	Description
3GPP	3rd Generation Partnership Project
ACK	Acknowledgement
ADC	Analog to Digital Convertor
AGC	Auto Gain Control
APDP	Average Power Delay Profile
ARQ	Automatic Repeat Request
AS	Angular Spread
AWGN	Additive White Gaussian Noise
BER	Bit Error Rate
BLER	Block Error Rate
BRP	Beam Refinement Protocol
BS	Base Station
CDF	Cumulative Distribution Function
CEF	Channel Estimation Field
CFO	Carrier Frequency Offset
CoMP	Coordinated Multipoint Transmission
CP	Cyclic Prefix
C-RAN	Cloud RAN
CSI	Channel State Information
BBU	Base Band Unit
C-plane	Control Plane
CPRI	Common Public Radio Interface
CQI	Channel Quality Indicator
CSI	Channel state information
CoMP	Coordinated Multi-Point transmission
DAC	Digital to Analog Convertor
DFT	Discrete Fourier Transform
DMG	Directive Multi Gigabit
DS	Delay Spread

EVM	Error Vector Magnitude
FD	Frequency Duplex
FEC	Forward Error Correction
FFT	Fast Fourier Transform
GUI	Graphic User Interface
HARQ	Hybrid automatic repeat request
ICIC	Intercell Interference Coordination
IDFT	Inverse Discrete Fourier Transform
IFFT	Inverse Fast Fourier Transform
ISD	Inter-Site Distance
ISS	Initiator Sector Sweep
HetNet	Heterogeneous Network
LA	Link Adaptation
LDPC	Low Density Parity Check
LLR	Log Likelihood Ratio
LLS	Link Level Simulator
LTE	Long Term Evolution
MAC	Media Access Control
MCS	Modulation and Coding Scheme
MeNB	Master e-nodeB
MIMO	Multiple-input multiple- output
MMIB	Mean Mutual Information per Bit
MMSE	Minimum Mean Square Error
mm-wave	Millimeter-Wave band (30 to 300 GHz) will be used for 6 to 100 GHz
MS	Mobile Station
MU	Multi-user
NLOS	Non-line-of-sight
OBO	Output Back-off
OFDM	Orthogonal Frequency Division Multiplexing
OFDMA	Orthogonal Frequency Division Multiple Access
PA	Power Amplifier
PDF	Probability Density Function
PDSCH	Physical Downlink Shared Channel

PDU	Protocol Data Unit
PER	Packet Error Rate
PF	Proportional Fair
PHY	Physical layer
PN	Phase Noise
PSDU	PHY Service Data Unit
QAM	Quadrature Amplitude Modulation
RBW	Resolution Bandwidth
RF	Radio Frequency
RRH	Remote Radio Head
RRU	Remote Radio Unit
RRM	Radio Resource Management
RS	Reed Solomon
RSRP	Reference Signal Received Power
RSRQ	Reference Signal Received Quality
RX	Receiver
RXSS	Receive Sector Sweep
SC	Single Carrier
SCME	Spatial Channel Model Extended
SeNB	Secondary e-nodeB
SINR	Signal to Interference and Noise Ratio
SLS	System Level Simulator
SM	Spectrum Mask
SNR	Signal to Noise Ratio
SQPSK	Spread QPSK
SS	Sector Sweep
STF	Short Training Field
TDMA	Time Domain Multiple Access
TX	Transmitter
TXSS	Transmit Sector Sweep
UE	User Equipment
U-plane	User Plane
PoC	Proof of Concept

PL	Path Loss
ZF	Zero Forcing

Executive Summary

Due to the popularization of smart phones and tablets in recent years, the traffic load on cellular networks is predicted to increase by 1000 times in the next 10 years. To face the severe issue of system capacity in cellular networks, MiWEBA has been carrying out a pioneering work in involving mm-wave into future 5G cellular networks by means of a novel C/U splitting architecture for mm-wave overlay heterogeneous networks. In order to demonstrate the effectiveness of our proposed architecture in achieving 1000 times more capacity, system level simulators were jointly developed and implemented by WP4 partners. The simulators include all fundamental technologies of the proposed novel architecture i.e. a C/U splitting scheme that supports global resource optimizations alongside many mm-wave smallcell BSs overlaid inside the coverage of conventional LTE macro cells.

This deliverable presented the overall view of all achievements in WP4 about radio resource management for MiWEBA architecture. Scenarios and use cases that had been studied in WP1 are revisited here to specify simulation environments including open area, street canyon, hotel lobby, and HetNet scenarios. Besides, the basics of the MiWEBA's exclusive system level simulator are described with the mm-wave channel model and massive MIMO antenna model developed in WP5, and the space-time traffic and BS power consumption models developed in WP4. Short-term and long-term radio resource management and optimizations are further developed and demonstrative evaluation results are presented. In the end, the final chapter extends the analysis to whole mm-wave frequency bands to indicate appropriate spectrum for 5G systems.

As our findings, this deliverable shows that the proposed MiWEBA architecture with proposed resource management algorithms in realistic scenarios can achieve more than 1000 times gain in system rate by installing 15 mm-wave small cell BSs per macro cell area. The protocol of location-based cell/beam discovery/selection is also developed to implement the context-based resource management. The location-based cell/beam discovery/selection is essential in particular for implementing resource optimizations and forming a self-organizing networks (SONs). Using this scheme, several optimization algorithms are developed and applied to boost energy-efficiency. As the baseline, the 1000x system rate is achieved by the mm-wave overlay HetNet with only 2x power consumption compared to the traditional homogenous network. Implementing dynamic ON/OFF according to the dynamic traffic map can further reduce this power consumption. To further enhance the capacity, dynamic cell structuring scheme is also developed to dynamically follow the hotspot zones (using the location-based cell/beam discovery protocol) and direct idle network resources towards them.

Finally all possible bands for 5G are investigated through the system level simulator to evaluate their performances for the future traffic requirements (1000x in 2020 and 1000000x in 2030). The evaluations show that among all available bands, 60GHz band with 20.22GHz bandwidth from 55.78GHz to 76.9GHz shows such a prospective capacity that makes it the most attractive band for the future 5G systems.

0 Introduction

0.1 Background for overall system performance evaluation

The goal of MiWEBA project is to integrate the millimeter-wave communication potential into the LTE cellular network framework. In order to accomplish this goal, MiWEBA introduces and investigates radically new network architecture along with innovative functionalities and new scenarios as the baseline for future 5G networks [1]. The novelty and the complexity of the research theme result in a large set of possible design choices. In the WPs of this project viable solutions e.g. C/U splitting, C-RAN based dynamic resource management etc. are being investigated. This particular deliverable integrates all the proposed technologies of MiWEBA into our developed system level simulator in order to show the viability of the project in designing future 5G cellular networks with mm-wave overlay HetNet and demonstrate its efficiency in terms of both spectrum and energy. Therefore, this deliverable provides a complete picture of the scenarios and use cases, our developed simulation tools and dynamic resource management frameworks. Both short-term and long-term resource optimization results are presented in distinct sections and in the end the integrated evaluation results are presented which illustrate the effectiveness of the proposed architecture toward the realization of 5G cellular networks.

0.2 Relation to other work packages

Our selected scenarios and use cases for performance evaluation presented in Chapter 1 are output from WP1 [2]. Chapters 2, 3 and 4 are related to D4.1, D4.3 and D4.4 of the same workpackage respectively. In Chapter 5, all mechanisms developed in other work packages e.g. C/U splitting (WP3), mm-wave antenna and propagation (WP5) [3] [4] are integrated and evaluated. Some short-term and long-term resource optimization algorithms presented in this deliverable are also planned to implement in the demo in WP6.

0.3 Structure of the document

Chapter 1 gives an overview of the scenario and use cases. The structure of the system level simulator is described in Chapter 2. Then, Chapters 3 and 4 describe short term and long term resource management, respectively. Finally, the evaluation results showing the impact of the proposed mm-wave Overlay HetNets are presented in Chapter 5.

1 Use cases and simulation scenarios

1.1 MiWEBA use cases

In this section we recall use cases we have detailed in Deliverable D1.1. Some of their parameterized scenarios as shown in Sect. 1.2 will be used to assess MiWEBA architecture performance in D4.5. MiWEBA use cases are divided into two groups: outdoor environment and indoor environment.

1.1.1 Outdoor environment

We identified three use cases for outdoor environment: *Urban Microcell in street canyon (like Street Canyon scenario in Sect. 1.2.2), Urban Microcell in open square (like Open Area scenario in Sect. 1.2.1), Urban Macrocell.*

Outdoor use cases range from a very small area with a single isolated mm-wave hot-spot to a larger scenario with several mm-wave small cells which provide a partial or full coverage of the selected area. Their features depend on the size of the area required to be covered with mm-wave access.

Typical use cases focus on areas located in the city centre where thousands of people may spend part of their daily life. The area is characterized by a several possible indoor and outdoor hotspots like bus stops, restaurants, enterprises, and recreation parks. Due to the high data rate requirements for multimedia broadband services in this kind of environments, the classic micro-wave based solutions may not be sufficient. In fact, indoor locations may suffer of poor signal strength while outdoor the inter-cell interference may strongly limit the achievable data rate.

For this dense area, the mobile operators may greatly benefit of the upgrade of their network through the deployment of mm-wave small cells, which will enhance the quality of experience of nearby users. Static users sitting in a bar or waiting for their bus may experience real time video streaming applications, gaming, voice over IP, etc. Device to device communications can be used by a group of friends to exchange photos collected during the last weekend spent together. Furthermore, nomadic users may receive real time information on their position, which may include interactive contents on nearby museums/shops as well as detailed instructions to reach their final destination in downtown.

Table 1.1 summarizes the 3 considered use cases:

Table 1.1. Outdoor use cases

	Description	D1.1 use cases and scenarios	Technology	Challenges
UMi street canyon	Street canyon street level urban scenario where mm-wave APs are deployed as a high-capacity microcell layout	Dense hotspot urban areas High-rate areas	Small cell APs with beamforming antennas	Increase distance and coverage Provide cooperation for interference coordination Use LOS and NLOS paths Provide mobility separated C-plane, context management
UMi open square	Urban scenario where mm-wave APs are deployed as a high-capacity microcell layout in a large and open square	Dense hotspot in a square High-rate areas Ultra high-rate hot spots	Small cell APs with beamforming antennas	Provide very high capacity in localized spaces No mobility issues C- and U-plane split
UMa	Urban scenario where mm-wave APs are deployed to increase the capacity and coverage of legacy macrocell layouts. Two-tier heterogeneous	Dense hotspot urban areas Mobility in the city Backhaul and fronthaul dense urban	Small cell APs and RRHs CRAN Dense smallcells	Increase capacity, density and coverage Provide CoMP, CoMP-JT and cooperative beamforming and

	network.	and metropolitan areas Larger areas		interference coordination Use mobility management with separated C-plane and context management Provide SON capabilities

1.1.2 Indoor environment

We identified three use cases for indoor environment: *indoor open office, indoor closed office* and *indoor shopping malls (like Hotel Lobby scenario in Sect. 1.2.3)*.

One of the use cases focuses on shopping malls, where people, while waiting for the lunch at one of the mall cafeteria, use their smartphone/tablet for web browsing or video streaming leading to a high density of traffic in a very small area. Moreover, the shop can also use interactive messages, which contain videos or images, to promote their products or inform customers about special offers.

Enterprise areas are another use case. Since enterprises buildings are characterized by different characteristics in terms of location, age, size, shape, number of rooms, etc., finding a unique solution to offer high data rate mobile services has not been feasible for cost and scalability reasons. In addition to these classic issues, today wireless solution for enterprises have to deal with the increasing capacity demands due to laptop, smartphones, and tablets. Moreover, seamless enterprise mobility is a strong requirement for enabling to conduct the business where most appropriated. Accordingly, mm-waves technologies can provide high data rate to static users in their offices while other systems such as macro cell based cellular network and small cells may provide reliable connectivity to mobile users.

Finally, users at home can rely on mm-waves technologies as an alternative to perceive high quality of experience in indoor. Indeed, due to the strong inter-cell interference, traditional dense femto cell deployments may not be a viable solution to provide the required bandwidth for applications like 3D TV live streaming, HDTV programs recording, video editing and transfer to media centres, real time multiplayer games, and HD video conferences.

Table 1.2 summarizes the 3 considered use cases:

Table 1.2. Indoor use cases

	Description	D1.1 use cases and scenarios	Technology	Challenges
Indoor open office	Mm-wave APs deployed in large and crowded open spaces with many people and pieces of furniture. They provide high-speed connectivity to static and nomadic users.	Dense hotspot enterprise	Small cell APs with beamforming antennas Some cooperation among APs	Provide very high capacity in localized spaces No mobility issues C- and U-plane split
Indoor closed office	Mm-wave APs deployed in small isolated room to provide high-speed wireless connectivity to users in the room	Dense hotspot home Isolated rooms	Small cell APs with beamforming antennas Some cooperation among APs	Improve indoor coverage with beamforming using LOS and NLOS paths Use cooperative transmissions and advanced antenna

				systems C- and U-plane split
Indoor shopping mall	Mm-wave APs deployed in large halls and shops with many people. They provide high-speed connectivity to nomadic users.	Dense hotspot shopping mall Large public areas	Small cell APs and RRHs CRAN Different level of cooperation among APs	Increase capacity Provide cooperative beamforming and interference coordination Use typically LOS path C- and U-plane split

1.2 Simulation scenarios

For the system level performance evaluation purposes, a number of use cases and environments, identified in the previous sections were mapped to the four base simulation scenarios: open area, street canyon, hotel lobby and HetNet LTE + mmWave communication system.

1.2.1 Open area

Open area simulation scenario resembles the sparse environment with no closely spaced high buildings, such as park areas, university campuses, stadiums, outdoor festivals, city squares or even rural areas (see Figure 1.1).

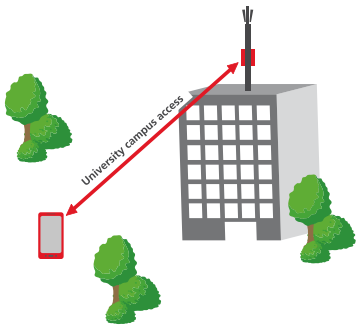

Figure 1.1 Open area scenario example: university campus

The open area scenario is used as a baseline setup for millimeter-wave communication system evaluation, and simulated for a large set of parameters and assumptions, summarized in Table 1.3.

Table 1.3. Open area scenario parameters

Parameter	Value
Small cell layout	Single cell, Hex grid (7 cells)
Number of sectors (APs)	3
ISD	25-100 m (50m baseline)
AP TX height	4m, 6m
UE height	1.5m
Surface material	asphalt
Surface ε_r	4 + 0.2j
Surface roughness σ	3 mm
Channel model	Q-D channel model, open area scenario

1.2.2 Street canyon

The street canyon simulation scenario represents typical urban environment: streets with pedestrian sidewalks along the high-rise buildings. The access link between the APs on the lampposts and the UEs at human hands is modeled in this scenario.

Deployment geometry is summarized in Table 1.4 and Figure 1.2

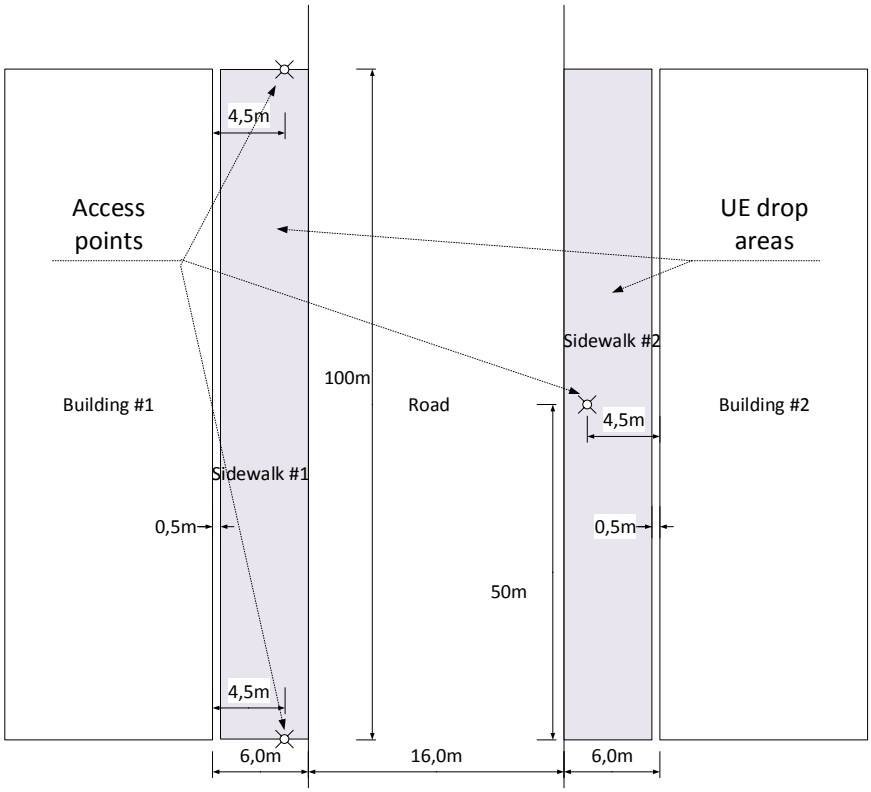

Figure 1.2: Street canyon scenario geometry

Table 1.4: Street canyon scenario parameters

Parameter	Value
AP height, H_{tx}	6 m
UE height, H_{rx}	1.5m
AP distance from nearest wall, D_{tx}	4.5 m
Sidewalk width	6 m
Road width	16 m
Street length	100 m
AP-AP distance, same side	100 m
AP-AP distance, different sides	50 m
Road and sidewalk material	asphalt
Road and sidewalk ε_r	4+0.2j
Ground roughness standard deviation σ_g	0.2 mm
Building walls material	concrete
Building walls ε_r	6.25+0.3j
Building walls roughness standard deviation σ_w	0.5 mm

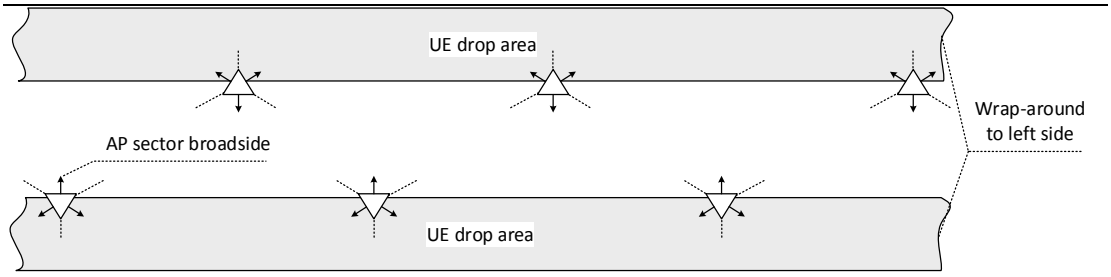

Figure 1.3 AP sectors and positions in the Street canyon simulation scenario

For the simulation purposes, the section of the street, shown in Figure 1.2 was duplicated and the wrap-around technique is applied to the street ends, as if the simulation area were on the cylinder surface (Figure 1.3)

UEs are uniformly dropped along the sidewalks (gray areas in Figure 1.2 and Figure 1.3), totally 540 UEs in simulation area, counting as 30 UE per sector of the each AP.

Assuming that each sidewalk width equal to 6m, and the length of the simulation area is 250m, this give UE density equal to 0.18 UE/m^2, or approximately one user per 5.5m^2.

1.2.3 Hotel lobby (large indoor public area)

The hotel lobby simulation scenario covers many indoor access large public area use cases. Hotel lobby channel model represents typical indoor scenario: large hall with multiple users within. Similar simulation scenarios were considered in [5], with statistical approach to the channel modeling, suitable for link layer simulations.

The basic parameters and geometry of the hotel lobby simulation scenario are summarized in Table 1.5 and illustrated in Figure 1.4.

Table 1.5: Hotel lobby (indoor access large public area) scenario parameters

Parameter	Value
AP height, H_{tx}	5.5 m
AP position	Middle of the nearest wall (see Figure 1.4)
UE height, H_{rx}	1.5m
Room height	6 m
Room width	15 m
Room length	20 m
Floor material	Concrete
Floor ε_{rf}	4 + 0.2j
Floor roughness standard deviation σ_f	0.1 mm
Walls material	Concrete
Walls ε_{rw}	4 + 0.2j
Walls roughness standard deviation σ_w	0.2 mm
Ceiling material	Plasterboard
Ceiling ε_{rc}	6.25+0.3j
Ceiling roughness standard deviation σ_c	0.2 mm

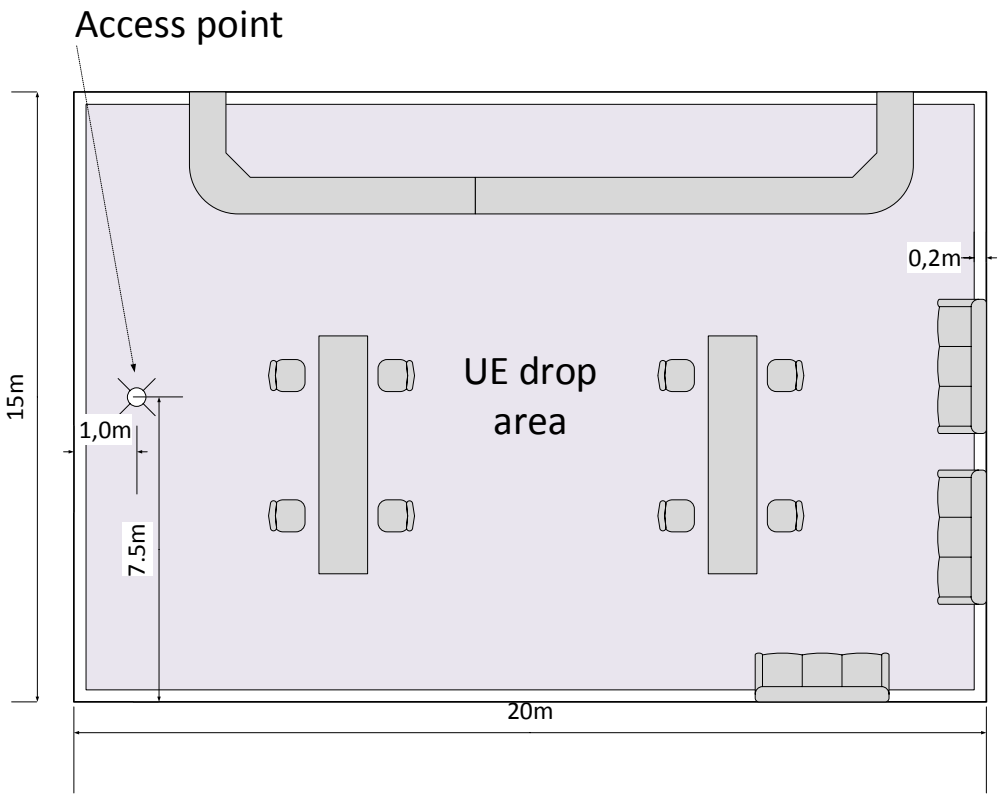

Figure 1.4: Hotel lobby (indoor access large public area) scenario

UEs are dropped throughout the room (gray areas in Figure 1.4).

AP has a single sector, directed to the center of the lobby. 50 UEs uniformly dropped in the area for each trial, with UE density 0.17 UE/m^2 (1 UE per 6 m^2) which is almost the same density as in street canyon.

1.2.4 HetNet LTE + mmWave scenario

HetNet scenarios allow to evaluate LTE+mmWave system performance characteristics of the whole heterogeneous communication system defined in MiWEBA. HetNet simulations assume random millimeter-wave APs (hot-spots) deployment within a large LTE cell (see Figure 1.5)

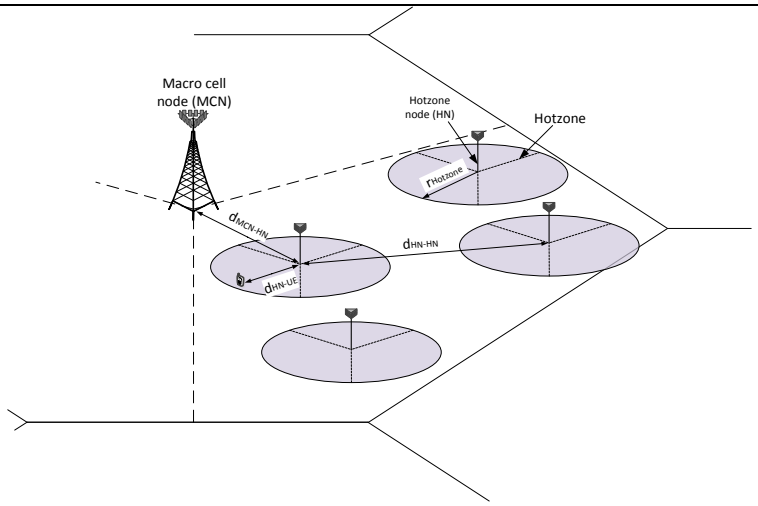

Figure 1.5 3GPP HetNet scenario with small cells

Parameters of the HetNet deployment are summarized in the Table 1.6

Table 1.6 Open-area Het-net deployment model parameters

Parameter	**Value**
Inter-site distance	500m
Number of Macro cells per site	3
Number of mmWave APs per macro cell, N_{HN}	1 , 3
$d_{MCN\text{-}HN\_min}$	75m
$d_{HN\text{-}HN\_min}$	40 m
AP height, H_{HN}	6 m
UE dropping	Clustered*
Number of users per macro cell, N_{users}	>100
Fraction of mmWave AP users, $P^{hotspot}$	9/10
$r_{Hotzone}$	40m
$d_{HN\text{-}UE\_min}$	5m
$d_{MCN\text{-}UE\_min}$	35m
UE height, H_{UE}	1.5m
Number of mmWave BS per hotzone	3

*Clustered UE dropping:

- Fix the total number of users, N_{users}, dropped within each macro geographical area.
- Randomly and uniformly drop the configured number of hotzone nodes, N_{HN}, within each macro geographical area (the same number N_{HN} for every macro geographical area).
- Randomly and uniformly drop N_{users_HN} users within $r_{Hotzone}$ radius of each hotzone node, where $N_{users\_HN} = \lfloor P^{hotspot} \cdot N_{users} / N_{HN} \rfloor$

Randomly and uniformly drop the remaining users, $N_{users} - N_{users\_HN} \cdot N_{HN}$ to the entire macro geographical area of the given macro cell (including the hotzone area).

2 System level simulator

2.1 Simulation parameters

In this section, fundamental parameters presented in D4.1 for the system level simulation are revisited. The system on which we focus is an mm-wave overlay HetNet which is constructed by wide area macro base station (macro BS) and small area coverage base stations (smallcell BS). It is assumed that macro BS LTE system works in 2GHz band and smallcell BS 802.11 ad system works in 60 GHz band.

2.1.1 Q-D Channel model

The novel Q-D channel modeling methodology, developed at the MiWEBA work package 5.1 [3], is used for channel simulations. MiWEBA Q-D channel modeling methodology is based on a number of experimental measurements [6] [7] and their theoretical analysis [8] [9]. The approach builds the millimeter-wave channel impulse response comprised of a few quasi-deterministic strong rays (D-rays), a number of relatively weak random rays (R-rays) – see Figure 2.1.

For each of the channel propagation scenario, the strongest propagation paths, these produce the substantial part of the received signal power, are determined. Then the signal propagation over these paths are calculated based on the geometry of the deployment and the locations of transmitter and receiver. Finally the signal power conveyed over each of the rays is calculated in accordance to theoretical formulas taking into account free space losses, reflection coefficients, polarization properties and receiver mobility effects like Doppler shift. Some of the parameters in these calculations may be considered as random values like reflection coefficients or as random processes like receiver motion. The number of D-rays, which are taken into account, is scenario dependent and chosen to be aligned with the channel measurement results. In Addition to the D-rays, a lot of other reflected waves are received from different directions, coming for example from cars, trees, lamp posts, benches, houses, etc. (for outdoor scenarios) or from room furniture and other objects (for indoor scenarios). These rays are modelled as R-rays and defined as random clusters with specified statistical parameters extracted from available experimental data or ray tracing simulation.

Open area, street canyon and hotel lobby channel models developed in [3] are applied to the corresponding scenarios (see Section 1.2).

For reference, in some scenarios, the simple LOS-only (free space propagation) channel is considered.

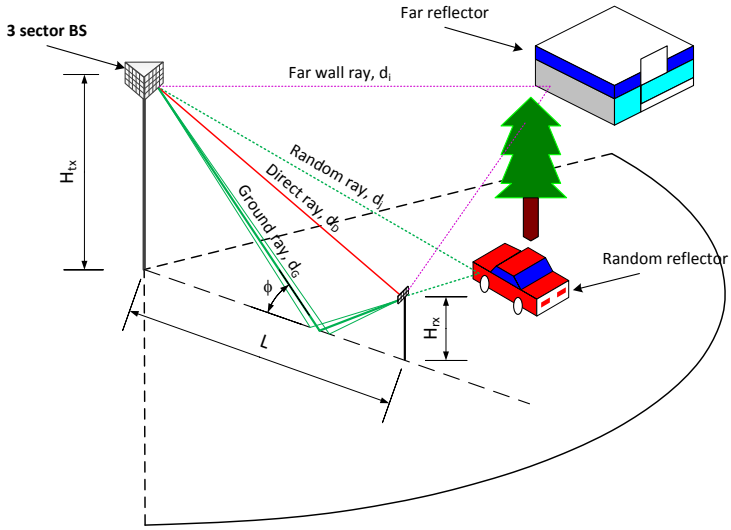

Figure 2.1 Q-D channel model illustration

2.1.2 HetNet evaluation parameters

Other parameters are based on the 3GPP standards and IEEE 802.11ad standards. Therefore some parameters e.g. CSI feedback error, signal overhead, etc. are not part of this deliverable. Parameters for the system level simulation are summarized in Table 2.1 and Table 2.2.

Table 2.1 LTE macro Parameters

Parameter	Value
Cell Layout	Hexagonal (ISD: 500 m)
Number of sectores	3
Carrier Frequency [GHz]	2.0
Available bandwidth [MHz]	10
BS Tx Power [dBm]	43
BS Antenna Height [m]	25
Anttena Pattern	3GPP sector antenna
Antenna gain [dBi]	17
Number of antennas	4
Delay spread [μs]	0.363
Path Loss [dB] (d in [m])	128.1+37.6*log10(d)
Transmission scheme	SVD-MIMO
Channel model	3GPP SCME [10]
Shadowing	log normal distribution with decorrelation distance: 50m standard deviation: 6dB
UE mobility	3 km/h linear walk

Table 2.2 Mm-wave Smallcell Parameters

Parameter	Value
Cell Layout	Random drop
Carrier Frequency [GHz]	60
Available bandwidth [MHz]	2160

Number of subcarriers	512 (for user data transmission: 336)
BS Tx Power [dBm]	19
BS Antenna Height [m]	4
Anttena Pattern	5dBi patch antenna
Number of antennas	8 antenna modules (each module has 8x2 elements)
Delay spread [μs]	0.015
Path Loss [dB] (d in [m])	$\begin{cases} 82.02 + 23.6\log_{10}(d/d_0), d \geq d_0 \\ 82.02 + 20\log_{10}(d/d_0), d < d_0 \end{cases}$ d_0:reference distance: 5m [3]
Transmission scheme	SVD-MIMO (Multi user MIMO is option)
Channel model	MiWEBA channel model, Outdoor open square [3]
Shadowing	log normal distribution with standard deviation: 5dB
UE mobility	3 km/h linear walk

LTE parameters are based on the 3GPP standards [11] [12]. We assume FD-LTE and perfect CSI feedback and the effects of H-ARQ are not considered. Additionally, any signalling overheads are not included. Mm-wave parameters are based on the IEEE 802.11ad standard [13]. In this simulator, only OFDM transmission is available. In the hotspot existing case, this study employs two types of hotspot models for short term evaluation and long term evaluation. Short term evaluation is based on the 3GPP evaluation model [11] and all smallcell BSs are deployed in the center of the hotspot. 90% of all users are within hotspots and remaining 10% users are randomly dropped. On the other hand long term evaluation is MiWEBA space-time traffic model which is developed based on the actual traffic data measured in an urban area in Japan.

2.2 Full buffer scenarios

2.2.1 Isolated and dense hexagonal deployments of mmWave APs

The HetNet system gives the insights on the overall system performance characteristics, but for separate millimeter-wave links analysis, the regular homogeneous system is more suitable. For that, two limit cases of the millimeter-wave small cells deployment are considered: the isolated cell and dense hexagonal deployment

- Isolated cell: In this case APs are dropped so rarely that we can neglect interference between them and estimate the mmWave network performance through simulating only three APs of a single cell [14].
- Dense deployment**:** In this opposite extreme case APs deployment has maximal density with the hexagonal structure and therefore the maximal inter-cell interference between APs is achieved.

Performance analysis of these two limit cases of interference level will allow to determine the upper and lower boundaries of the millimeter-wave hotspots throughput and capacity.

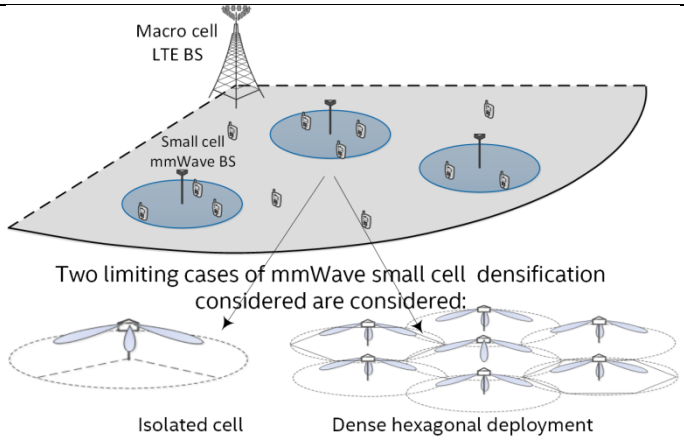

Figure 2.2 Two limit inter-cell interference cases: isolated cell and dense hexagonal deployment

2.2.2 Frequency reuse

For long-term interference management within a millimeter-wave cells the frequency reuse pattern is applied. Three non-overlapping channels each with 2 GHz bandwidth allocated similar to the 802.11ad standard are considered as available. The millimeter-wave cell with 3-sectors gives us two approaches of these channels usage (see Figure 2.3):

- Frequency reuse 3. Each serving sector operates in only one of 3 channels.
- Frequency reuse 1. Each serving sector can operate in the whole band using all 3 channels

Frequency reuse-3 is preferable as it reduces the interference impact. At the same time for some cases frequency reuse 1 can provide better system performance from the spectral efficiency point of view.

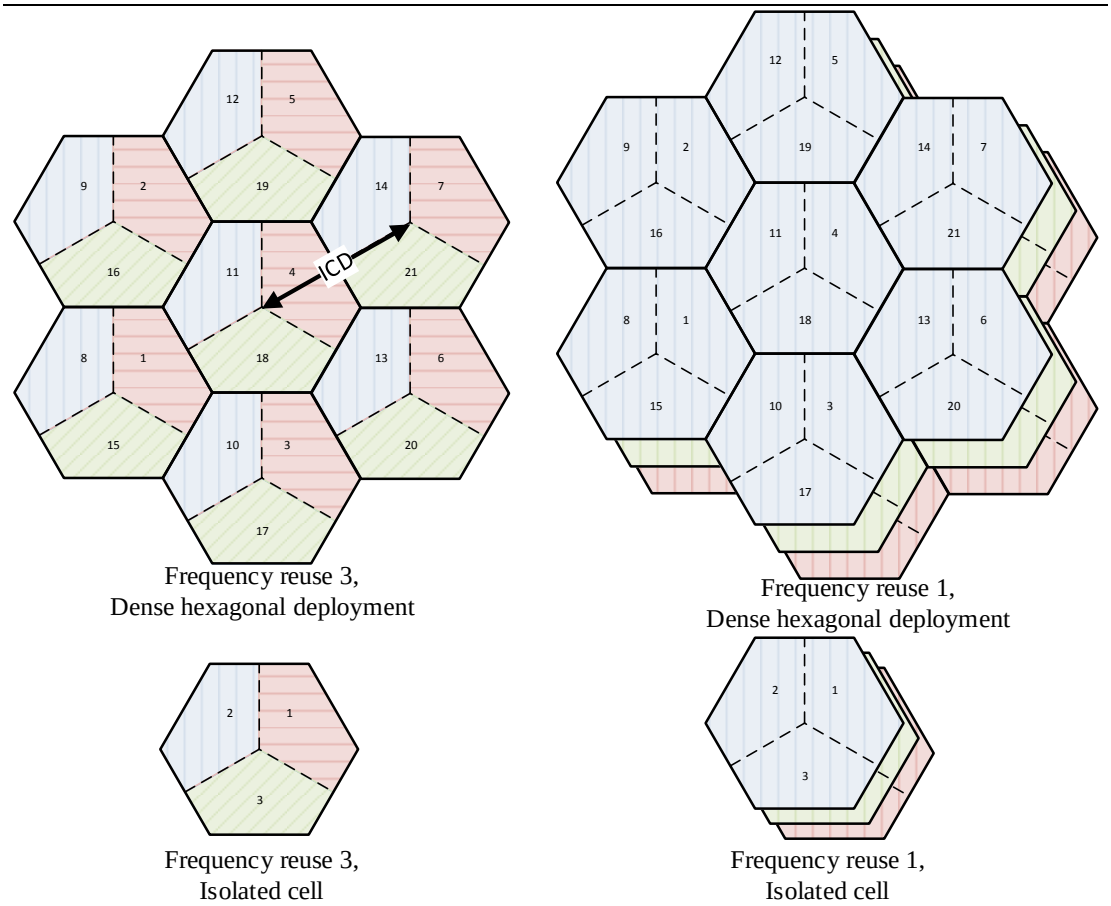

Frequency reuse 3, Dense hexagonal deployment

Frequency reuse 1, Dense hexagonal deployment

Frequency reuse 3, Isolated cell

Frequency reuse 1, Isolated cell

Figure 2.3 Frequency reuse for isolated and dense hexagonal deployments

Deployment parameters for two frequency reuse cases are summarized in Table 2.3.

Table 2.3 Deployment parameters

Parameter	Value
Environment description	Dense hexagonal deployment: – Three APs (antenna height - 6m) each serving its own 120° sector are placed at the centre of the hexagons – Inter-Cell Distance (ICD) = 100m
Channels allocation	Frequency reuse-3 Frequency reuse-1
UEs location	UE (antenna height – 1.5m) are placed randomly (uniform distribution) within the N_{cells} cells considering predefined number of UEs (N_{UEs}) per cell sector $N_{UEs} = 50$ Dense deployment: $N_{cells} = 7$ ($N_{AP} = 21$) Isolated cell: $N_{cells} = 1$ ($N_{AP} = 3$)

2.3 Non-full buffer scenario

In non-full-buffer scenario, traffic demand of each users are set. Mm-wave system can transmit a huge amount of data in a blink. However since the coverage is limited, only a few users can get benefits. In order to use mm-wave resource effectively, users whose traffic demand is relatively high should be accommodated into mm-wave system appropriately. This simulation employs Gamma distribution traffic model with bias [15] which is made from actual traffic data in urban area, Japan. Figure 2.4 and Table 2.4 are a CDF of the user traffic and distribution parameters respectively.

If the property of traffic distribution will not change in the future, we can predict future traffic demand by controlling the scale parameter of Gamma distribution.

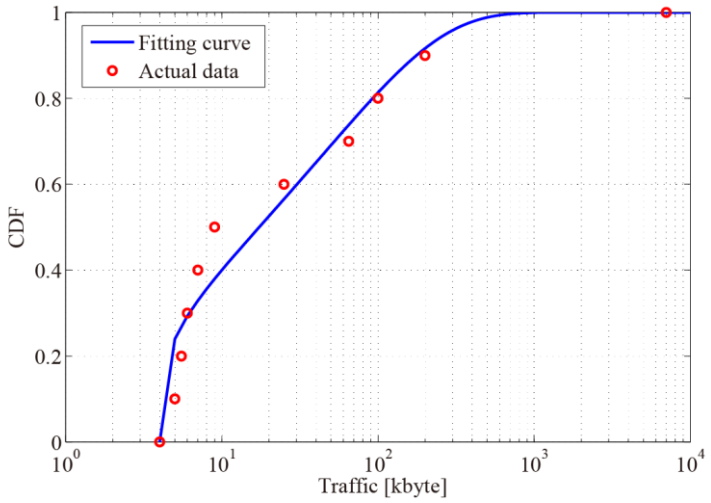

Figure 2.4 Traffic distribution CDF

Table 2.4 Gamma distribution parameters

Parameter	Value
Scale parameter	2.012×10^5
Shape parameter	0.2892
Bias	4 kbps

2.3.1 Space-time traffic model

In short term evaluation, users are dropped based on the 3GPP hotspot model [11] and all smallcell BSs are deployed in the center of the hotspot. 90% of all users are within hotspots and remaining 10% users are randomly dropped. On the other hand, in long term evaluation, users are dropped based on the MiWEBA space-time traffic model [16] which is developed based on the actual traffic data measured in an urban area in Japan. The space-time traffic distribution is estimated based on the statistical information of each user traffic mentioned above and the total hourly traffic measured in 100 meters by 100 meters. More details are explained in Section 4.2.2.1. MiWEBA space-time traffic model can express the hotspot variation of every hour. Figure 2.5 and Figure 2.6 show BS deployment and user distribution of each scenario.

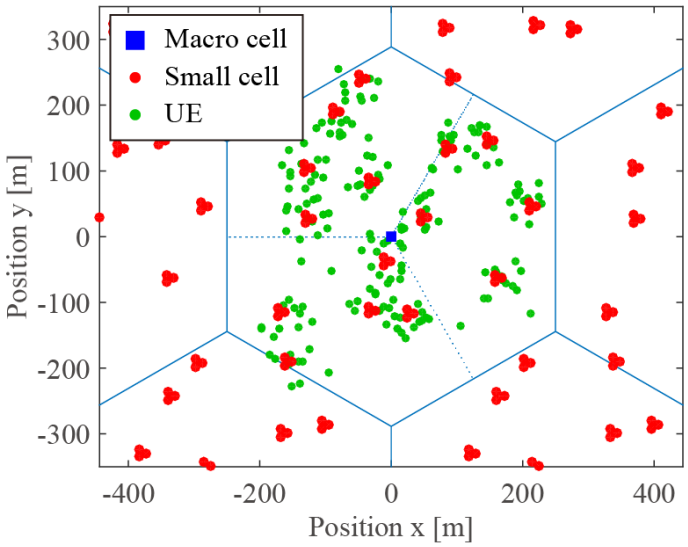

Figure 2.5 Short term evaluation deployment

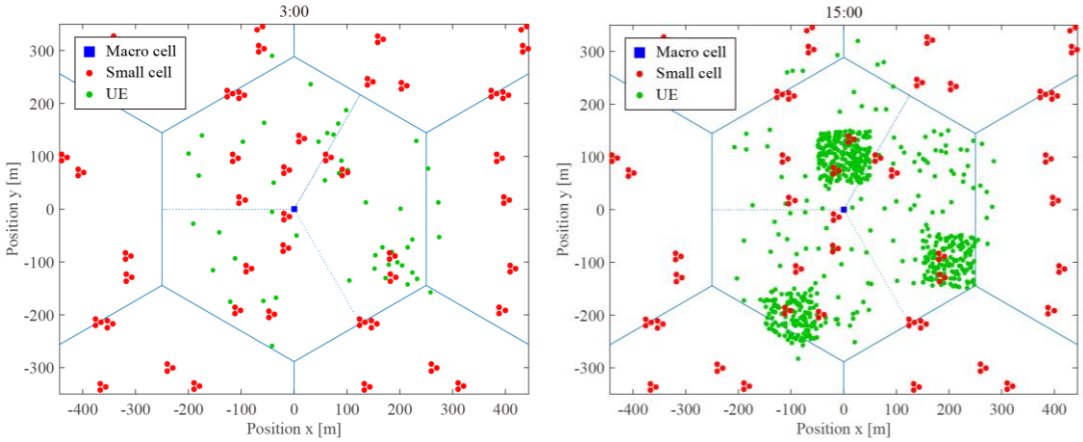

Figure 2.6 Long term evaluation deployment (left: 3:00, right: 15:00)

2.3.2 BS power consumption model

In order to appropriately investigate the effectiveness of the On-demand smallcell BS ON/OFF, this study introduces a practical base station power consumption model of 2GHz, 3.5GHz, and 60GHz band based on GreenTouch [17] and Earth project model [18], which is summarized in Table 2.5. The transition duration between ON and idle is assumed to be negligibly small and the power consumption is assumed to be a constant value regardless of the impinged traffic load.

Table 2.5 BS power consumption of each band

Parameter	Value
BS ON	835W (2GHz DL)/ 14W (3.5GHz DL)/ 60W (60GHz DL)
BS idle	19W (2GHz)/ 2W (3.5GHz)/ 2W (60GHz)

3 Short term resource management

3.1 Full buffer scenario

3.1.1 Basic assumptions

System level simulations with full buffer mode allow analyzing the potential of system throughput and capacity, regardless of the type of data traffic. Several trials (new positions of the random UEs, new direct and interfering channel drops) are simulated to get stable averaged results. The duration of simulation, i.e. number of simulated frames, is typically much shorter than that for non-full buffer simulations and usually proportional to the number of scheduled users. A full buffer proportional-fair scheduler is used to assign time-frequency resources to the deployed UEs.

The basic assumptions on the full buffer system level simulations are shown in Table 3.1. Detailed considerations of the most of the parameters are show in the following sections.

Table 3.1. Basic SLS assumptions

Parameters	Assumption
Number of trials	10, 20
Frames per trial	100
Allocations per frame	1, 25 ,50
Channel model/Pathloss	LOS-only, Q-D channel models
Carrier / BW	60 GHz / 2 GHz x 3 channels
Transmission scheme	MU-MIMO, SVD-based TX, ZF
Receiver type	Interference-unaware MMSE
Channel estimation	Perfect
Link adaptation	Outer loop, 10%
Scheduling type	Greedy PF MU scheduling

3.1.1.1 Resource block structure

In the frequency selective channels the SC approach to signal modulation and scheduling may lead to a serious performance degradation. To overcome the multipath effects, OFDM (orthogonal frequency division multiplexing) approach is used. In case of point-to multipoint links, this approach enhanced to the OFDMA – orthogonal frequency division multiple access, where different groups of OFDM subcarriers (subbands) are assigned to the different users. In the presented simulation results, for OFDMA system with 1024 total and 600 data subcarriers, different resource blocks are used:

- Whole frame allocations (2 GHz in frequency, 1 frame in time, 600 subcarriers)
- 25 allocations per frame (each resource block is continuous 80 MHz allocation in frequency and 1 frame in time, 24 subcarriers)
- 50 allocations per frame (each resource block is continuous 40 MHz allocation in frequency and 1 frame in time, 12 subcarriers)

3.1.1.2 MU-MIMO (Massive MIMO) and user scheduling

UE grouping and MU-MIMO greedy scheduler

In full-buffer scenario, scheduling algorithm assigns the available time-frequency resources to the UEs, on the base of the pre-defined metrics. The proportional fair (PF) metric, inversely proportional to the amount of resources already allocated to the UE in previous frames is used. For the multiuser (MU-MIMO) transmissions, the scheduler also takes responsibility for UE grouping for simultaneous transmission on the same time-frequency slot. For MU group the best UEs are picked up one by one considering maximization of total group PF metric. The process stops when addition of one more user reduces the metric.

TX beamforming algorithms

The perfect channel estimation and feedback is assumed in the presented full buffer system level simulations. Channel quality information and channel state information obtained from user feedback are used. During the scheduling the beam forming vectors are defined, using the interference mitigation techniques applied to TX side such as zero forcing if enabled.

3.1.2 Basic simulation results

3.1.2.1 Open area simulation scenario

Cell size selection

The largest possible small cell size can be determined by the minimum required SINR and the pathloss exponent. However, regarding the throughput metric, some quasi-optimal cell size exists. From the first view, it seems that the cell throughput is increased by decreasing the cell radius – the higher order modulations are used for UEs that is close to AP. However, for fixed UE density and MU-MIMO mode, very small cells have small number of UE to multiplex, due to lack of UEs. So, an optimal cell size exists that meets for both mentioned factors. To determine the size, the set of SLS simulations with different cell radius was performed in the open area environment for Isolated and Dense cases. The results are summarized in Table 3.2 and Table 3.3. It can be seen that for R=50 m (ISD = 100m) the highest level of UE multiplexing is reached and such cells may be recommended for further analysis and future deployments. Note, that this value is selected for the baseline antenna configuration of 8x16 in a smallcell BS. Obviously, for larger antenna array the optimal cell size becomes bigger.

Table 3.2 Isolated small cells metrics for different cell size, 8x16 antenna

Cell radius [m]	Smallcell BS throughput, [Gbps]	Number of UEs dropped into one sector	Avg number of UEs in MU-MIMO group	Avg. UE throughput, [Mbps]	Cell edge UE throughput, [Mbps]
r = 25	10.6	5	2.94	2119	1320
r = 50	10.2	20	**4.82**	512	291

r = 75	7.2	45	4.35	161	87
r = 100	4.7	80	2.90	59	24

Table 3.3 Hexagonal dense small cells metrics for different cell size, 8x16 antenna

Cell radius [m]	**Smallcell BS throughput, [Gbps]**	**Number of UEs dropped into one**	**Avg number of UEs in MU-MIMO**	**Avg. UE throughput, [Mbps]**	**Cell edge UE throughput, [Mbps]**
r = 25	6.7	5	2.66	1333	696
r = 50	7.3	20	**4.32**	365	206
r = 75	5.5	45	3.80	123	66
r = 100	3.9	80	2.66	49	24

Figure 3.1 and Figure 3.2 shows the UE throughput distribution among the cell for isolated and dense scenarios respectively.

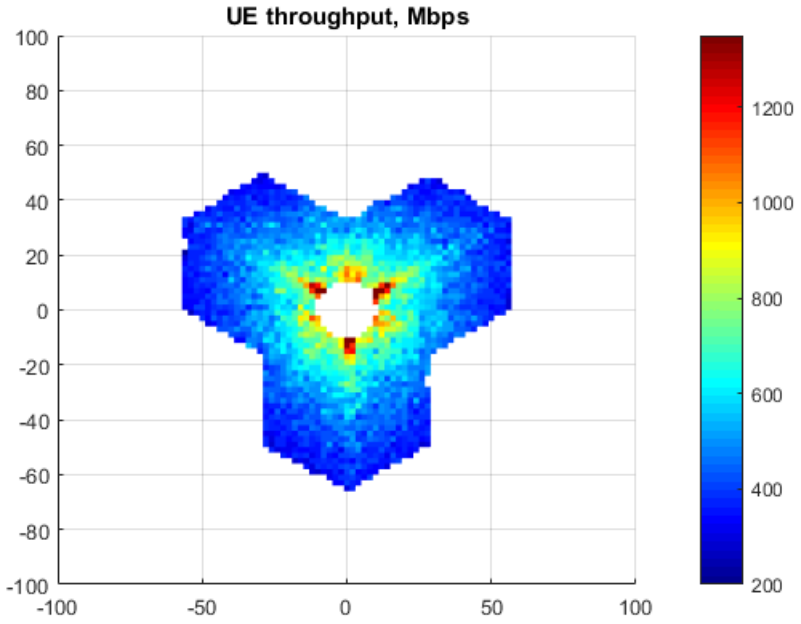

Figure 3.1 UE throughput distribution for cell radius 50m, isolated cell

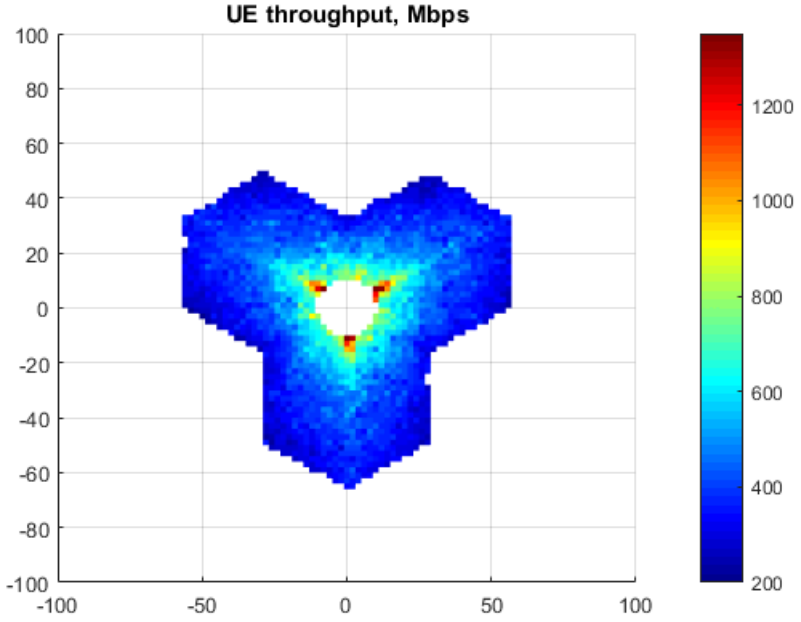

Figure 3.2 UE throughput distribution for cell radius 50m, dense scenario

Line of Sight channel approximation

As a reference point, for comparison of all performance results in different environment and channel models, the open area LOS-only channel approximation is used.

Different techniques were evaluated in Isolated cell and Dense hexagonal interference scenarios. To investigate the scheduling impact with respect to the resource granularity, two resource block sizes investigated: the whole band (2GHz,

see Table 3.4) with single allocation per frame and 80 MHz (25 allocations per frame, see Table 3.5). All these results are obtained for 8x16 antenna configuration.

Table 3.4 Open area LOS channel, single allocation per frame

Scenario	Smallcell BS throughput, [Gbps]	Avg. number of UEs in MU-MIMO group	Avg. UE throughput, [Mbps]	Cell edge UE throughput, [Mbps]
Reuse-1 SU isolated	4.3 x 3	1	86	35
Reuse-3 SU isolated	4.6	1	92	42
Reuse-3 isolated	9.4	5.10	187	111
Reuse-1 isolated	8.7 x 3 (+178%)	4.88	173	104
Reuse-1 dense	2.2 x 3 (-30%)	2.64	44	17
Reuse-3 dense	7.8 (-17%)	4.88	156	92

Table 3.5 Open area LOS channel, 25 allocations per frame

Scenario	Smallcell BS throughput, [Gbps]	Avg. number of UEs in MU-MIMO group	Avg. UE throughput, [Mbps]	Cell edge UE throughput, [Mbps]
Reuse-3 isolated	12.0	5.77	239	143
Reuse-1 isolated	11.2 x 3 (+180%)	5.66	225	137
Reuse-1 dense	3.3 x 3 (-18%)	2.87	65	29
Reuse-3 dense	9.1 (-24%)	5.35	182	110

The results for LOS-only channel approximation in the open area scenario may serve as good reference point for comparison with realistic channel model results. At the same time, it gives initial insights on the impact of interference scenario and frequency reuse to the system performance.

The scenario with least interference level is Reuse-3 isolated: no inter-sector interference and no interference from other cells. The Reuse-1 in isolated scenario almost triples (+180%) the throughput. The increased interference prevents system from achieving exact x3 gain due to frequency reuse (see Section 2.2.2).

In the dense environment, increased level of interference will strongly affect the performance of the system. Reuse-3 scenario with only inter-cell interference present has degradation about 20% in comparison with interference-free case. Moreover, Reuse 1 does not provide throughput increase. Simulations show that this huge performance loss caused not only by the interference level, but rather by unpredictability of interference level, leading to the usage of minimal MCSs. It can be shown that various methods of interference and scheduling coordination may improve the situation (see Section 3.1.3)

Q-D channel model

The Q-D channel model represents realistic propagation conditions, and shows the impact of multipath propagation and fading on the final performance metrics [19].

Like in the LOS-only channel results, two resource block sizes investigated: the whole band (2GHz, see Table 3.6) with single allocation per frame and 80 MHz (25 allocations per frame, see Table 3.7).

Table 3.6 Open area Q-D model, single allocation per frame

Scenario	Small cell BS throughput, [Gbps]	Avg. number of UEs in MU-MIMO group	Avg. UE throughput, [Mbps]	Cell edge UE throughput, [Mbps]
Reuse-3 isolated	9.9	5.29	198	118
Reuse-1 isolated	9.3 x 3 (+181%)	5.19	185	114
Reuse-1 dense	2.1 x 3 (-36%)	2.60	41	17
Reuse-3 dense	7.0 (-29%)	4.74	139	83

Table 3.7 Open area Q-D model, 25 allocations per frame

Scenario	Small cell BS throughput, [Gbps]	Avg. number of UEs in MU-MIMO group	Avg. UE throughput, [Mbps]	Cell edge UE throughput, [Mbps]
Reuse-3 isolated	11.3	5.58	226	140
Reuse-1 isolated	10.7 x 3 (+184%)	5.50	213	134
Reuse-1 dense	3.4 x 3 (-10%)	2.88	67	31
Reuse-3 dense	8.8 (-22%)	5.23	176	110

The results for the Q-D model of the open area scenario are very similar to the LOS-only approximation results. This means that very low frequency selectivity of the open area channel.

3.1.2.2 Street canyon simulation scenario

Street canyon scenario is described in Sect. 1.2.2. Unlike in the open-area scenario, in the street canyon in addition to the ground ray (which have rather small delay in comparison with LOS path), several new wall reflected paths are observed, with larger delays. The channel becomes frequency selective with deep gaps in signal power at certain frequencies (see Figure 3.3).

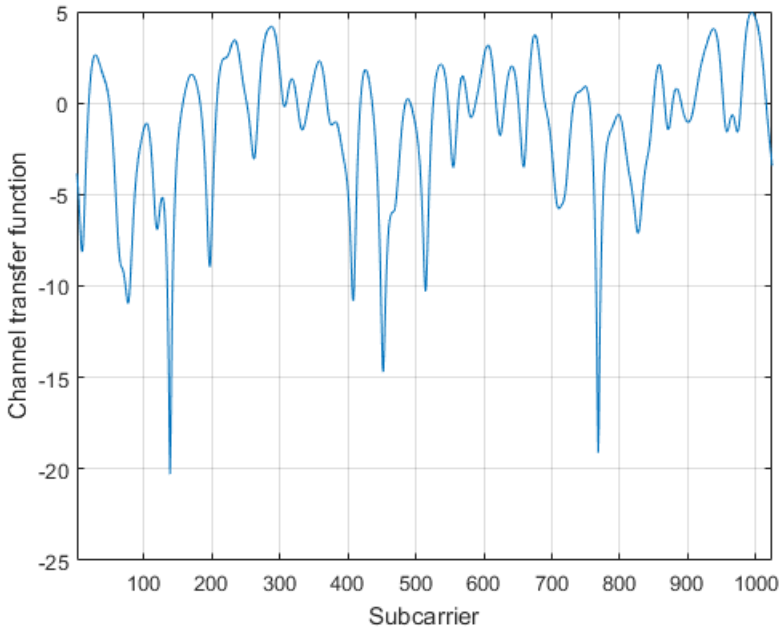

Figure 3.3 Example of the Street Canyon channel transfer function

To overcome the frequency selectivity, the whole band should be divided at smaller resource blocks (sub-bands). Simulation results, summarized in Table 3.8, are presented for single allocation per frame, 25 allocation and 50 allocations. For comparison purposes, the results for LOS-only, flat channel are also presented.

Table 3.8 Street canyon simulation results

	Scheduling/feedback granularity	**Small cell BS throughput, [Gbps]**	**Avg number of UEs in MU-MIMO group**	**Avg. UE throughput, [Mbps]**	**Cell edge UE throughput, [Mbps]**
LOS only	1 x 2000MHz band	15.5	3.99	516	225
Q-D	1 x 2000MHz band	4.9	2.67	163	28
	25 x 80MHz sub-bands	13.5	3.88	452	221
	50 x 40MHz sub-bands	**14.9**	**4.08**	**497**	**247**

The multipath properties of propagation channel in the street canyon can be seen by comparing the results of Q-D model in Table 3.8 with the reference results of LOS-only. It can be seen that using the resource allocation block equal to whole channel produces significant degradation, while dividing the band into smaller allocated subbands improves the situation. For 40 MHz subbands the performance in the multipath environment is very close to ideal situation with flat LOS channel. The average number of multiplexed UEs in that case is about 4.

Figure 3.4 and Figure 3.5 shows the BS throughput and UE throughput CDFs respectively.

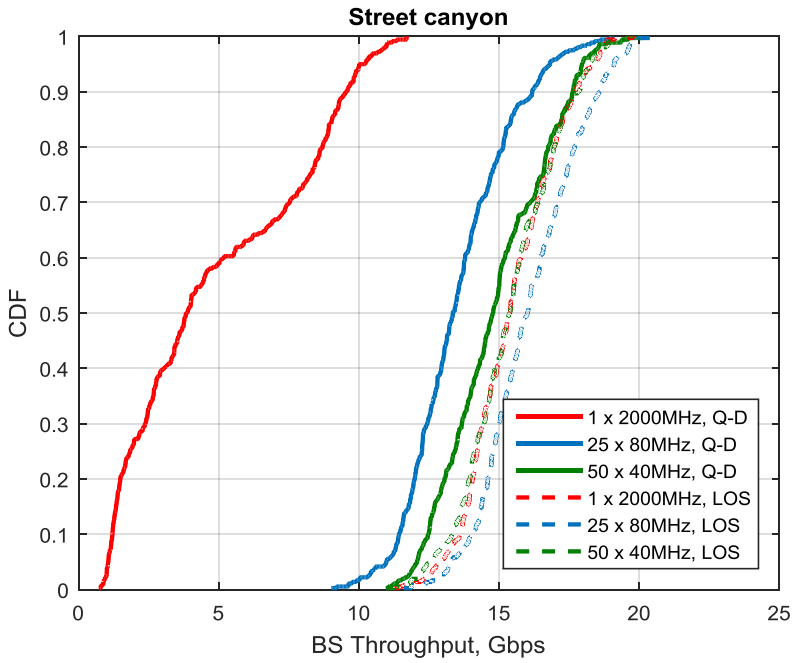

Figure 3.4 BS throughput CDF, street canyon scenario

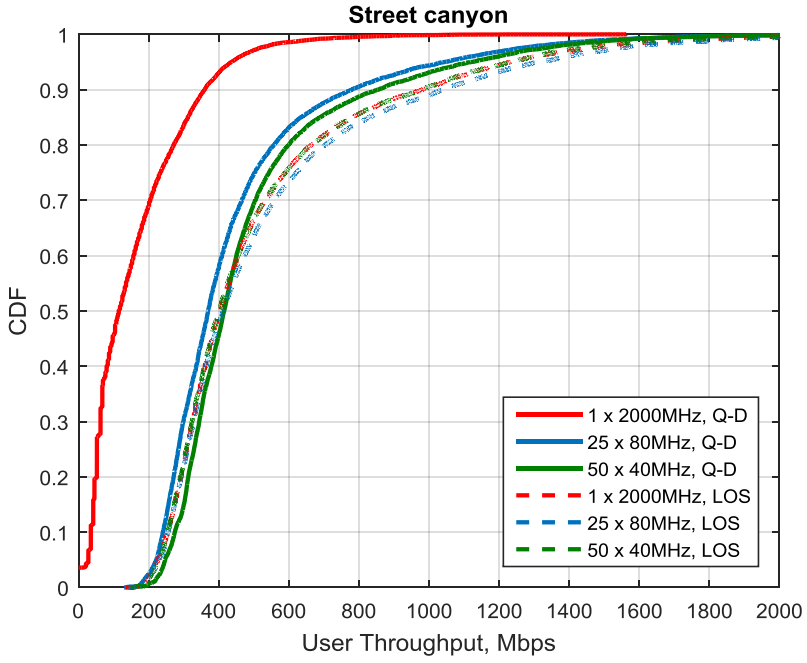

Figure 3.5 UE throughput CDF, street canyon scenario

The UE throughput CDFs in Figure 3.5 gives insights on the achievable throughputs for street canyon scenario with 1 UE per 5.5m^2 density. In such overpopulated environment, 10% of UEs may have larger than 1 Gbps throughput, and half of users – larger than 0.4 Gbps.

3.1.2.3 Hotel lobby simulation scenario

The Hotel lobby channel is also characterized by strong multipath components and high frequency selectivity. The Q-D model takes into account all paths up to and including second order reflections. Thus, sub-band approach with division of the frame into a number of smaller s is also required here.

Simulation results for Hotel lobby scenario (Section 1.2.3) are summarized in Table 3.9. It can be seen that with smaller allocation size, the performance in realistic Q-D channel becomes closer to the ideal LOS-only case.

The spatial multiplexing rate (average number of UEs in MU group) is high, despite the highly multipath environment with strong interference between reflected rays.

Table 3.9 Hotel lobby simulation results

Scheduling/feedback granularity		**Small cell BS throughput, [Gbps]**	**Avg number of UEs in MU-MIMO group**	**Avg. UE throughput, [Mbps]**	**Cell edge UE throughput, [Mbps]**
LOS (25 x 80MHz sub-bands)		23.7	6.5	475	273
Q-D	1 x 2000MHz band	10.9	4.4	217	107
	25 x 80MHz sub-bands	17.9	5.3	358	206
	50 x 40MHz sub-bands	**18.8**	**5.4**	**376**	**242**

Figure 3.6 shows the UE throughput CDFs for different simulated modes of operation.

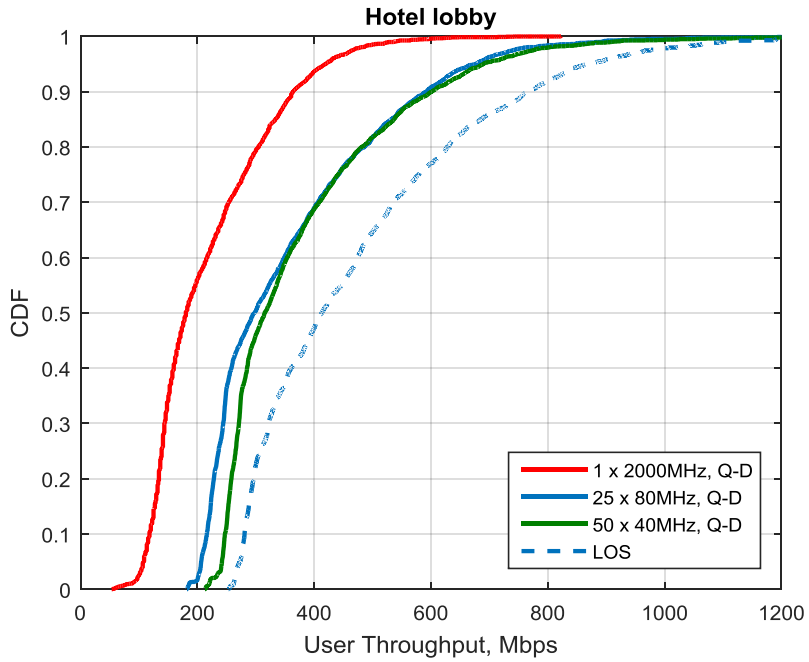

Figure 3.6 UE throughput CDFs for Hotel Lobby scenario

The UE throughput CDFs in Figure 3.6 shows on the achievable throughputs for street canyon scenario with 1 UE per 6m^2 density. Similar to the street canyon, 10% of UEs may have larger than 1 Gbps throughput, and half of users – larger than 0.3 Gbps.

3.1.3 Coordinated resource management in Hotspot deployments

3.1.3.1 Coordinated beamforming and scheduling

Performance of different Coordinated Multipoint (CoMP) schemes in millimeter-wave hotspots was evaluated. For the open-area scenario, both isolated and dense deployment cases, the Coordinated Scheduling (CS) and Coordinated Beamforming (CB) schemes are applied. For dense environment, the coordination cluster was selected equal to seven cells (three sectors in each, totally 21 transmitters). For the CS/CB CoMP simulations, all transmissions in coordination cluster are managed in the centralized manner, jointly optimizing the beamforming to reduce mutual interference and scheduling assignments to increase the throughput. In more details, considered schemes are described in [20] [21] [22] [23].

The intra-cell interference in CS/CB CoMP scheme is also suppressed using the zero-forcing algorithm. So, it will be fair to compare the CS/CB CoMP performance with the performance of the system with intra-cell interference ZF suppressing scheme only.

To avoid the complexity of optimal beamforming calculations, the CoMP scheme with the Coordinated Scheduling (CS) only can be used. This scheme does not perform any zero-forcing algorithms or other beamforming optimizations, but the scheduling is performed jointly for all BSs in the cluster on the base of the total cluster proportional fair metric maximization. Here the UEs still report to their

serving BSs the information about the interfering channels to other BSs of the CoMP cluster. While performing the scheduling the CPU does not change the reported beamforming. It just takes into account the interference which current beamforming makes to all UEs and picks up the UEs into the MU groups maximizing the total system throughput (minimizing the intra-cell and inter-cell interference).

3.1.3.2 CoMP simulation results

In Section 3.1.2.1 we have evaluated millimeter-wave system performance for different frequency reuse schemes (reuse 1 and reuse 3) and interference scenarios (isolated and dense). It was show that in comparison with reference interference free scenario (isolated cell in reuse 3), other schemes have degradation that is very significant in dense interference environment. Additionally, even in interference free scenario, the system is suffered from inter-stream interference during the MU-MIMO transmissions. All this mentioned sources of interference can be mitigated or avoided by application of spatial processing algorithms and coordinated resource management.

The Zero-Forcing (ZF) procedure is applied at the TX side to minimize mutual interference of the MU spatial streams. Coordinated Scheduling (CS) will match scheduling decision on several stations for throughput optimization. The Coordinated Scheduling / Coordinated beamforming (CS/CB) will also adjust beams of small cell BSs to minimize the interference.

Table 3.10 summarized the performance evaluation results for isolated interference case of the open area scenario.

Table 3.10 CoMP techniques in Isolated scenario, Open area LOS channel

Scenario	Small cell BS throughput, [Gbps]	Avg number of UEs in MU-MIMO group	Avg. UE throughput, [Mbps]	Cell edge UE throughput, [Mbps]
Reuse-3	9.4	5.10	187	111
Reuse-3 ZF	10.8 (+15%)	5.82	217	120
Reuse-1	8.7 x 3 (+178%)	4.88	173	104
Reuse-1 ZF	9.8 x 3 (+213%)	5.46	197	109
Reuse-1 CS	9.0 x 3 (+187%)	4.96	180	111
Reuse-1 ZF +CSCB	10.2 x 3 (+226%)	5.50	204	116

It can be seen that Reuse 1 may almost triple the throughput by itself, and various CoMP schemes helps to mitigate the additional interference to a negligible levels.

Table 3.11 show similar evaluation for dense interference scenario in Reuse 3. It can be seen that various CoMP techniques may increase the system throughput up to 20-30%. The last row in the table shows the performance for the case of ideal knowledge of the suitable MCSs. The small difference between realistic and ideal scheme illustrates how close we get to the performance limits.

Table 3.11 CoMP techniques in Dense scenario, Open area LOS channel

Scenario		Small cell BS throughput, [Gbps]	Avg number of UEs in MU-MIMO group	Avg. UE throughput, [Mbps]	Cell edge UE throughput, [Mbps]
Dense, Reuse 3	Reuse 3	7.8	4.88	156	92
	Reuse 3, ZF	8.7 (+12%)	5.43	176	100
	Reuse 3, CS CoMP	9.3 (+19%)	4.50	187	116
	Reuse 3, ZF + CSCB	10.1 (+29%)	4.55	202	121
	Reuse 3, CSCB + clairvoyant MCS	10.5 (+35%)	4.51	209	128

The BS throughput CDFs for all evaluated scenarios are summarized in Figure 3.7. As we can see, the curve corresponding to for Dense Reuse-3 +CS almost matches the curve corresponding to Isolated Reuse-3. That means that implementation of CS CoMP scheme allows to compensate the performance degradation connected with the inter-cell interference.

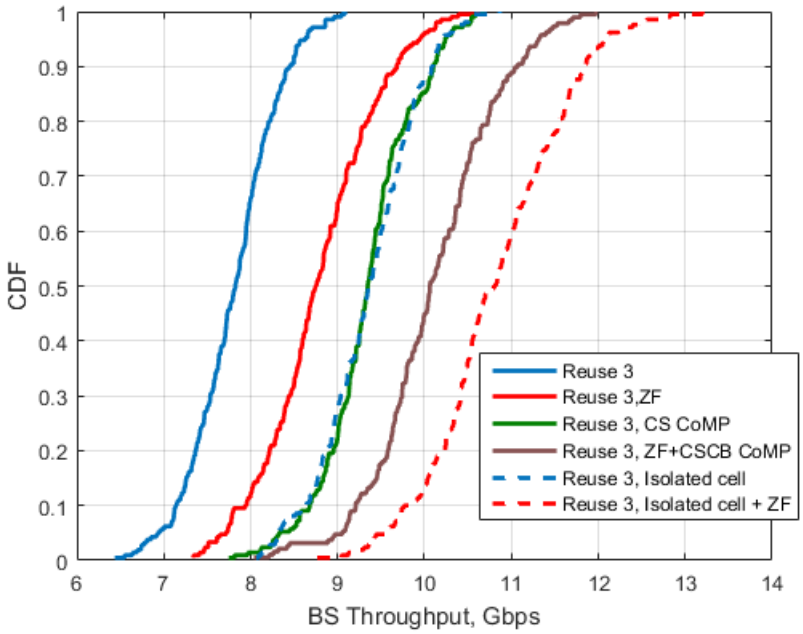

Figure 3.7 BS throughput for open area dense scenario for different reuses

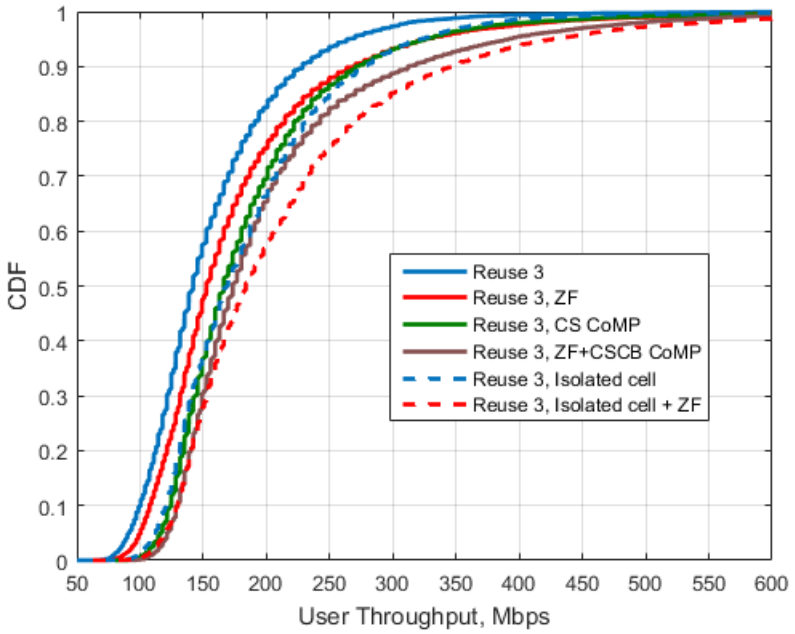

Figure 3.8 UE throughput for open area dense scenario for different reuses

Figure 3.8 shows the UE throughput performance of the considered schemes and algorithms. It can be seen that most advanced ZF+CSCB CoMP scheme may increase the percentage of users with throughput larger than 200Mbps from baseline 17% to almost 35% - two times increase.

3.1.4 Analysis with partially adaptive antenna arrays

3.1.4.1 Array antenna system

Array antenna system is key technology to achieve high performance in the millimeter-wave communication systems, especially in outdoor scenarios. Highly directional large aperture antenna arrays [4] are used at the AP to overcome high propagation loss and ensure multiuser operation. For system level evaluation purposes, the fully adaptive arrays (FAA) are considered, assuming that each antenna element can transmit independent signal with complex weights, allowing adaptive beamforming without limitations.

In addition, the modular antenna arrays (MAA) are considered as practical solution [24]. The MAA consist of multiple independent antenna subarrays, each with its own RF part and phase shifting circuitry (see Figure 3.9). The modules have common baseband and can be adjusted to act as a single antenna array, with some limitations caused by elements grouping (partially adaptive antenna array). Such design gives the possibility to create large aperture antenna array in a cost-effective manner, from the low-cost modules and also solves the problems of feeding lines and heat dissipation.

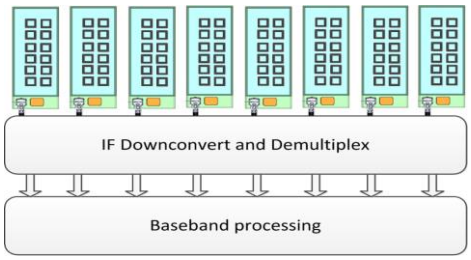

Figure 3.9 Modular antenna array architecture

Parameters of the antennas and antenna arrays used for simulation are summarized in Table 3.12

Table 3.12. Antenna system parameters

BS antenna array	Array type	FAA, MAA
	Height	4, 6 m
	Configuration	8x16 elements
	TX power	19 dBm
	Element gain	5 dBi
	Array gain	26 dBi
UE antenna	Height	1.5m
	Gain	Omni

The structure of MAA limits the beamsteering capability of the array, since single module is able to control just phase shifting, and not full complex weights. However, it is noted that the performance of MAA in single-user scenario is nearly the same with that of FAA, since the MAA can create single beam almost as effective as that of precise weighting (beamforming) in the FAA.

In the case of MU-MIMO scenario with group of users, the situation changes. Partially adaptive structure of MAA due to the constraints in degrees of freedom will

not be able to form beams with maximal gains towards arbitrary located group of users. For example, for the MAA with vertical module placement, the array may have limited ability for vertical beamforming to several users and almost full adaptation ability in horizontal plane. Thus, in multi-user mode in the mmWave small cell with such type of the MAA, the users for simultaneously scheduled group should be selected from the same "ring" around the AP, with the same elevation angle and distance (see Figure 3.10a), while FAA may effectively form equivalent beams in every direction and provide better selection of scheduled users from the whole cell (see Figure 3.10b).

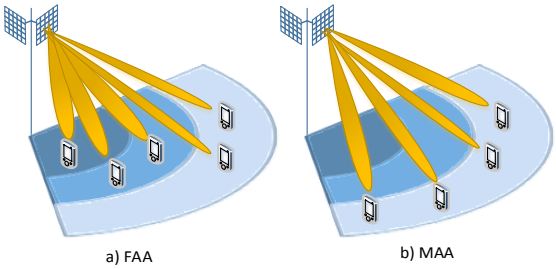

Figure 3.10 MU-MIMO for FAA case (a) and MAA case (b)

In more details, the FAA beamforming matrix (weights matrix) is a rectangular matrix with same number of elements as corresponding array (see Figure 3.11a) with the same number of RF circuits, while the MAA beamforming in the baseband requires vector processing (Figure 3.11b), with second dimension of beamforming made in the analog part, by the built-in modules of phase shifters.

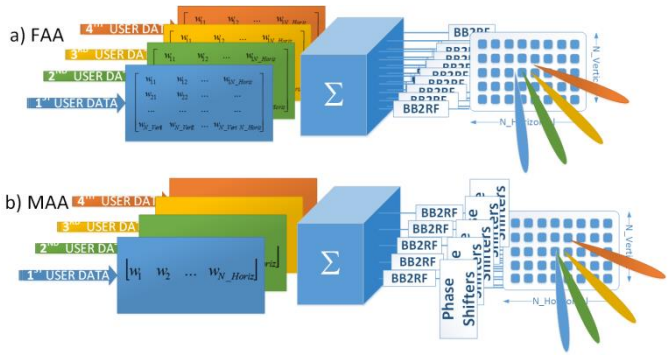

Figure 3.11 Illustration of MU beamforming for FAA case (a) and MAA case (b)

The scalability of the MAA technology opens the way for creation of very large aperture antenna arrays with high gain and high EIRP. This can potentially lead to a violation of regulatory limits such as those specified by the FCC, or similar regulations in other countries. For example, the FCC limits signal power density in 59.05-64.0 GHz band by 18 $\mu W/cm^2$ at 3 m distance [25]. This is equivalent to limiting the peak EIRP (transmit power plus antenna gain) to 43 dBm, which can be easily achieved by MAA with 16 modules of 8x2 elements each. In such case, extra available power may be used to create several equivalent beams to different users in MU-MIMO mode without violating the FCC limits, as it will be described further

3.1.4.2 Simulation results

The obtained system level evaluation results is summarized in Table 3.13, Table 3.14 and Table 3.15 for 8x16, 8x32 and 8x64 arrays respectively. The total throughput through smallcell BS operated in MU-MIMO mode is analysed for different combinations of Isolated vs. Dense scenarios, and the fully adaptive arrays (FAA) vs. partially adaptive arrays (MAA).

It can be seen that difference between isolated cell throughput and cell throughput in hexagonal deployment is about 30-35%. Estimation of the performance of the MAA shows that for base configurations (8x32 and 8x64 elements) the cell throughput degradation in comparison with the FAA case is about only 4-5%. It should be noted, that for free space environment the degradation was about 10-20% under the same assumptions on antennas and cell size.

Table 3.13 Throughput metrics for 8x16 antenna array configuration

	Ant. type	Avg number of UEs in MU-MIMO group	Max number of UEs in MU-MIMO group	Avg user throughput, Mbps	AP throughput, Gbps
Isolated cell	FAA	5.0	9	186.4	9.3
	MAA	4.3	8	167.6	8.4
Dense deployment	FAA	4.6	8	148.6	7.4
	MAA	3.9	8	135.2	6.8

Table 3.14 Throughput metrics for 8x32 antenna array configuration

	Ant. type	Avg number of UEs in MU-	Max number of UEs in MU-MIMO	Avg user throughput,	AP throughput, Gbps
Isolated cell	FAA	7.1	15	380.6	19.0
	MAA	6.7	14	346.9	17.3
Dense deployment	FAA	7.0	15	294.5	14.7
	MAA	6.7	14	273.3	13.7

Table 3.15 Throughput metrics for 8x64 antenna array configuration

	Ant. type	Avg. number of UEs in MU-MIMO group	Max number of UEs in MU-MIMO group	Avg. user throughput, Mbps	AP throughput, Gbps
Isolated cell	FAA	13.8	26	753.1	37.7
	MAA	12.8	25	692.8	34.6
Dense deployment	FAA	15.5	24	589.6	29.5
	MAA	14.1	24	555.4	27.8

Figure 3.12, Figure 3.13 and Figure 3.14 show the main characteristic of the MU-MIMO algorithm – the distribution of the resulting MU-MIMO rank, i.e. the number of simultaneously served and spatially multiplexed users.

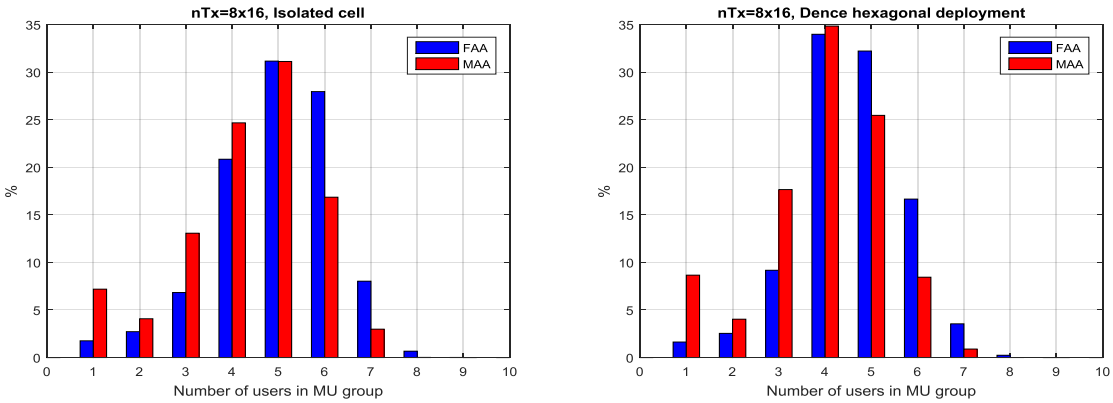

Figure 3.12 MU rank for 8x16 antenna array configuration

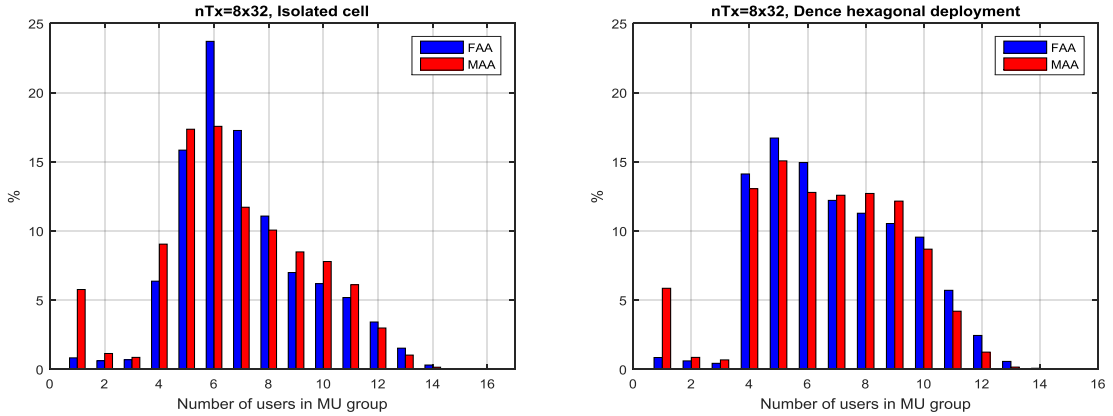

Figure 3.13 MU rank for 8x32 antenna array configuration

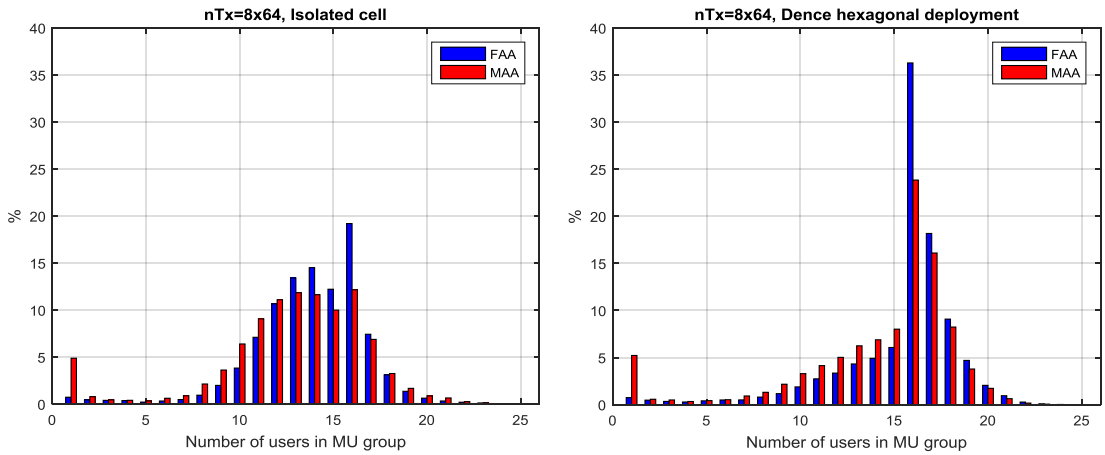

Figure 3.14 MU rank for 8x64 antenna array configuration

It can be seen that, in the realistic multipath environment, the partially adaptive antenna array setup (MAA) demonstrates degradation about 5-15% in comparison with ideal fully adaptive scheme (FAA).

Comparing the isolated cell and hexagonal dense scenarios, it is found that the interference from adjacent small cells, in the worst case of dense small cell deployment, leads to throughput degradation up to 35-38%. Despite that, the application of MU-MIMO technique allows achieving up to 30 Gbps total throughput per small cell for university campus scenario. The relatively large performance degradation due to inter-cell interference opens possibilities for further mmWave small cells throughput enhancement via interference cancellation and different small cell coordination techniques.

3.1.5 LTE+mmWave HetNet system performance

In this section we will introduce the simulation results for LTE+mmWave HetNet system in full buffer traffic case as the upper-bound of the performance of basic MiWEBA mmWave overlaid heterogeneous network.

Deployment scenario parameters for the LTE+mmWave HetNet system evaluation are discussed in Section 1.2.4. The basic simulation assumptions summarized in Table 3.16.

Table 3.16 LTE+mmWave HetNet evaluation assumptions

Parameters		**Assumption**	
		LTE (Macro)	mmWave
Deployment		Heterogeneous hexagonal deployment 21 cells (Cell size = 500m)	
Number of small cells per macro cell area		1, 3	
Number of UE per macro cell area		50, 150. Clustered UE dropping	
Number of subcarriers		1024 (for user data transmission: 600)	
mmWave blockage probability		0.03	
BW		10 MHz	2 GHz, reuse-3
Channel model		IMT Uma	Q-D open area (D5.1)
BS antenna element	Element gain	17dB	5 dBi
	Horizontal beamwidth	70°	80°
	Vertical beamwidth	10°	80°
	Front2Back	25dB	25 dB
BS antenna array	Configuration	2 elements	8x16 full adaptive arrays
	TX power	46 dBm	19 dBm
UE antenna element		0 dBi, omni-directional	
Transmission scheme		DL MU-MIMO	
Feedback	Type	SVD-based	

(beamforming and SINR)	Periodicity	10 ms	
	Resource block granularity	5 PRB	25 x 80MHz subbands
Link adaptation	Outer loop target FER	10 %	
Scheduling	Type	Proportional-fair MU greedy scheduling	
	Traffic load	Full buffer	
mmWave association criterion		SNR threshold (9dB)	

3.1.5.1 User Association procedure

Static user association were implemented for HetNet mmWave evaluation. The UEs are assigned to LTE BS or one of mmWave APs once per trial, for all simulation duration. Such approach allows only RSSI (SNR) based association, since the interference level and corresponding SINR value varies per frame.

Taking into account margin for the interference level, the threshold value for the UE to mmWave AP association was selected equal to 9 dB. UEs with less SNR are assigned to the LTE BS.

Additionally, the chance of full mmWave blockage is introduced in simulations, with blockage probability equal to 3%. UEs in blockage automatically assigned to the LTE BS.

3.1.5.2 Simulation results

Two cases of the hotspots (small cells) deployments considered in this section: single mmWave small cell (3 APs) per LTE sector (see Figure 3.15) and three mmWave small cells (3 APs at each) per LTE sector (see Figure 3.16). In these figures, red circle is the macro BS, green circle denotes smallcell BS and pink dots are UEs. Corresponding system level performance metrics are summarized in

Table 3.17 and 3.18 respectively.

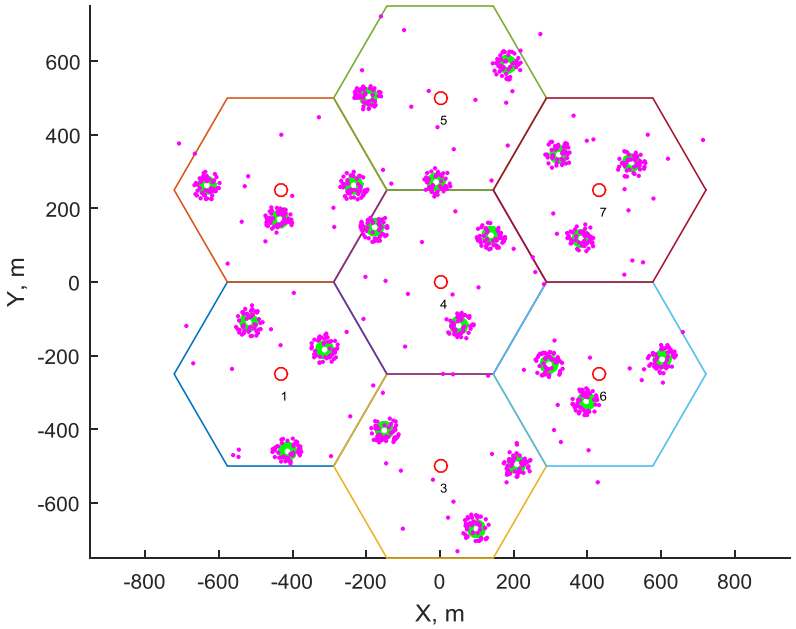

Figure 3.15 Deployment with single mmWave Small cell per LTE sector

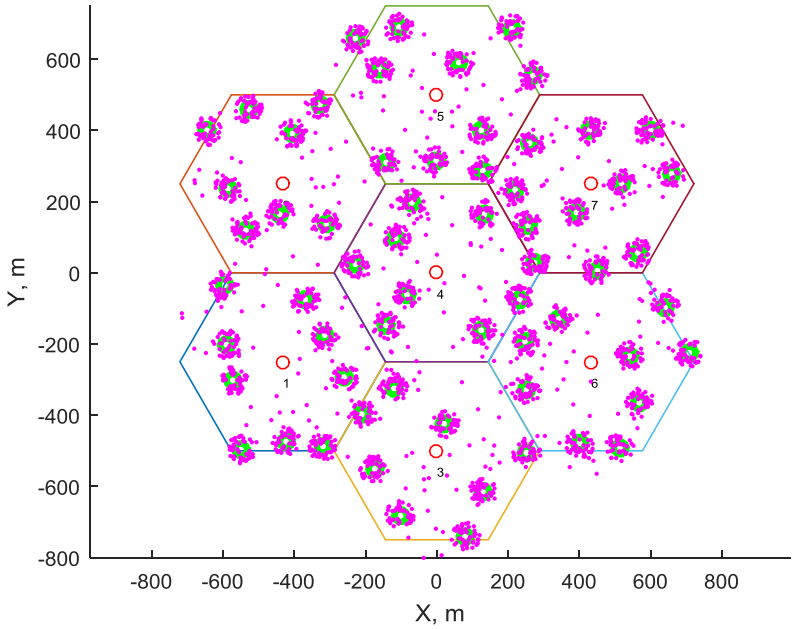

Figure 3.16 Deployment with 3 small cells per LTE sector

Table 3.17 Single mmWave Small cell per LTE sector results

	% of assigned users	Avg UE throughput, Mbps	Avg BS throughput, Mbps	Avg number of UEs in MU group
LTE	10.3	3.9	20.28	1.07

mmWave AP	89.7	714.1	10567	4.34
LTE+mmWave macrocell area	100	641.0	31721	-

Table 3.18 Three mmWave Small cell per LTE sector results

	% of assigned users	**Avg UE throughput, Mbps**	**Avg BS throughput, Mbps**	**Avg number of UEs in MU group**
LTE	7.2	1.85	20.01	1.11
mmWave AP	92.8	606.8	9433	4.29
LTE+mmWave macrocell area	100	563.2	84917	-

Simulation results shown in

Table 3.17 illustrate the drastic macrocell area throughput increase (more than 1000 times). This impressive increase caused by the fact that due to clustered UE deployment, about 90% of UEs deployed in a hotspot zones close to the mmWave APs and served by them in the mmWave band.

Figure 3.17 shows the macrocell throughput CDF for the case of one mmWave small cell per LTE sector. Two regions on the UE throughput CDF curve clearly illustrate the percentage of LTE-associated users (lower part of the curve, 10.3%) and mmWave AP-associated users (89.7%).

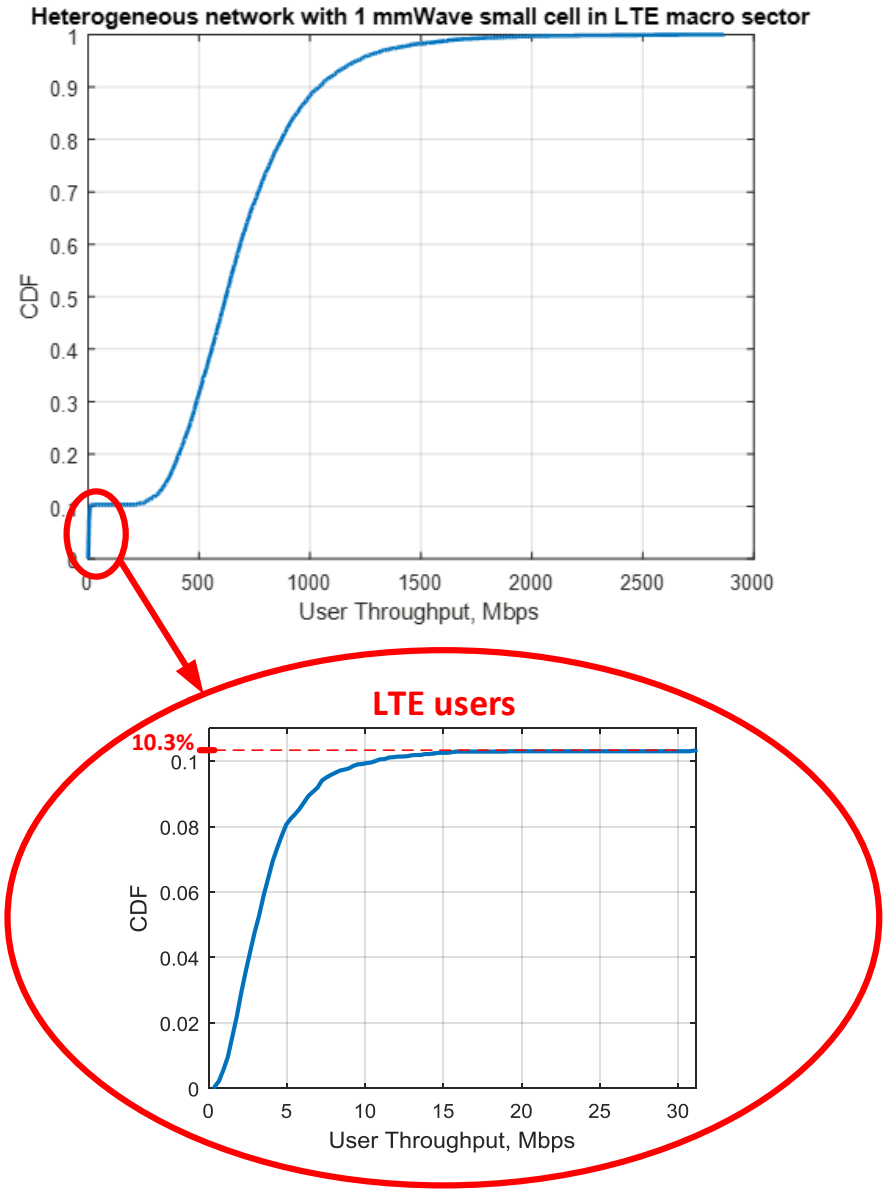

Figure 3.17 Throughput CDF for HetNet with 1 mmWave AP per LTE sector

In the second investigated HetNet scenario (Table 3.18 Three mmWave Small cell per LTE sector results), three hotspot zones were deployed per LTE sector (Figure 3.16 Deployment with 3 small cells per LTE sector). It can be seen that with the increasing of the mmWave coverage, the percentage of users associated with LTE is decreased and mmWave throughput per AP degraded only a little, due to mutual interference between mmWave APs. In this case, with three hotspots, the total LTE+mmWave macro cell throughput increase is even more spectacular: about 4000 times.

Such impressive performance increase caused by three main factors of mmWave systems: the channel bandwidth increase (x200, from 10MHz to 2GHz), efficient MU-MIMO implementation in the mmWave band based on large-aperture antenna arrays (4-5 times spatial multiplexing gain) and network densification: placement of

the hotspots in the macro cell area (9 times performance gain for 3 small cells with 9 APs in total).

It should be noted, that considered macro deployment (ISD=500m) allows placement of 8-9 mmWave small cells (cell radius = 50m), covering the whole macro cell area with dense deployment, considered in Section 2.2.1. In this case, employing effective CoMP techniques (see Section 3.1.3) network densification gain may reach 20-25 times.

3.2 Non-full buffer scenario

3.2.1 Context based user association optimization problem

In order to utilize the mm-wave resources efficiently, user association method should be optimized for the mm-wave overlaid heterogeneous network. In this section we will introduce a novel user association method which considers achievable throughput and traffic demand of each user simultaneously. To evaluate the system performance, system rate is introduced which expresses the total throughput of the system. The system rate is defined as follows

$$R = \sum_{u \in \mathrm{M}} \min\left(\frac{W_{\mathrm{M}} C_{u,\mathrm{M}}}{|\mathrm{M}|}, L_u \right) + \sum_{s=1}^{N_{\mathrm{S}}} \sum_{u \in \mathrm{S}_s} \min\left(\frac{W_s C_{u,s}}{|\mathrm{S}_s|}, L_u \right) \tag{3-1}$$

where W_{M} and W_s are the available bandwidth for macro and smallcell respectively. $C_{u,\mathrm{M}}$ and $C_{u,s}$ are link capacity from macro and *s*-th smallcell. $|\mathrm{M}|$ and $|\mathrm{S}_s|$ represent the number of users belong to macro BS and *s*-th smallcell BS respectively. N_{S} is the total number of smallcell BSs deployed within one macrocell area. L_u is traffic demand of user *u*. This system rate definition expresses the balance between achievable rate and traffic demand. If the achievable rate is much higher than the traffic demand, the user rate equals to the traffic demand and vice versa.

3.2.2 User association algorithm

Optimal BS of each user can be found by solving this optimization problem.

$$\left(\mathrm{M}^*, \mathrm{S}_1^*, \ldots, \mathrm{S}_{N_{\mathrm{S}}}^*\right) = \arg \max_{\mathrm{M}, \mathrm{S}_1, \ldots, \mathrm{S}_{N_{\mathrm{S}}}} R \tag{3-2}$$

$$\text{subject to} \begin{cases} \mathrm{M} \cap \mathrm{S}_s = \phi \\ \mathrm{S}_i \cap \mathrm{S}_j = \phi \text{ for } \forall i \neq j \end{cases} \tag{3-3}$$

The constraint explains that each user can connect only one BS from either macro or smallcell BSs. This optimization problem can be solved by the following 3 steps.

1. BS index allocation
2. Problem partitioning
3. Solving combinatorial optimization problem

3.2.2.1 BS index allocation

First of all, all user are allocated smallcell BS index of connection candidate. BS index allocation is done based on the link capacity.

$$s_u^* = \arg\max_s C_{u,s} \tag{3-4}$$

By this index allocation, macrocell area is divided like a Voronoi diagram as shown in Figure 3.18.

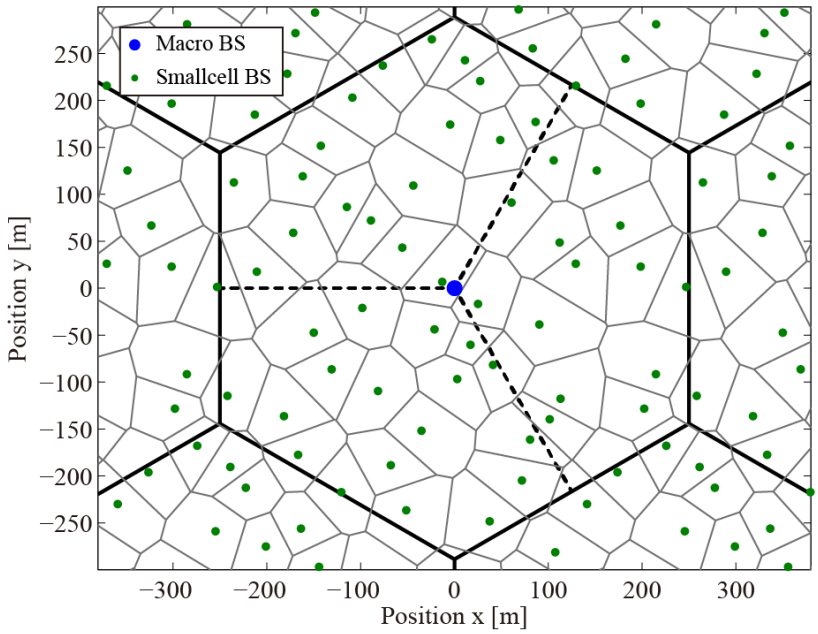

Figure 3.18 Divided macrocell area

3.2.2.2 Problem partitioning

In this section, Optimization problem is partitioned based on the previous macrocell partitioning.

$$\begin{aligned} R &= \sum_{u\in \mathrm{M}} \min\left(\frac{W_{\mathrm{M}} C_{u,\mathrm{M}}}{|\mathrm{M}|}, L_u\right) + \sum_{s=1}^{N_{\mathrm{S}}} \sum_{u\in \mathrm{S}_s} \min\left(\frac{W_s C_{u,s}}{|\mathrm{S}_s|}, L_u\right) \\ &= \sum_{s=1}^{N_{\mathrm{S}}} \sum_{u\in \mathrm{M}_s} \min\left(\frac{W_{\mathrm{M}} |\mathrm{M}_s|}{|\mathrm{M}|} \frac{C_{u,\mathrm{M}}}{|\mathrm{M}_s|}, L_u\right) + \sum_{s=1}^{N_{\mathrm{S}}} \sum_{u\in \mathrm{S}_s} \min\left(\frac{W_s C_{u,s}}{|\mathrm{S}_s|}, L_u\right) \\ &= \sum_{s=1}^{N_{\mathrm{S}}} \left[\sum_{u\in \mathrm{M}_s} \min\left(\frac{\alpha_s W_{\mathrm{M}} C_{u,\mathrm{M}}}{|\mathrm{M}_s|}, L_u\right) + \sum_{u\in \mathrm{S}_s} \min\left(\frac{W_s C_{u,s}}{|\mathrm{S}_s|}, L_u\right) \right] \\ &= R_s \end{aligned} \tag{3-5}$$

where $|\mathrm{M}_s|$ is the number of users within *s*-th partitioned macrocell area. $\alpha_s = \frac{|\mathrm{M}_s|}{|\mathrm{M}|}$ is the spectrum splitting ratio for each smallcells. According to this problem partitioning, the optimization problem is rewritten as follows,

$$\left(\mathrm{M}_s^*, \mathrm{S}_s^*\right) = \arg\max_{\mathrm{M}_s, \mathrm{S}_s} R \tag{3-6}$$

$$\text{subject to } \mathrm{M}_s \cap \mathrm{S}_s = \phi \tag{3-7}$$

3.2.2.3 Solving combinatorial optimization problem

Finally, optimal cell association can be achieved by solving a combinatorial optimization problem. The optimization problem can be transformed to a combinatorial optimization problem by introducing an association binary index $x_u = \{0,1\}$. If user *u* connects to macro BS, $x_u = 1$, and if user *u* connects smallcell BS, $x_u = 0$. In order to solve this problem, firstly the number of macro users is fixed as,

$$|\mathrm{M}_s| = k = \sum_{u=1}^{\mathrm{U}} x_u \tag{3-8}$$

where U is a total number of users within partitioned macrocell area.

According to this condition, the optimization problem can be transformed as follows,

$$\begin{aligned} R_s &= \sum_{u\in \mathrm{M}_s} \min\left(\frac{\alpha_s W_{\mathrm{M}} C_{u,\mathrm{M}}}{|\mathrm{M}_s|}, L_u\right) + \sum_{u\in \mathrm{S}_s} \min\left(\frac{W_s C_{u,s}}{|\mathrm{S}_s|}, L_u\right) \\ &= \sum_{u=1}^{\mathrm{U}} \min\left(\frac{\alpha_s W_{\mathrm{M}} C_{u,\mathrm{M}}}{k}, L_u\right) x_u + \sum_{u=1}^{\mathrm{U}} \min\left(\frac{W_s C_{u,s}}{\mathrm{U}-k}, L_u\right)(1-x_u) \\ &= \left[\sum_{u=1}^{\mathrm{U}} \min\left(\frac{\alpha_s W_{\mathrm{M}} C_{u,\mathrm{M}}}{k}, L_u\right) - \sum_{u=1}^{\mathrm{U}} \min\left(\frac{W_s C_{u,s}}{\mathrm{U}-k}, L_u\right)\right] x_u + \sum_{u=1}^{\mathrm{U}} \min\left(\frac{W_s C_{u,s}}{\mathrm{U}-k}, L_u\right) \\ &= \mathbf{f}_k^T \mathbf{x}_k + C_k \end{aligned} \tag{3-9}$$

where $\mathbf{f}_k$ and $\mathbf{x}_k$ are U dimensional function value vector and user index vector. C_k is not related to the association index value. Since the number of macro users is fixed as *k*, there is an implicit constraint.

$$\mathbf{1}_k^T \mathbf{x}_k = k \tag{3-10}$$

where $\mathbf{1}_k$ is a vector that all elements are 1. According to this transformation, the optimization problem becomes as follows,

$$\underset{\mathbf{x}_k}{\text{maximize}}\ \mathbf{f}_k^T \mathbf{x}_k \tag{3-11}$$

$$\text{subject to}\ \mathbf{1}_k^T \mathbf{x}_k = k \tag{3-12}$$

This problem can be solved by sorting algorithm. $\mathbf{f}_k$ is sorted with descending order and $\mathbf{x}_k$ is also sorted with the same order. Then optimal user combination can be obtained by extracting the top of k users from sorted vector $\mathbf{x}_k$. This solution is for the case of $|\mathrm{M}_s| = k$ therefore k should be optimized as follows.

$$\begin{aligned} k^* &= \arg\max_k \mathbf{f}_k^T \mathbf{x}_k + C_k \\ k &\in \{0,1,\ldots,\mathrm{U}\} \end{aligned} \tag{3-13}$$

3.2.3 Simulation results

Fundamental simulation parameters are revised in Table 3.19.

Table 3.19 Simulation parameters

Parameter	Value
Cell Layout	Random drop
Number of smallcell BSs	15 (each BS has 3 sectors)
BS Tx Power [dBm]	19
Average traffic value	62Mbps/user

The simulation results are summarized in Figure 3.19 and Table 3.20.

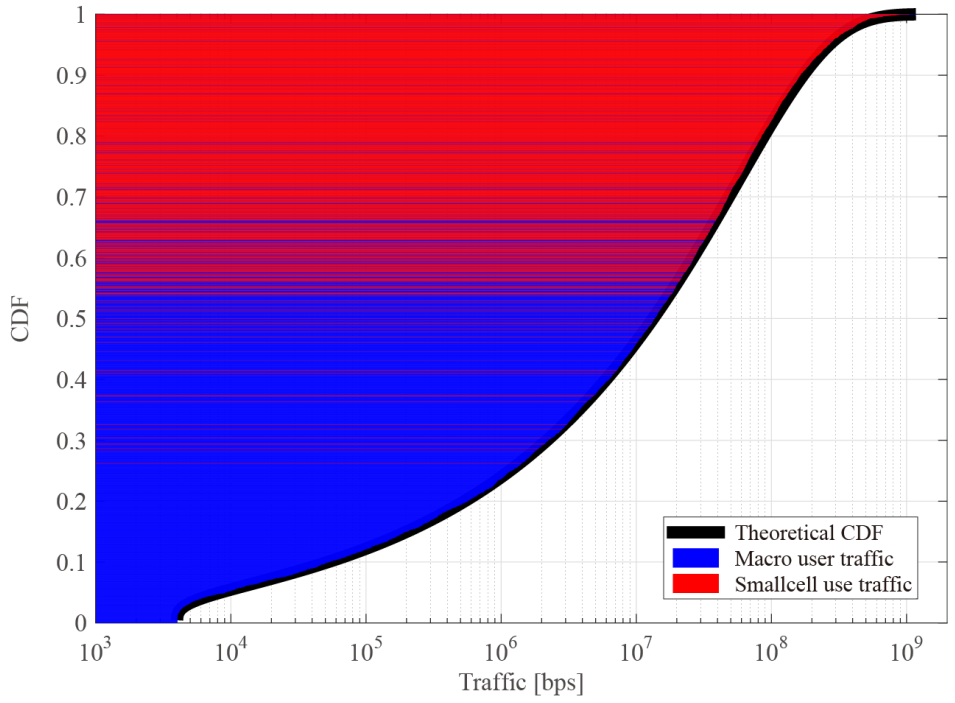

Figure 3.19 Association status

Figure 3.19 shows the association status of all users. Obviously, high traffic users are preferentially accommodated into smallcell BSs thanks to the proposed user association method.

Table 3.20 Simulation Results

	HomoNet	HetNet
System rate	123.53 Mbps	195.40 Gbps
Average user rate	22.26 kbps	35.21 Mbps
Macro cell throughput	122.13 Mbps	108.88 Mbps
Smallcell throughput		627.39 Mbps

In this realistic non-full-buffer simulation, we can obtain over 1000 times gain by installing mm-wave small cell BSs. Since macro BS accommodates the low traffic users, macro cell throughput becomes lower than that of HomoNet case.

4 Long term resource management

4.1 Dynamic cell search & beam training protocol

This section describes and evaluates the dynamic cell/beam search protocol. In this recursive protocol, the estimated location of the UE is used to assign cell/beams to search for the UE and the search result is used to dynamically update the location estimation. This enables the C-RAN to obtain an accurate traffic map that can be used to apply further network optimization algorithms.

4.1.1 Location-based cell/beam discovery/selection protocol

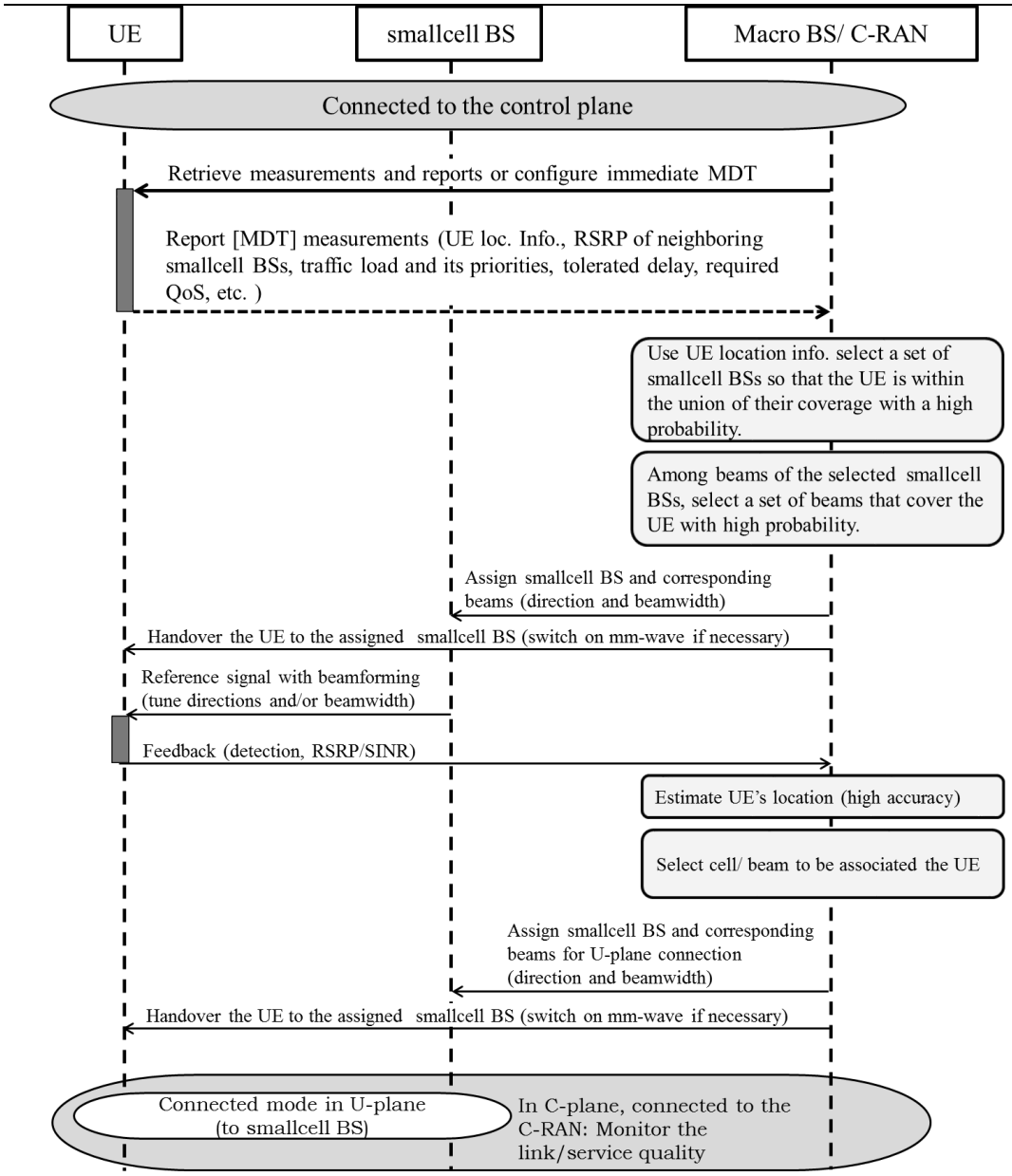

Figure 4.1 Functional structure of the protocol in the case when the UE is discovered by at least one of the selected cell/beams

The function of the protocol is shown in Figure 4.1. Initially, the UE is connected to the macro BS in the C-plane and its location is estimated by the macro BS. The macro BS/C-RAN selects and sends commands to several smallcell BSs to activate particular beams and transmit synchronization signals. The set of smallcell BSs and their corresponding beams are selected based on the probability of reaching/discovering the UE, *Pr*. The cell/beam selection is divided into two successive processes. At first, a few smallcell BSs are selected for each UE according to the probability of discovering that UE. Then, among beams of the selected smallcell BSs, a set of beams are selected that will cover the UE with high probability. Figure 4.2 summarizes this process. For multi-user scenario, the

selection and search is performed iteratively and the result of beam search for a UE is also used in subsequent iteration(s) for other UE(s).

As Figure 4.1 shows, when the UE detects a reference signal of at least one smallcell BS, it sends a C-plane feedback to the macro BS. C-RAN updates its estimation of the UE's location and decides on assigning one of the smallcell BS/beams that reached the UE. On the other hand, if the UE does not send any detection feedback to the macro BS, the C-RAN assumes that none of the selected beams covered the UE. According to this information, the estimation of the UE's location is updated and the C-RAN selects other smallcell BSs/beams to search for the UE.

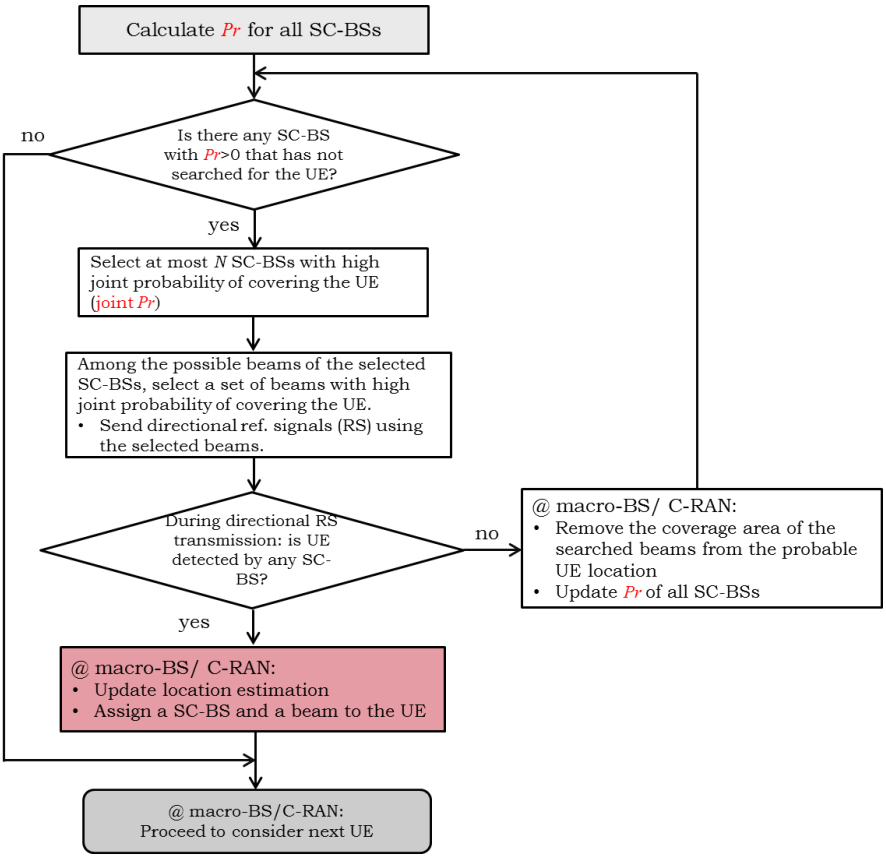

Figure 4.2 The flowchart of location-based cell/beam discovery/selection according to the probability of discovery (Pr)

4.1.2 Performance evaluation

The step-by-step function of the protocol is described in detail in D4.4 [16]. Here the performance metrics of the protocol are evaluated. A HetNet is considered that consists of a macro cell BS and arbitrary number of mm-wave smallcell BSs in random places within the macro cell area as shown in Figure 4.3. The number of smallcell BSs can vary from only one to at most 61 smallcell BSs with inter cell distance of 100 meters. It is assumed that the UE is equipped only with omnidirectional antenna, while smallcell BSs transmit with directional antennas. Initially, the macro BS estimates the location of the UE. In the numerical evaluations, it is assumed that the standard deviation of the initial estimation's error is 200 meters which is twice of the minimum inter-site distance between smallcell BSs.

A multi-user scenario is considered in which three UEs are uniformly distributed in the macro cell area. The protocol uses the results of the search for one UE, to update the location estimation of the next UE. Whether the next UE is discovered or not during the search for current UE, its location is estimated according to the coverage of the beams that participated in current search. Therefore, the average number of required beams for the second and the third UEs are reduced dramatically.

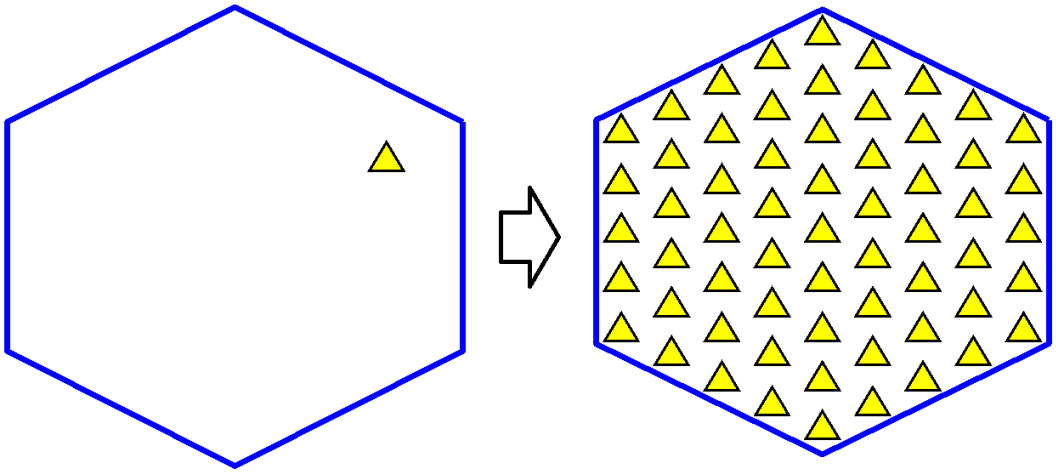

Figure 4.3 Network scenario from the lowest smallcell BS density, to the highest density: a number of smallcell BSs with the minimum inter-site distance of d are randomly distributed within the macro cell area.

Figure 4.4 shows the average number of smallcell BSs activated to search for the UEs. In the average five smallcell BSs are to be activated and search for the UE before it is found. However, for the second and third UEs, additional five or ten smallcell BSs are not required and these UEs are discovered faster with fewer smallcell BSs by using the information collected during the search for the first UE. It should be noted that fewer available smallcell BSs in the network naturally leads to fewer activated smallcell BSs for search, however obviously the probability of discovering a smallcell BS/beam for a UE will be lower. Figure 4.4 is obtained for 200 meters standard deviation error in UEs' initial location estimations. Also the transmit power of smallcell BSs is set to 19dBm which is the value obtained from the equipment developed in MiWEBA. Different transmission powers and/or location estimation errors ends in different results.

Another performance metric is the total number of beams of all smallcell BSs activated to discover the UE, which is shown in Figure 4.5. It can be seen that for two/three UEs the total number of activated beams is less than twice/triple of the number for discovering one UE. The same discussion as for the number of activated smallcell BSs is valid for the total number of activated beams. Also considering both Figure 4.4 and Figure 4.5 together gives an estimate of the number of activated beams per activated smallcell BS.

Table 4.1 Parameters for the evaluation of the location-based cell/beam discovery protocol

Minimum inter-site distance between smallcell BSs (d)	100 meters
Distribution of the UEs in the macro cell area	Uniform
Error of the macro BS's estimate of the UEs' locations, ε	$\varepsilon=(\varepsilon_x, \varepsilon_y)$ $\varepsilon_x, \varepsilon_y \sim N(0,\sigma^2)$

	$\sigma^2=2d^2$
Smallcell BS Transmit power	19dBm
Threshold received power (Detection threshold of the UE)	-75dBm
Smallcell BSs' antenna height	5m
UE antenna height	1.5
Smallcell BS mm-wave antenna pattern [3]	36 beams per smallcell BS with the following beam pattern: $G(\varphi,\theta)=10\log\left(\frac{16\pi}{6.76\theta_{3\text{dB}}\varphi_{3\text{dB}}}\right)$ $-12\left(\frac{\varphi-\varphi_0}{\varphi_{3\text{dB}}}\right)^2-12\left(\frac{\theta-\theta_0}{\theta_{3\text{dB}}}\right)^2$ $\theta_{3\text{dB}}=10^\circ$ $\varphi_{3\text{dB}}=10^\circ$ Tilt angle, θ_0=5° Azimuth angle, φ_0: adjustable
Path loss [dB]	$PL_{dB}=\alpha+10n\log_{10}(d/d_0)$ $d_0=5\text{m}, \alpha=82.02, n=\begin{cases}2.36 & d>d_0\\ 2 & d\le d_0\end{cases}$

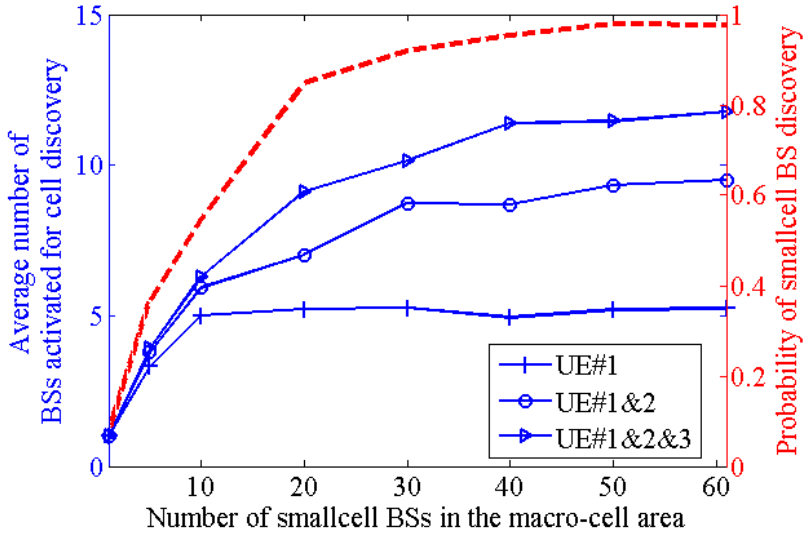

Figure 4.4 Average number of smallcell BSs activated for cell/beam discovery (blue lines) beside the probability of discovering at least one smallcell BS/beam for a UE in the macro cell area (red line)

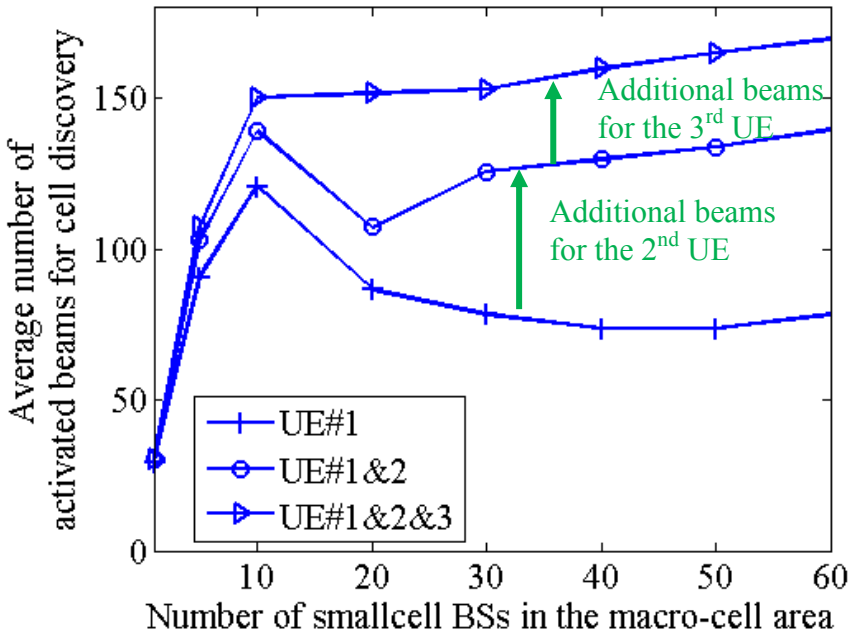

Figure 4.5 Average number of beams from all smallcell BSs activated to detect a UE

To summarize, in the location-based cell/beam discovery protocol, the C-RAN involves estimated location of the UE in cell discovery process, and concurrently updates the estimated location. Also, the recent history of the search is used to accelerate the search and discovery. Finally, the protocol enables the C-RAN to obtain an accurate traffic map that can be used to apply further network optimization algorithms, such as dynamic smallcell ON/OFF and dynamic cell structuring for CoMP joint transmission, to build novel self-organizing networks (SONs).

4.2 Dynamic smallcell BS ON/OFF for energy efficiency

4.2.1 Energy efficient mm-wave smallcell activation and beam control for delay-constrained services

In this section we present and evaluate an optimal controller that 1) adapts the activity (on/off) of an mm-wave BS to the variation of downlink traffic load and 2) selects the best momentary beam to serve the scheduled UEs, according to the load, latency constraints, and available capacity.

This algorithm assumes that the cell association problem has been previously solved (for instance by using the methodology proposed in Section 4.1)

The main challenge is to efficiently characterize the time-spatial variations of the system parameters at each beam, which needs to model the system through a large number of states. To achieve this goal, we assume the presence in the network of a local buffer that stores traffic and dynamically forwards it according to the controller decision (see Figure 4.6). To take advantage of such architecture, it is necessary to maximize the data transmitted each time an mm-wave BS is active, i.e. lowering its queue status as much as possible.

At a given time slot, several beams may serve the same active UE; however, larger the mismatch between the beam direction and the user location, lower the user

experienced SINR. Depending the QoS constraints and reported channel measurements, the controller can decide either to share the available capacity amongst multiple neighbouring users, or serving fewer UEs, which will experience higher throughput.

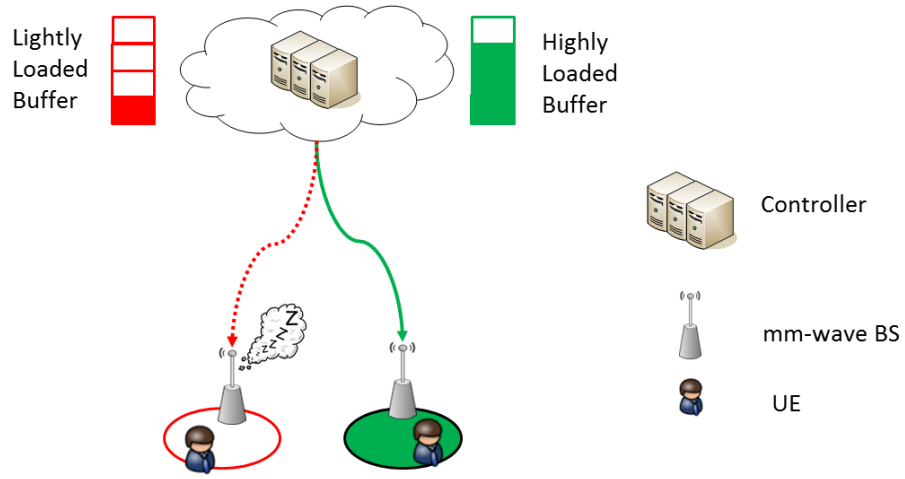

Figure 4.6 The proposed system model.

4.2.1.1 System model and problem statement

At the timeslot *t*, we assume that the controller implements an action $a_t \in A = \{0,1,\ldots, N\}$, where $a_t=0$ corresponds to keep the BS in sleep mode and $a_t=i$, indicates that the *i*th beam is activate for data transmission. Accordingly, the buffer status S_t is updated

$$S_t = min\{S_{t-1} - B_i, 0\} + D_t, \tag{4-1}$$

where B_i [bits] is amount of data that can be transmitted by activating the *i*th beam and D_t represents the new incoming data. Therefore, the controller perceives a cost C_t associated to the selected action, which can be measured as follows

$$C_t = P_t + \beta \cdot D_t, \tag{4-2}$$

where P_t is the mm-wave BS power consumption, D_t the data lost due to unsatisfied latency constraints, and β is a coefficient $\left[\frac{W}{bits}\right]$ that trades off power consumption and QoS.

By following the classic methodology proposed in the literature, we use a linear power model with slope Δ to characterize the instantaneous power consumption at the mm-wave BSs (see D4.4)

$$P_t = \begin{cases} P_0 + \Delta \cdot P_{TX}, & 0 < P_{TX} \leq P_{max} \\ P_s, & P_{TX} = 0 \end{cases}, \tag{4-3}$$

where P_0 is the static component of the power consumption when the BS is active, P_{TX} is the RF emitted power, P_{max} is the RF power at full load, and P_s is the power consumption at sleep mode.

Finally, since we aim to minimize the energy consumption and avoid packet loss due to the cell switch on/off mechanisms, the activation and beam control optimisation problem of mm-wave smallcell BS can be stated as follows

$$\min_{A} \sum_{t} P_t$$
$$\text{s.t.} \quad \sum_t D_t = 0 \tag{4-4}$$

4.2.1.2 Fuzzy Q-learning based optimization protocol

Design of the optimal controller that optimizes the objective function defined in Section 4.2.1.1 is hard task due to the large size of the network state set and the combinatorial nature of the problem. Accordingly, to solve the problem with a limited complexity, we separate the mm-wave BS activation problem and the selection of the transmission beam.

First, we define a latency threshold that indicates whether an urgent transmission has to occur soon. We set the latency threshold equals to the time required by the maximum number of HARQ retransmissions (N_{RETX})

$$T_{RETX} = N_{RETX} \cdot T_{Fdbk} \tag{4-5}$$

Where T_{Fdbk} is the delay for receiving the ACK/NACK feedback after the UE attempts the packet decoding.

Let denote B as the set of beam that can be activated at a given BS; in the proposed protocol, when the latency or threshold is passed, the controller identifies the subset of beam $\bar{B} \subseteq B$ that can serve the urgent traffic; then it select the beam ($\bar{b}^*$) that maximizes the cell data rate according to

$$\bar{b}^* = \underset{\bar{B}}{\text{argmax}}\big(\min(R_b, L_b)\big) \tag{4-6}$$

Where R_b is the capacity (in bits) associated with the beam b and L_b is the associated load (in bits).

In the case where the latency threshold is not passed, the selected beam b^* simply corresponds to

$$b^* = \underset{B}{\text{argmax}}\big(\min(R_b, L_b)\big) \tag{4-7}$$

After, the beam selection, the controller uses fuzzy logic to represent the beam state and then fuzzy q-learning (FQL) to decide whether the selected beam has to be activated or not. Let S be a finite set referred to as the beam state set and defined as $S = L \times R \times T$, where L, R, and T respectively describe the size (in bits) of the queue that can be served by the selected beam, the beam capacity, and the how urgent is the associated traffic (i.e., the time to live of the oldest packet present in the queue).

The goal is to find an optimal policy, i.e. a state-action mapping that minimizes the expected cumulative cost of the agent when visiting the state space S. However, in general, it is difficult to define appropriate state and action spaces for Reinforcement Learning problems. The discretization of the state space has to be rather fine to cover all possibly relevant situations and there can also be a wide variety of actions to choose from. As a consequence, there exists a combinatorial explosion problem when trying to explore all possible actions from all possible states.

To solve dimensionality problems, the fuzzy inference system (FIS) is a suitable candidate. In fact, it aims to perform as a control system considering that, many times, real problems cannot be efficiently expressed through mathematical models. In fuzzy logic, unlike standard conditional logic, the truth of any statement is a matter of degree. In other words, differently from classic binary logic, the statement "x is a member of X" is not necessary true of false and the degree to which any fuzzy statement is true is denoted by a value between 0 and 1.

In our model, the beam state vector *S* is represented by fuzzy state set $\bar{S} = \{\bar{s}_1,\dots,\bar{s}_n\}$ composed by $L = 3$ linguistic variables; accordingly, we can the fuzzy inference rules as follows:

IF input state vector $\boldsymbol{s}$ is $\bar{s}_i$

Then action a_0 with $q(\bar{s}_i, a_0)$

or action a_1 with $q(\bar{s}_i, a_1)$,

where a_j belongs to the set of actions defined in Section 4.2.1.1 and $q(\bar{s}_i, a_j)$ is the fuzzy Q-value for the state-action pair $(\bar{s}_i, a_j)$. The FQL has two outputs: one corresponds to the inferred action and the other represents the Q-value for the state-action pair ($\boldsymbol{s}$, a):

$$a = \frac{\sum_i^n w_i \cdot a_i}{\sum_i^n w_i} \tag{4-8}$$

$$Q(\boldsymbol{s}, \mathrm{a}) = \frac{\sum_i^n w_i \cdot q(\bar{s}_i, a_i)}{\sum_i^n w_i}, \tag{4-9}$$

Where w_i represents the truth value (i.e., the output of fuzzy-AND operator) of the rule representation of FQL for $\bar{s}_i$, and a_i is the action selected for state $\bar{s}_i$. Q-values have to be updated after the action selection process according to $q(\bar{s}_i, a_i) = q(\bar{s}_i, a_i) + \alpha \cdot \Delta q(\bar{s}_i, a_i)$, where α is the learning rate, $\Delta q(\bar{s}_i, a_i) = (C(\boldsymbol{s}, \mathrm{a}) + \delta Q(\boldsymbol{y}, \mathrm{a}') - Q(\boldsymbol{s}, \mathrm{a})) \cdot \frac{w_i}{\sum_i^n w_i}$, $C(\boldsymbol{s}, \mathrm{a})$ represents the cost obtained applying action a in state vector $\boldsymbol{s}$, and $Q(\boldsymbol{y}, \mathrm{a}')$ is the next-state optimal Q-value defined as:

$$Q(\boldsymbol{y}, \mathrm{a}') = \frac{\sum_i^n w_i \cdot q(\bar{y}_i, a_i^*)}{\sum_i^n w_i}, \tag{4-10}$$

and $a_i^* = \underset{a_j^* \epsilon A}{argmin} q(\bar{y}_i, a_j^*)$ is the optimal action for the next state $\bar{y}_i$, after the execution of action a_i in the fuzzy state $\bar{s}_i$.

The proposed FQL algorithm consists of a four layer Fuzzy Inference System (FIS), where the first layer has as input the three linguistic variables defined by the term sets:

$T(t) =$
$\{Very\ Much\ Urgent, Very\ Urgent, Urgent, Almost\ urgent, Not\ Urgent\}$,

$T(l) =$
$\{Very\ Much\ Loaded, Higly\ Loaded, Loaded, MidLoaded, LightlyLoaded, UnLoaded\}$
, and

$T(r) =$
$\{Very\ Low\ Capacity, MidCapacity, HighCapacity, Very\ High\ capacity\}$.

In this layer, there are $z = |T(l)| + |T(t)| + |T(r)|$=16 output nodes, each one describing (via a trapezoidal membership function $\mu(x)$, to which degree the small cell state variables belong to the appropriate fuzzy sets (fuzzification process). Let denote as $O_{1,k}$ with $1 \leq k \leq z$ the output of this layer.

The second Layer is named as the rule nodes layer and is composed by $n = |T(l)| \cdot |T(t)| \cdot |T(r)|$=150 nodes. Each node gives as output the truth value of the i-th fuzzy rule $O_{2,i}$ with $1 \leq i \leq n$ which is the product of four membership values corresponding to the term set inputs.

The third layer is also composed of $n = 150$ nodes named as action-selection nodes. The selection of the per node action a is based on the ε-greedy action selection policy. Each node $1 \leq i \leq n$ generates two output values as follows:

$$O_{3,i}^{A} = \frac{O_{2,i} \cdot a_i}{\sum_i^n O_{2,i}}, \tag{4-11}$$

$$O_{3,i}^{Q} = \frac{O_{2,i} \cdot q(\bar{s}_i, a_i)}{\sum_i^n O_{2,i}} \tag{4-12}$$

The fourth layer is has two output nodes, action node O_4^A and Q-value node O_4^Q, which represent the results of the defuzzification process.

$$O_4^A = \sum_i^n O_{3,i}^A \tag{4-13}$$

$$O_4^Q = \sum_i^n O_{3,i}^Q \tag{4-14}$$

4.2.1.3 Control protocol

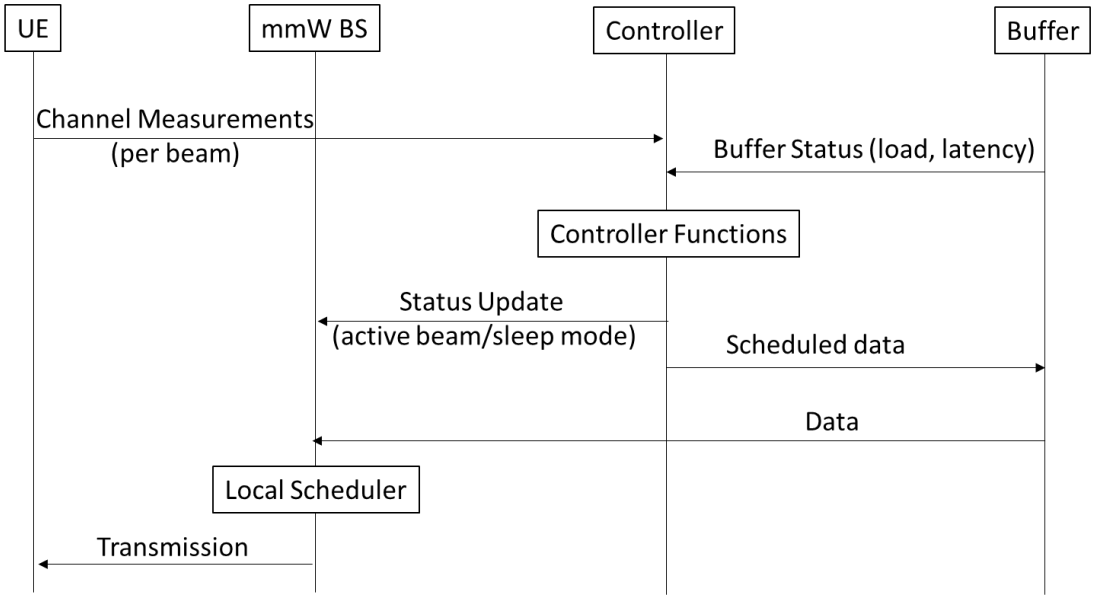

Figure 4.7 The signalling flow of the proposed energy efficient framework.

The signalling flow required by proposed energy efficient controller is depicted in Figure 4.7. It is important to stress that the controller and the data buffer can be deployed at the mm-wave BS level for a fast activation/deactivation management. On the contrary, a centralised architecture is feasible (for instance by locating the controller at the macro BS level or at BBU) to reduce costs and enable joint access/backhaul controller of a cluster of neighbouring mm-wave BSs.

The controller receives instantaneous channel measurements per beam and UE, which are used to estimate the average beam capacity. On the contrary, information on the buffer status, enables the controller to evaluate the beam load as well as which are the latency constraints per beam, i.e. which beam can be used to serve urgent traffic.

4.2.1.4 Performance evaluation

In this section we assess the proposed energy efficient solution to manage the mm-wave smallcell BSs Activation and Beam Control presented in 4.2.1.2 and 4.2.1.3. We compare the proposed solution with a simpler beam scheduling algorithm that, when a transmission is required, identifies the couple (beam, user) that maximizes the link spectral efficiency (i.e., SINR). This reference algorithm is evaluated both in case where energy saving functions are not implemented and in the case where the mm-wave smallcell BS is deactivated only when its queue is empty. As simulation environment, we consider a hotspot characterized by a dense user deployment, where deployment and traffic parameters are described in Section 1.1.1 and Section 2.3 respectively. Additionally, we consider the open area channel model described in D5.1 and the power model defined in D4.4. Results are averaged over 50 runs each one simulating 10 seconds of network activity.

The consumed energy per successful transmitted bit of the three compared mechanisms is shown in Figure 4.8. First we can note that average consumed energy

per received bit decreases with the user rate requirements. Additionally, results show that introducing an activation/deactivation scheme can lead up to 40% of energy saving. Furthermore, the proposed solution can result in an additional 18% of energy saving by exploiting the delay energy saving tradeoff.

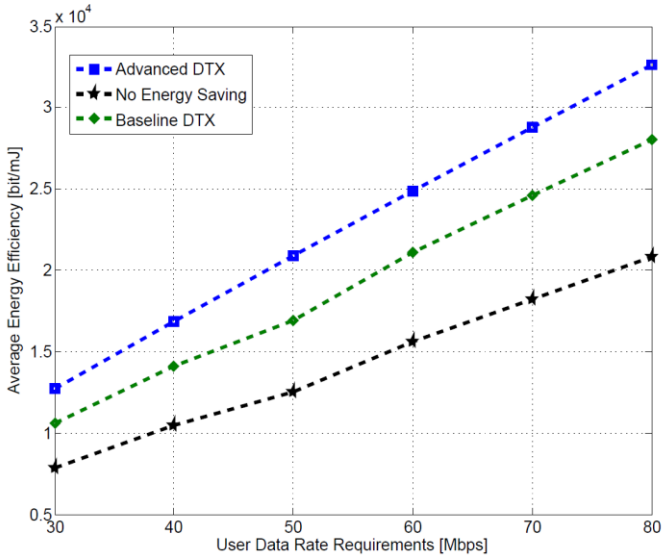

Figure 4.8 mm-wave smallcell BS Energy Efficiency vs Traffic rate requirements.

The effect of the energy-latency tradeoff is underlined in Figure 4.9. Although the baselined DTX scheme (as well as the baseline scheme without energy saving solution) does not affect the user perceived latency, the proposed solution introduces notable latency, always respecting the QoS constraints.

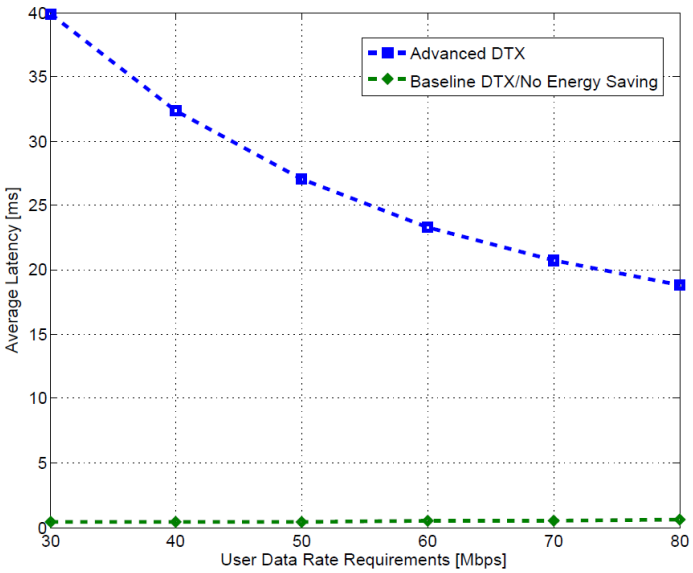

Figure 4.9 User Latency vs Traffic rate requirements.

4.2.2 On-demand smallcell BS ON/OFF to maximize system rate over consumed power

4.2.2.1 Dynamic traffic modeling

Modelling and simulation of a cellular network typically assumes that UEs are uniformly scattered in each cell. This implies a statistically uniform distribution of

traffic load over space, but in reality the spatial traffic distribution is highly non-uniform across different cells. In reality, traffic distribution over space shows considerable geographical disparity and varies hour by hour which is dependent upon users' daily activity. It is crucial to develop a dynamic traffic model based on that the network can dynamically adapt to the variation in a cost-effective way.

Service providers perform various measurements on the traffic requirements of UEs and the total traffic of different areas. In this paper, the measurement results provided by one of the biggest operators in Japan are employed to demonstrate such dynamic traffic distribution modelling. Two different sets of measurements were provided: traffic generated by a UE, and the total hourly traffic of an area measured at a metropolitan area of Tokyo in 2014.

Table 4.2 parameters of the packet length distribution

Shape parameter, k	0.2892
Scale parameter, θ	2.012×10^5
Traffic bias	4 kbps

User traffic measurements are used to model the statistics of the traffic demand of a UE in the actual environment. In that model, the packet generation of each UE is a Poisson process with 8 sec. average time interval between packets and the length of each packet follows the Gamma distribution plus a constant bias. The probability density function (PDF) of the Gamma distribution is defined as follows:

$$f(a) = a^{k-1}\frac{e^{-a/\theta}}{\Gamma(k)\theta^k} \tag{4-15}$$

here the parameters of the PDF of the packets' lengths are listed in Table 4.2.

The total hourly traffic L is measured in 100 meters x 100 meters areas. An example of the measured total traffic in one hour from 10:00 to 10:59 (T=10) is shown in Figure 4.10. A few high load areas are recognizable in the whole area. By interpolation on the hourly total traffic measurements, the total traffic distribution in at each time is estimated:

$$L((x,y),t) \text{ in kbps for: } t \in [0,23:59) \tag{4-16}$$

The number of UEs in each area (x,y) at the considered time instant, $N_{UE}((x,y),t)$, is estimated based on the instantaneous total traffic load, $L((x,y),t)$, and the statistics of the traffic load of each UE. The traffic load of each UE, can be considered to be static (equal to the average traffic load) or stochastic. Accordingly, the instantaneous number of UEs can be modelled either statically or dynamically.

Static modeling

In static modelling, the instantaneous number of UEs in an area is obtained by dividing the instantaneous total traffic load to the average traffic load of a UE, $\overline{L}_{UE}$:

$$N_{UE}((x,y),t) = \frac{L((x,y),t)}{\overline{L}_{UE}} \tag{4-17}$$

The average traffic of a UE, $\overline{L}_{UE}$, can be obtained either directly form measurements or according to the user traffic model.

Dynamic modeling

In dynamic modelling, a number of UEs are considered where each UE has a stochastic instantaneous traffic load and sum of the instantaneous traffic of all the UEs is almost equal to the instantaneous total traffic of the area. Therefore, in different simulation iterations, for different numbers of UEs are obtained. The flowchart that describes the implementation of the dynamic modelling is shown in Figure 4.11. Figure 4.12 shows the number of UEs in the 100 meters × 100 meters square area located at point (1100,600) for both dynamic and static models.

Static modelling results in a deterministic number of UEs at each area at each time of day. Quite the contrary, dynamic modelling provides a stochastic number of UEs at each area at each time.

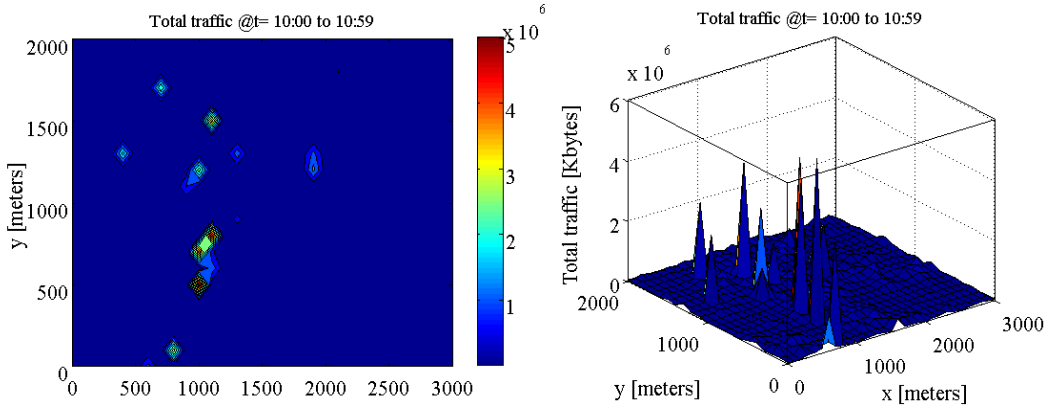

Figure 4.10 An example of the measured total traffic in one hour.

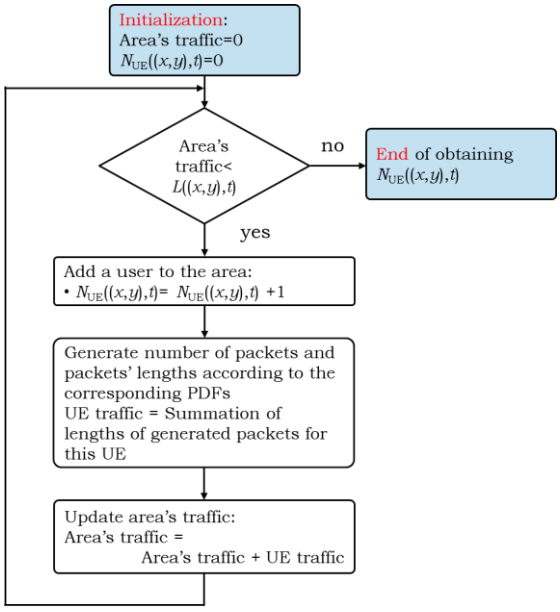

Figure 4.11 Flowchart of dynamic modelling of $N_{UE}((x,y),t)$ for a specific location and time.

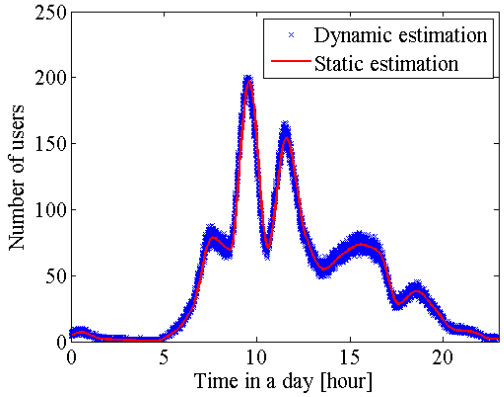

Figure 4.12 The number of UEs in the 100 meters × 100 meters square area at point (1100,600).

Traffic generated for numerical simulation

The practical dynamic traffic model based on measurement data at a busy crossroad of the Tokyo metropolitan city is employed to evaluate the effectiveness of the proposed algorithm in the next section. The generated traffic pattern throughout a whole day is depicted in Figure 4.13 where we can observe the traffic (represented by the number of UEs existing the evaluated environment) varies dynamically. Especially, during midnight and early morning, the traffic is low as expected. On the other hand, the traffic peak is at noon where many hotspots appear as seen in Fig. 4-9. In other words, the generated traffic can correctly predict the traffic trend of the considering metropolitan area.

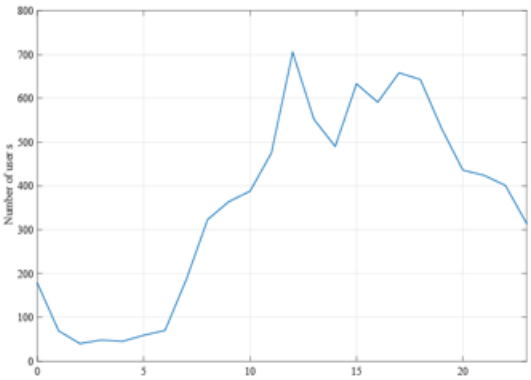

Figure 4.13 Traffic variation through a day.

4.2.2.2 Optimization problem

This section presents our on-demand cell activation algorithm, which is a joint optimization problem of cell association and smallcell BS ON/OFF status. The objective function is to improve the system rate over consumed energy of the system. As for BS deployment, general hexagonal structure with three sector macro cells is assumed as shown in Figure 4.14 where the macro BS is located at the center of hexagonal structure and smallcell BSs are overlaid on the macro cells randomly and operated in a different frequency band from macro BSs. In this work, two scenarios of respectively current 3.5GHz and mm-wave 60GHz bands are considered. It is noted that the cell association in this work is applied only for U-plane, while the C-

plane of all UEs are connected to the macro BS in advance. In order to maximize the system performance, the system rate over consumed energy r in bits/J which is defined as the ratio between the total system rate and the total system consumption power of all BSs is introduced as follows r :

$$\rho = \frac{\sum_{u\in\mathcal{M}} \min\left(\frac{W_{\mathrm{M}} C_{u,\mathrm{M}}}{|\mathcal{M}|}, L_u\right) + \sum_{s=1}^{n_{\mathrm{S}}} \sum_{u\in S_s} \min\left(\frac{W_{\mathrm{S}} C_{u,s}}{|S_s|}, L_u\right)}{P_{\mathrm{B}} + n_{\mathrm{S}} P_{\mathrm{S1}}} \tag{4-18}$$

where definition of variables can be referred to Sect. 3.2.2. $n_{\mathrm{S}} \pounds N_{\mathrm{S}}$ is the total number of activated smallcell BSs and N_{S} is the total number of smallcell BSs deployed within one macro cell area. L_u in bps is a traffic demand of user U. $P_{\mathrm{B}} = P_{\mathrm{M1}} + P_{\mathrm{M0}} + N_{\mathrm{S}} P_{\mathrm{S0}}$ is the network's baseline consumption power which is contributed from P_{M1} (macro BS's surplus consumption power when activated), P_{M0} (macro BS's power consumption when idle) and P_{S0} (smallcell BS's consumption power when idle). $P_{\mathrm{S}} = P_{\mathrm{S1}} + P_{\mathrm{S0}}$ is the consumption power of a small cell where P_{S1} is the surplus consumption power when the smallcell base station is activated [16].

On the offloading point of view, BS should accommodate appropriate UEs to improve system rate efficiently e.g. smallcell BS accommodates UE of high traffic demand. On the energy saving point of view, smallcell BSs should be switched off as many as possible at the expense of degrading the system rate. For a fixed number of activated BSs, the denominator of r becomes a constant. Therefore, the joint optimization problem can be decomposed into finding the optimal user association to maximize the total system rate for a fixed set of activated BSs and finding the optimal set of activated BSs to maximize the system rate over consumed energy. Detailed optimization process can be found in [16].

4.2.2.3 Performance evaluation

According to the previous sections, we evaluate the performance of the on-demand dynamic ON/OFF algorithm with respect to our measurement-based traffic model, using a practical power consumption model of base stations, both presented in [16]. Our evaluation metrics includes the power consumption ratio and the system rate over consumed energy.

Simulation scenarios and parameters

Macro BSs are deployed in the hexagonal grid and uses 2GHz band. On the other hand, smallcell BSs are deployed non-uniform randomly in the macro cell area which are apt to be near the hotspot areas of the day. Each smallcell BS has three sectors and employs the frequency reuse with reuse factor 3. Smallcell BS uses 3.5GHz band or 60GHz band. In 60GHz smallcell BS, the transmit antenna is assumed as the large antenna array constructed with multiple antenna array modules (WP5). Users are dropped into the evaluated network coverage randomly. User density and its time variation are according to D4.4. The average value of traffic demand of each user is assumed to be a 1000 times higher than that of the current traffic, which means 62

Mbps. The remaining simulation parameters can be found in Sect. 2.1 or summarized in Table 4.3.

Table 4.3 Simulation parameters.

Parameter	Value
Bandwidth (Macro / 3.5 GHz / 60 GHz)	10 MHz / 100 MHz / 2 GHz
Number of macro cells	7 (1 evaluate, 6 interference)
Number of macro sectors	3
Number of SC-BSs (per 1 macro cell)	15 (5 per macro sector)
Number of UEs (per 1 macro cell)	time varying
Number of BS antennas (Macro / 3.5 GHz / 60 GHz)	4 / 4 / 8
Number of UE antennas (Macro / 3.5 GHz / 60 GHz)	2 / 2 / 1
Macro ISD	500 m
BS antenna height (Macro / 3.5 GHz / 60 GHz)	25 m / 10 m / 4 m
UE antenna height	1.5 m
Tx power (Macro / 3.5 GHz / 60 GHz)	43dBm / 30dBm/ 19dBm
Additional consumption power of BS (Macro / 3.5 GHz / 60 GHz)	ON: 835W / 14W / 60W OFF: 19W / 2W / 2W
Pathloss model (Macro / 3.5 GHz / 60 GHz)	$128.1+37.6\log_{10}(d[\text{km}])[\text{dB}]$ / $140.7+36.7\log_{10}(d[\text{km}])[\text{dB}]$ / $PL(d)=\begin{cases}82.02+23.6\log_{10}\left(\frac{d}{d_{\text{ref}}}\right), & d \geq d_{\text{ref}}\\ 82.02+20\log_{10}\left(\frac{d}{d_{\text{ref}}}\right), & d < d_{\text{ref}}\end{cases}$
Channel model (Macro / 3.5 GHz / 60 GHz)	3GPP SCME urban macro scenario/ 3GPP SCME urban micro scenario/ Measurement-based Rician fading model
Noise power density	-174 dBm/Hz
Average traffic demand	62 Mbps

Power consumption models of 3.5GHz and 60GHz

In order to appropriately investigate the effectiveness of the proposed algorithm in 5G HetNet, this study introduces a practical base station power consumption model of each band based on GreenTouch and Earth project model, which is summarized in Table 4.3. The transition duration between ON and idle is assumed to be negligibly small and the power consumption is assumed to be a constant value regardless of the impinged traffic load.

Table 4.4 provides the power consumption ratio of HetNet over HomoNet for our simulation scenario of 15 smallcell BSs within a macro coverage, assuming that all BSs are ON. Seen from the result, the requirement for surplus power consumption of HetNet against conventional HomoNet is almost ignorable in contrary to the system rate gain 1000x of HetNet. In other words, HetNet is more energy-efficient in their nature. It should be emphasized that mm-wave HetNet seems to require more power than micro-wave HetNet. However, it is merely due to the value of additional consumption power of 60GHz BS when ON (60W) is based on our developed prototype and it must be reduced dramatically in commercial products.

Table 4.4 Power consumption ratio of HetNet over HomoNet (all ON case)

Frequency	Ratio
3.5GHz	1.25
60GHz	2.05

Simulation results

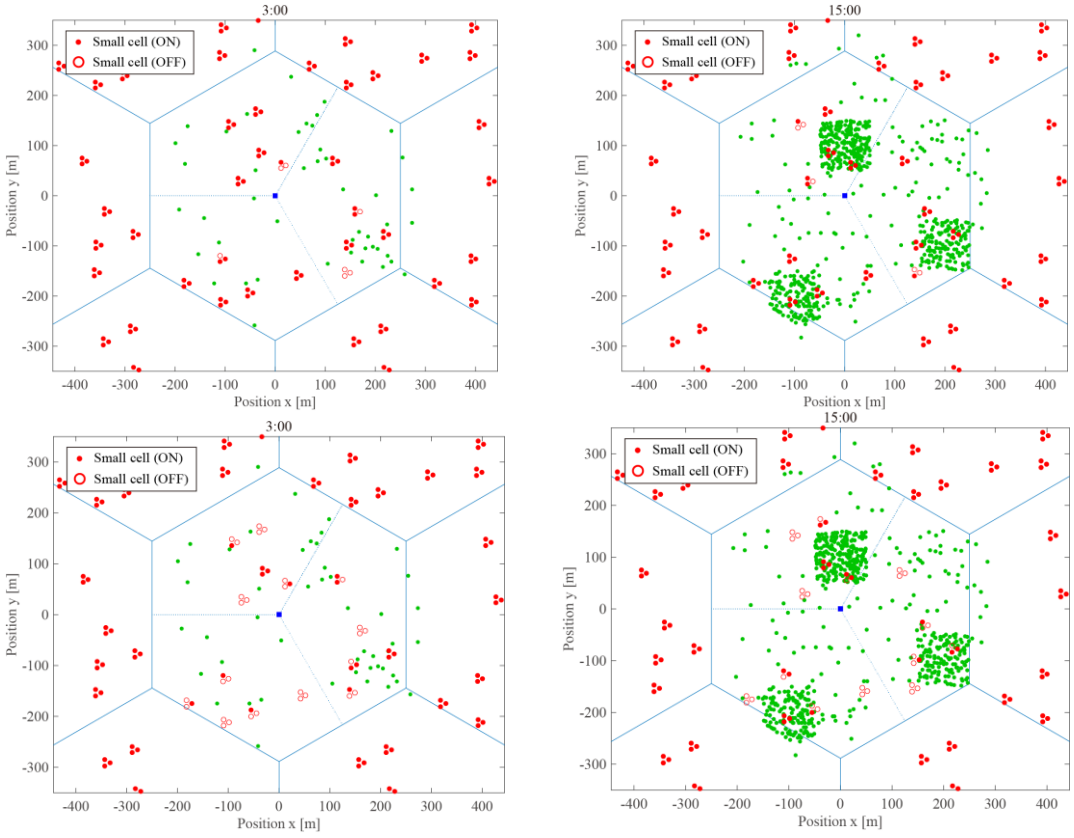

Figure 4.14 ON/OFF status (left: 3AM, right: 3PM, top: 3.5GHz, bottom: 60GHz).

The effectiveness of the on-demand ON/OFF algorithm can been observed in Fig. 4-9 which depicts the optimization results (BS ON/OFF status) of both 3.5GHz and 60GHz smallcells for two representative scenarios of low traffic load at 3AM and peak hour at 3PM. As seen in the evaluated macro cell area of the figure, more BSs are deactivated at 3AM rather than that at 3PM, obviously for the case of 60GHz smallcells. The deactivation effect is not remarkable for 3.5GHz HetNet due to this system's limited capacity against future 1000x traffic demand.

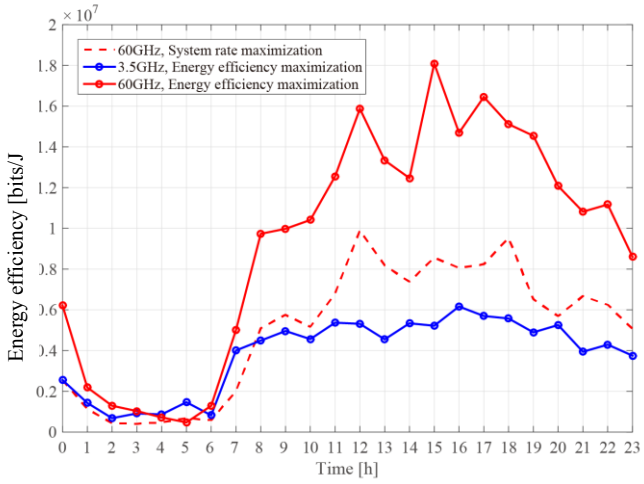

Figure 4.15 System rate over consumed energy performance.

For the traffic throughout a day, the evaluation results are depicted in Figure 4.15. In this figure, the horizontal axis shows the hours of a day and the vertical axis shows the system rate over consumed energy r. The blue lines show the results of 3.5GHz smallcells while the red lines show these of mm-wave smallcells. The figure reveals that the energy efficiency also varies in a similar way as the traffic pattern. Interestingly, the system becomes more energy-efficient at higher traffic load since at low traffic load, some of smallcell BSs are still needed to be activated to support a portion of high traffic demand users, which makes the system inefficient in terms of consumed energy. The result also indicates that mm-wave HetNet is more efficient than microwave HetNet at especially peak hours, owing to the mm-wave's wider bandwidth and smaller consumption power. It means that mm-wave HetNet is recommended as a strong candidate for 5G in terms of energy efficiency. For reference, the results of system rate optimization (Sect. 3.2.1) without taking into account consumed energy i.e. maximizing only the numerator of r are also shown in dashed lines, which have worse performance than our approach. The reason is clear due to the lack of a BS deactivation mechanism in D4.3 where all BSs should be turned on. Overall, our simulation results show the importance of introducing mm-wave HetNet in terms of energy efficiency to support the future higher traffic demand in 5G.

4.3 Dynamic cell structuring for CoMP Joint Transmission

The study on the traffic measurements in current cellular networks shows that, several hotspot zones are expected to appear and disappear based on the time in a typical day [16]. In case of mm-wave smallcell BSs, dynamic cell assignment and beamforming tackles the requirements of hotspot zones. The narrow beamwidth of mm-wave smallcell BSs makes it possible to apply beam coordination schemes even within a small area. In case of LTE or micro-wave smallcell BSs, by optimizing the beam direction and antenna tilt the coverage of smallcell BSs can be shifted to the hotspot zone. However, because of the wide beamwidth of LTE smallcell BSs, the interference among the shifted coverages is inevitable. Therefore, a multi-user Joint Transmission (JT) scheme is adapted to make benefit of all smallcell BSs that can cover the hotspot zone.

4.3.1 Algorithm for dynamic cell structuring for CoMP JT

A HetNet is considered in which there are several smallcell BSs in a macro-cell area. It is assumed that smallcell BSs are connected to the C-RAN and can adjust their antenna beam directions and transmission power and perform joint transmission CoMP in a cluster. The wide beamwidth of an LTE smallcell BS can cover a group of UEs within a hotspot zone. Also several smallcell BSs can shift their coverages to cover the hotspot zone. In such a case, a cluster of these smallcell BSs can service the group of users in the hotspot zone in an orchestrated fashion. Large optimal cooperative clusters are formed around small high-user density zones. A cluster is a group of smallcell BSs that cooperatively perform JT to several UEs. The set of smallcell BSs for each cluster, {j}, and the antennas' beam angles of each smallcell BS, (φj,θj), and their transmission power are optimized so that the system rate of the network is maximized:

$$\left(P_{\mathrm{t}}^{(j)}{}_{\forall j\in\{\hat{j}\}},\left(\hat{\varphi}_j,\hat{\theta}_j\right)_{\forall j\in\{\hat{j}\}},\{\hat{j}\}\right)=\arg\max_{\left(P_{\mathrm{t}}^{(j)},(\varphi_j,\theta_j),\{j\}\right)}\sum_{\forall i}R_i \tag{4-19}$$

In this equation, R_i is the communication rate of UE_i and therefore the optimization criterion is the summation over communication rates of all UEs. Also, j indicates the index of smallcell BSs and (φ_j,θ_j) are the azimuth and tilt angle of the j-th SC-BS and $P_{\mathrm{t}}^{(j)}$ is the transmission power of this smallcell BS. This optimization problem is solved in three consecutive steps:

1. The azimuth and tilt angle of a candidate smallcell BS are optimized to point the coverage of the smallcell BS to the corresponding hotspot zone.
   1.1. If there are multiple candidates of antenna direction that transfer the coverage to the hotspot zones, the one direction that produce lowest interference for other hotspots is selected.
2. The candidate smallcell BS is activated with the optimized beam direction. This will increase the capacity/rate in the corresponding hotspot, yet degrades the rate for other hotspots by interfering to their communication links.
   2.1. Step by step, the transmission power of this smallcell BS is reduced from maximum transmit power and the capacity of the corresponding cluster and other clusters are monitored. The transmission power that not only increases the capacity of this hotspot, but also increases the sum capacity in the network is selected as the optimal transmit power.
   2.2. If such a transmit power is not found, the candidate smallcell BS is deactivated and is discarded from the cluster.

Different clusters for different hotspots, grown simultaneously. The above steps are performed in different clusters synchronously to assure the balance between clusters and the resources associated to different hotspots.

4.3.2 Performance evaluation

For system evaluation, a macro cell area tiled by LTE smallcell BSs at 3.5GHz is considered. These parameters are selected similar to 3GPP specifications for pico cells except that the omnidirectional antennas are replaced by sectorized antennas of

macro cells [16]. As shown in Figure 4.16, two hotspot zones are considered within the macro-cell area and one of them is considered to be moving by time in order to demonstrate the dynamism of the cell structuring and cluster optimization. In the center of each hexagonal cell of Figure 4.16, there is an access point that consists of three base stations (smallcell BSs) and each smallcell BS covers a 120° sector of its cell. Other parameters are listed in Table 4.5.

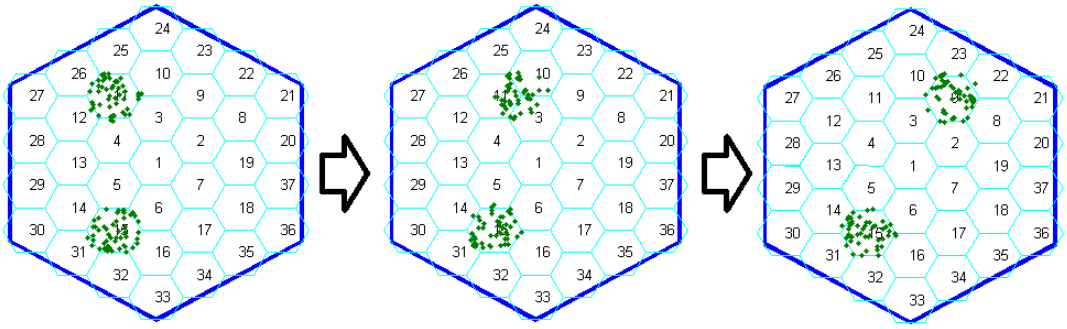

(a) (b) (c)

Figure 4.16 Dynamic change of hotspot zones within macro cell area

Table 4.5 Dynamic cell structuring and large scale CoMP for LTE smallcell BSs at 3.5GHz

Inter-site distance between smallcell BSs (d)		100 meters
Distribution of the UEs		Uniform within each hotspot
Smallcell BS Transmit power (maximum)		24dBm
Smallcell BSs' antenna height		5m
UE antenna height		1.5
Smallcell BSs' antenna pattern	Normalization factor of the antenna gain	14dBi
	Antenna horizontal pattern	$-\min\left\{12\left(\frac{\varphi-\varphi_0}{\varphi_{3\text{dB}}}\right)^2, 25dB\right\}$ $\varphi_{3\text{dB}} = 70^o$ Azimuth angle, φ_0: adjustable
	Antenna vertical pattern	$-\min\left\{12\left(\frac{\theta-\theta_0}{\theta_{3\text{dB}}}\right)^2, 20dB\right\}$ $\theta_{3\text{dB}} = 10^o$ Tilt angle, θ_0: adjustable
Path loss [dB]		140.7 + 36.7 $\log_{10}$(distance [km])
Bandwidth		20 MHz
Noise power density		-174 dBm/Hz

For the three steps of the dynamic scenario, local clusters with optimized cell structures can be formed as depicted in Figure 4.17 to Figure 4.19. In scenario (a), the cell #11 and #15 are hotspot zones and all users are located in one of these two

areas. The three smallcell BSs of these two cells form intra-site CoMP clusters to service the users in their corresponding cells. In each cell, the antenna direction of smallcell BSs is optimized so that the interference effect on the other hotspot zone will be minimal. As can be seen in Figure 4.17, the cells are structured in a way to avoid pointing to the other hotspot.

Then as shown in Figure 4.18, in scenario (b), one of the hotspots moves and locates between three different cells. In this case an inter-site cluster is formed for this hotspot. The structure of the other cluster in cell #15 is also updated to reduce interference towards the shifted hotspot.

Finally in Figure 4.19, the moving hotspot is in cell #9. A new intra-site cluster is formed for this hotspot and the structure of the other cluster in cell #15 is again updated to reduce interference in the direction of the new hotspot.

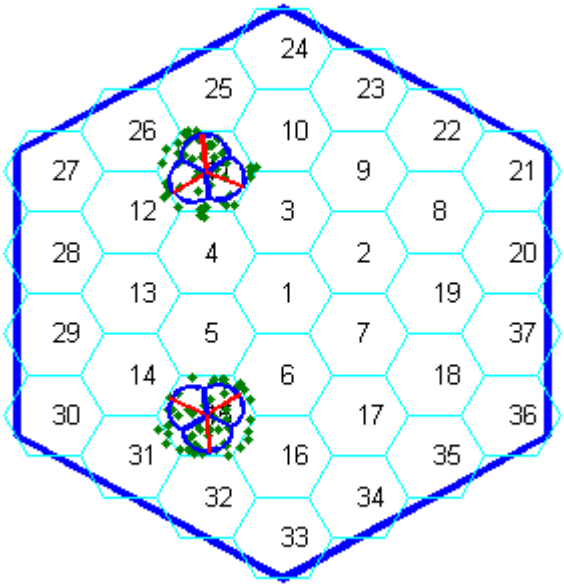

Figure 4.17 Local (1-tier) clusters with optimized cell structures for hotspot zones of Figure 4.16 (a)

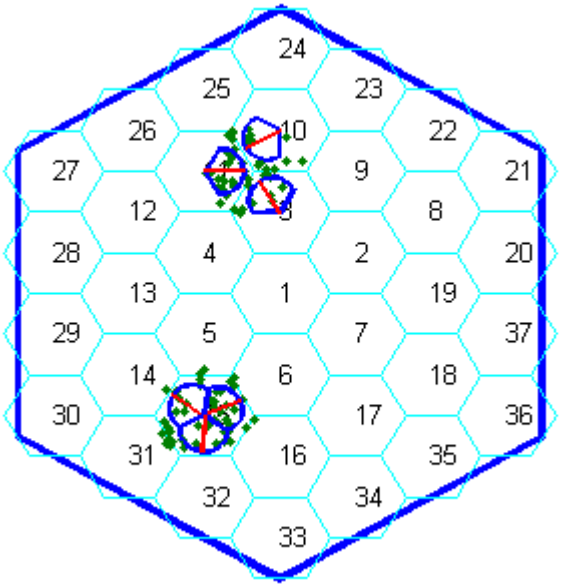

Figure 4.18 Local (1-tier) clusters with optimized cell structures for hotspot zones of Figure 4.16(b)

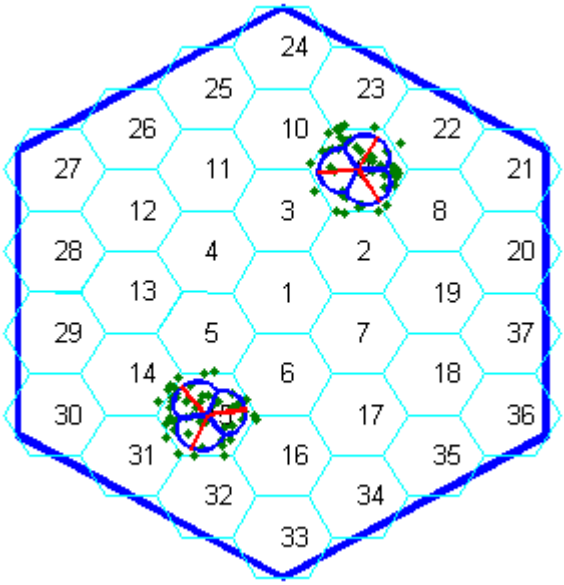

Figure 4.19 Local (1-tier) clusters with optimized cell structures for hotspot zones of Figure 4.16 (c)

In general, the cluster for a hotspot zone can benefit from idle smallcell BSs of other cells [16]. For the dynamic scenario of Figure 4.16, the smallcell BSs in the second tier around each hotspot can join the cluster with proper cell structuring and transmit power adjustment. Figure 4.20 to Figure 4.22 show the optimized two-tier clusters for each of the three steps of the scenario.

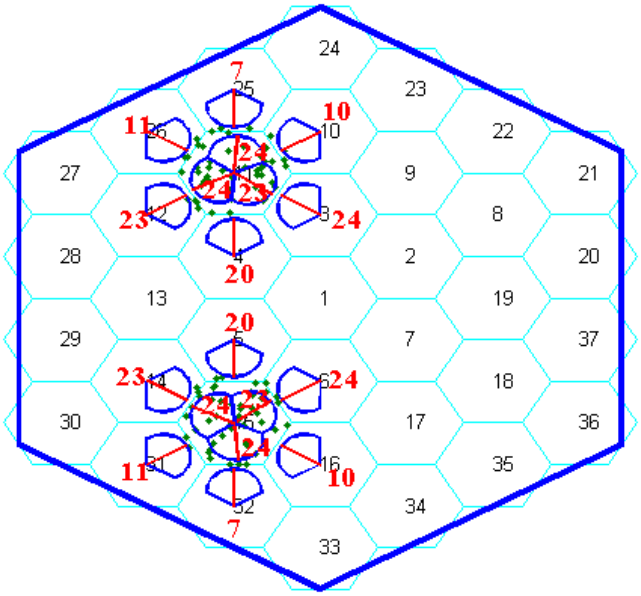

Figure 4.20 Two-tier clusters with optimized cell structures for hotspot zones of Figure 4.16 (a). The optimized transmit power of each smallcell BS in dBm is written beside it.

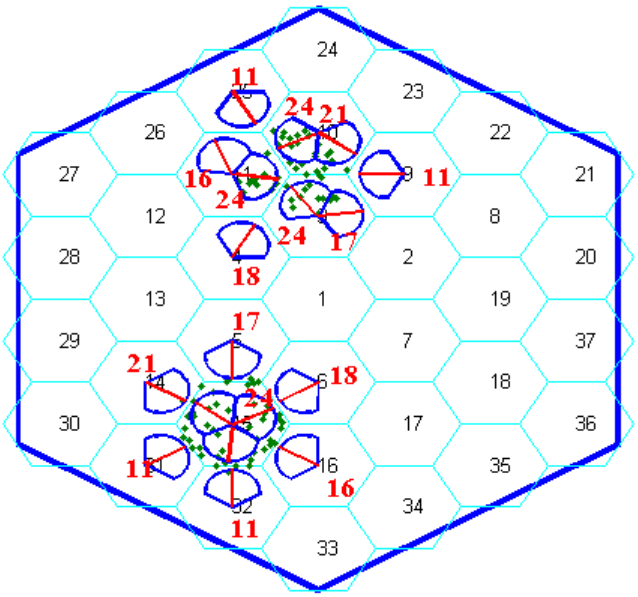

Figure 4.21 Two-tier clusters with optimized cell structures for hotspot zones of Figure 4.16 (b). The optimized transmit power of each smallcell BS in dBm is written beside it.

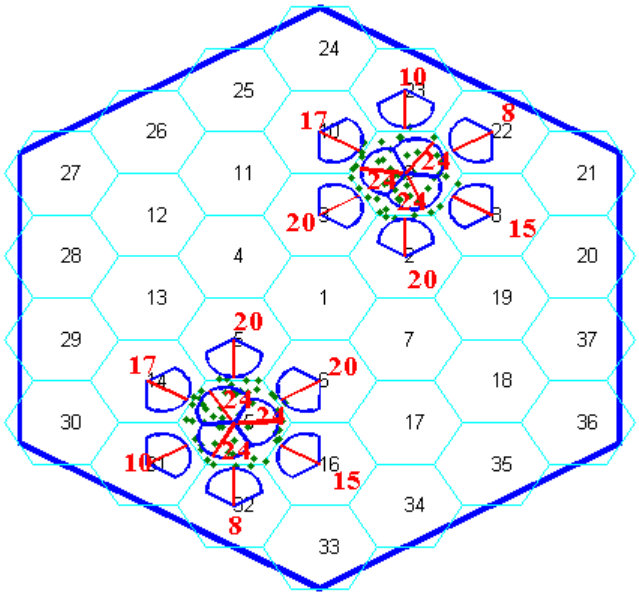

Figure 4.22 Two-tier clusters with optimized cell structures for hotspot zones of Figure 4.16(c). The optimized transmit power of each smallcell BS in dBm is written beside it.

The total capacity (spectrum efficiency) of the network as well as the share of each hotspot are evaluated and listed in Table 4.6. The dynamic cell structuring along with CoMP obtains more than three times of the single-cell communication rate. In the single-cell scheme each UE is assigned to the strongest BS and the BSs service their assigned UEs without any coordination with other BSs. JT CoMP increases the capacity by eliminating the interference within each cluster. If the CoMP cluster can be extended to a larger cluster the capacity improves even farther. When the second tier with optimized cell structure and transmit power is added to the cluster, the system rate increases by another factor of 2. However, it should be noted that addition of second tier adds six more smallcell BSs to the CoMP cluster, while the capacity is only doubled compared to the 1-tier cluster due to the different pathloss between 1st and 2nd tiers. In this analysis, we focused on the lower frequency of 3.5GHz band with wider beam (sector) width. However, if we see the whole mm-wave frequency bands, there must be a trade off between the CoMP JT and the coordinated beamforming since the achievable beam width given a space depends on the frequency. Such a trend should be considered in the selection of spectrum for 5G systems.

Table 4.6 Comparison between optimized dynamic cell structuring /CoMP and conventional communication

Dynamic Scenario of Figure 4.16		**Step (a)**	**Step (b)**	**Step (c)**
Single cell communication	Sum rate of hotspot 1 (moving) / sum rate of hotspot 2 (fixed at cell #15) [bps/Hz]	9.5 / 9.5	11 / 9	9.5 / 9.5

	Total sum rate [bps/Hz]		19	20	19
Local cluster (one-tier as in Figure 4.17 to Figure 4.19)	Sum rate of hotspot 1/ sum rate of hotspot 2 [bps/Hz]		36 / 37	33 / 37	39 / 39
	Total sum rate [bps/Hz]		73	71	78
Extended cluster (two-tier as in Figure 4.20 to Figure 4.22))	Fixed P_t (24dBm)	Sum rate of hotspot 1/ sum rate of hotspot 2	65 / 65	54 / 76	75 / 75
		Total sum rate [bps/Hz]	130	130	150
	Optimized P_t (Figure 4.20 to Figure 4.22)	Sum rate of hotspot 1/ sum rate of hotspot 2	80 / 80	62 / 87	87 / 87
		Total sum rate [bps/Hz]	160	150	174

5 Indications for 5G system design

5.1 Frequency bands for 5G

Our research work so far has focused on the 60 GHz because off-the-shelf devices are available. However the 5G investigation focuses not only on 60GHz but also whole frequency bands in range of 6GHz to 100GHz. Basically, higher frequency has wider bandwidth and sharper antenna gain, however, has severe pathloss. We'll evaluate the performance of system rate by considering this trade off.

Actually many research activities are developing other mm-wave bands. METIS [26] had widely investigated about 5G. Especially they listed the availability of the spectrum from 6GHz to 300GHz [27]. MiWaveS [28] focuses on the 60GHz (57GHz–66GHz), 71GHz–76GHz and 81GHz–86GHz (E-band) to realize ultra high speed wireless access networks and backhaul links. 5G PPP called for the 1st 5G

projects in 2014 and totally 18 projects have been selected from the 83 proposals. Especially among them, METIS II [29] and mmMAGIC [30] are related to above 6GHz. NTT docomo has done several experiments with 8 vendors to realize 5G [31]. The experiment with Ericsson achieved over 4Gbps of peak data rate and 2Gbps of average data rate with 10km/h mobility. The system uses 15GHz frequency band with 400MHz bandwidth and 4 stream MIMO. The experiment with Nokia Networks achieved over 2Gbps peak data rate with walking speed by using 70GHz frequency band with 1GHz bandwidth. They will also plan to do the experiment with Samsung by using 28GHz frequency band with 500MHz–1GHz bandwidth and with Mitsubishi Electric by using 44GHz frequency band with 100MHz bandwidth.

According to these R&D activities, [32] and [27] made a list of the candidate spectrum for 5G. The former picked up five bands which are allocated to the fixed service and have several GHz bandwidth. On the other hand, the latter listed many candidates between 6GHz to 300GHz and also classified these candidates into three groups, high, medium, and low priorities. Based on these lists and the spectrum regulation in Japan, China, US, and EU, the possible candidates are carefully picked up and listed in Table 5.2-1. In the MiWEBA project, the bands which have the bandwidth over 1GHz and have potential to receive consensus in terms of regulation are selected. Mm-wave has characteristic of large propagation loss and therefore requires directional antenna to compensate this propagation loss. Because of these two factors, interference toward other systems is estimated to be lower than that of the conventional frequency band. For this reason, Licensed Shared Access (LSA) [32] which shares licensed band among multiple systems under a certain rule to guarantee the link quality is expected to be useful. From this aspect, this paper assumes that the frequency band from 55.78GHz to 76GHz which includes unlicensed band of 57GHz to 66GHz can be used as a continuous spectrum. Since the aeronautical radio navigation system should be secured, finally five candidates are selected from Table 5.1. Table 5.2 summarizes these candidate spectrum bands.

Table 5.1 Spectrum allocation status

Frequency [GHz]	Bandwidth [GHz]	Allocation status			
		JP	CHN	US	EU
27.94-29.45	1.5	Fixed satellite	Fixed/Mobile Fixed satellite	Fixed satellite	Aeronautical radio navigation
31.8-33.4	1.6	Unused	Fixed Radio navigation	Radio navigation Space research Inter satellite	Radio navigation Earth exploration satellite (active) Space research (active)
40.5-43.5	3	Fixed	Fixed Fixed satellite	Fixed satellite	Fixed Aeronautical radio navigation
45.5-47.0	1.5	Unused	Mobile	Mobile	Fixed
47.2-50.2	3	Unused	Fixed	Fixed	Fixed
55.78-57.0	1.22	Fixed/Mobile	Earth exploration satellite (passive)	Earth exploration satellite (passive)	Maritime radio navigation
57.0-66.0	9	Fixed	Fixed	Fixed	Fixed

			Earth exploration satellite		
66.0-71.0	5	Unused	Mobile	Mobile	Fixed
71.0-76.0	5	Fixed/Mobile	Fixed	Fixed	Fixed
81.0-86.0	5	Fixed/Mobile	Fixed	Fixed	Earth exploration satellite Fixed Radio navigation

Table 5.2 Spectrum candidates for 5G

(1)	(2)	(3)	(4)	(5)
31.8GHz–33.4GHz (Channel BW: 1.6GHz)	45.5GHz–47.0GHz (Channel BW: 1.5GHz)	47.2GHz–50.2GHz (Channel BW: 1.5GHz x2)	55.78GHz–76.0Hz (Channel BW: 2GHz x10)	81.0GHz–86.0GHz (Channel BW: 1.6GHz x3)

The values within the parenthesis represent possible channel bandwidth. The 1st and 2nd candidate have only single channel. The 3rd, 4th, and 5th candidates may have 2, 10, and 3 channels respectively. For convenience, we assume that the 4th band has 10 channels of 2GHz bandwidth however the existing channelization rule in 60GHz unlicensed band should be retained practically

5.2 mmWave interpolated channel model

Various research groups have analyzed the characteristics of the mm-wave propagation in outdoor environments. Especially, New York University (NYU) has done the substantial propagation experiments [33]. NYU also made pathloss models at 28GHz and 73 GHz bands based on their experimental results [34]. On the other hand, MiWEBA project has conducted the experiment of outdoor 60GHz propagation and made pathloss and channel models [35] [3]. Since outdoor mm-wave propagation models are still under research, there is no appropriate model for the mm-wave bands mentioned Section 5.2. Therefore, the methodology of making pathloss model using interpolation is applied to create pathloss model for each candidate band. Since there is also no appropriate model for the instantaneous channel fluctuation, this paper employs the 60GHz model of [3] at this moment.

Generally, if the carrier frequency is f, the pathloss is proportional to f^a. Therefore it can be derived as follows,

$$PL = 10a\log_{10}(f) + b \tag{5-1}$$

where a is a frequency-dependency factor. According to the Friis transmission equation, $a \geq 2$ should be satisfied. The passloss models of 28GHz, 60GHz, and 73GHz are as follows,

$$PL_{28\text{GHz}} = 72.0 + 29.2\log_{10}\left(d/d_{0,28\text{GHz}}\right) \tag{5-2}$$

$$PL_{60GHz} = 82.02 + 23.6\log_{10}\left(d/d_{0,60GHz}\right) \quad (5\text{-}3)$$

$$PL_{73GHz} = 82.7 + 26.9\log_{10}\left(d/d_{0,73GHz}\right) \quad (5\text{-}4)$$

where $d_{0,28GHz}$(5m), $d_{0,60GHz}$(5m), $d_{0,73GHz}$(4m) represent the reference distances of 28GHz, 60GHz, and 73GHz respectively. By using these existing pathloss models and interpolation method [36], coefficients a and b can be estimated. Meanwhile the pathloss value is also proportion to the distance between transmitter and receiver. Therefore the coefficients a and b can be derived as a function of the distance. Then these coefficients can be estimated by using MMSE (Minimum Mean Square Error) criterion.

$$J(a(d),b(d)) = \sum_{i=1}^{I}\left(PL_{original}(f_i,d) - PL(f_i,d)\right)^2 \quad (5\text{-}5)$$

$$\left(\hat{a}(d),\hat{b}(d)\right) = \arg\min_{a(d),b(d)} J(a(d),b(d)) \quad (5\text{-}6)$$

$$\text{subject to } a(d) \geq 2 \quad (5\text{-}7)$$

where f_i and d are center frequency and distance between Tx and Rx respectively. I is the number of frequency samples for the interpolation. In this paper $I = 3$. $PL_{original}(f_i,d)$ is the original pathloss model described by Eqs. (5-2), (5-3), (5-4). $PL(f_i,d)$ is an unified pathloss model in Eq. (5-1). Figure 5.1 and Figure 5.2 show the estimated values of the coefficients a and b.

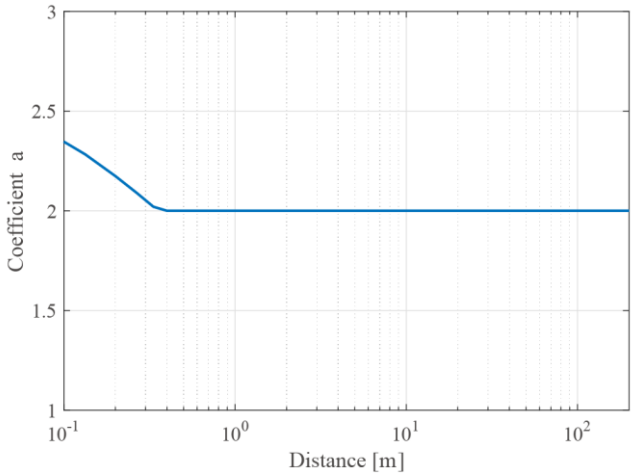

Figure 5.1 Estimated value of the coefficient a

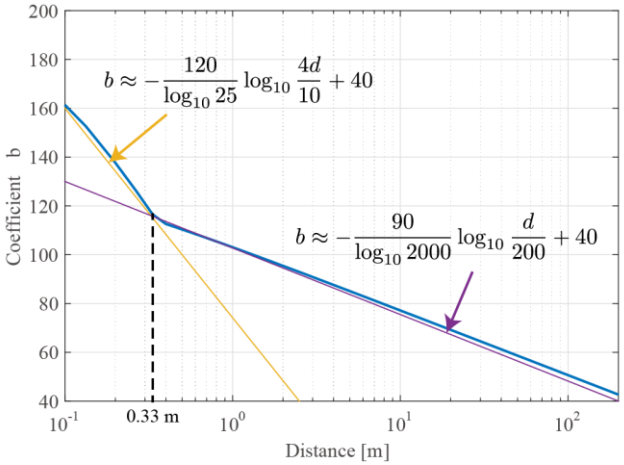

Figure 5.2 Estimated value of the coefficient b

At almost all distances, coefficient a equals to two. On the other hand, b has a break point around $d = 0.33\text{m}$. Therefore, the coefficient b can be modeled by the combination of two logarithm functions as follows,

$$b = \begin{cases} -\dfrac{120}{\log_{10} 25} \log_{10} \dfrac{4d}{10} + 40, & d < 0.33 \\ -\dfrac{90}{\log_{10} 2000} \log_{10} \dfrac{d}{200} + 40, & d \geq 0.33 \end{cases} \tag{5-8}$$

Figure 5.3 shows the comparison between the original pathloss model and the unified model by using estimated coefficients $\hat{a}(d)$, $\hat{b}(d)$. In the original pathloss model compared between 28GHz and 60GHz, there is a cross point at d = 60[m] because of the difference of experimental environments and applicable ranges. The unified pathloss model agrees well with original models from d = 1 to 10 meters and has good approximation by resolving the discrepancy of the cross point.

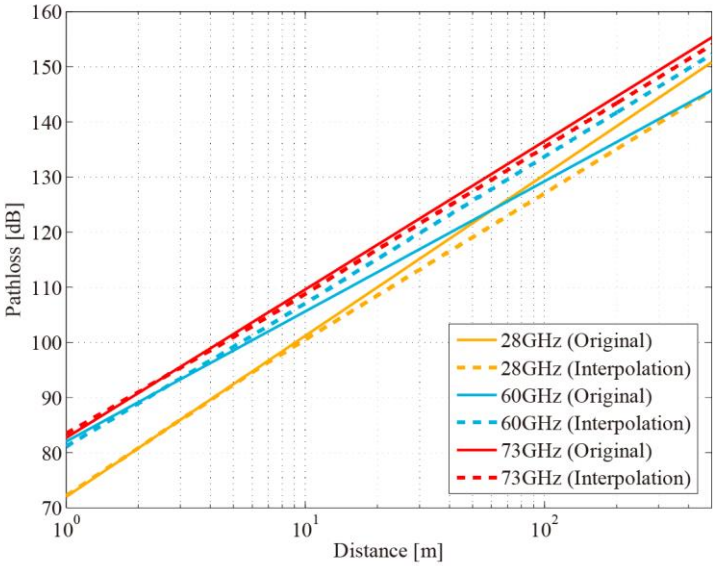

Figure 5.3 Pathloss comparison between original and interpolated model

5.3 System level analysis

According to the simulation parameters derived in the Section 2, performance of each candidate band for 5G is evaluated with respect to the system rate gain which is defined by the system rate of HetNet divided by that of homogeneous network. In this simulation, The Tx power of smallcell BS is assumed as 19dBm per channel. Antenna aperture is assumed to be fixed as the same size of that of 60GHz case. Therefore, antenna gain is proportion to the square of the center frequency. This paper assumes 26dBi gain (128 antenna element, 5dBi element gain) can be obtained at 60GHz case and configures the gain for other cases based on the above assumption.

Firstly, we compare the pathloss values of candidate bands. Figure 5.4 shows each pathloss value with respect to the distance. For the pathloss calculation, the center frequency of each candidate band is used. From this figure there is about 10dB difference on pathloss between 30GHz and 80GHz bands. The results of the system rate gain analysis by using this pathloss value are shown in Table 5.3. In this simulation, we evaluated two types of traffic scenario. The first one is 1000x higher traffic than that of current demand, corresponding to the 2020 (average traffic demand of each user is 62Mbps). The second one is 1000000x higher traffic than that of current demand, corresponding to the 2030 (average traffic demand of each user is 62Gbps). The number of each candidate is corresponding to the numbers in the Table 5.2-2.

From Table 5.3, it is clear that (4) shows the best performance. Since (3) and (5) have wide bandwidth, system rate gain are higher than that of (1) and (2). Although (5) has large pathloss value, it shows better performance than that of (3) thanks to the antenna gain enhancement and wide bandwidth. This results indicate that the system which can have large bandwidth should have higher priority for future 5G systems.

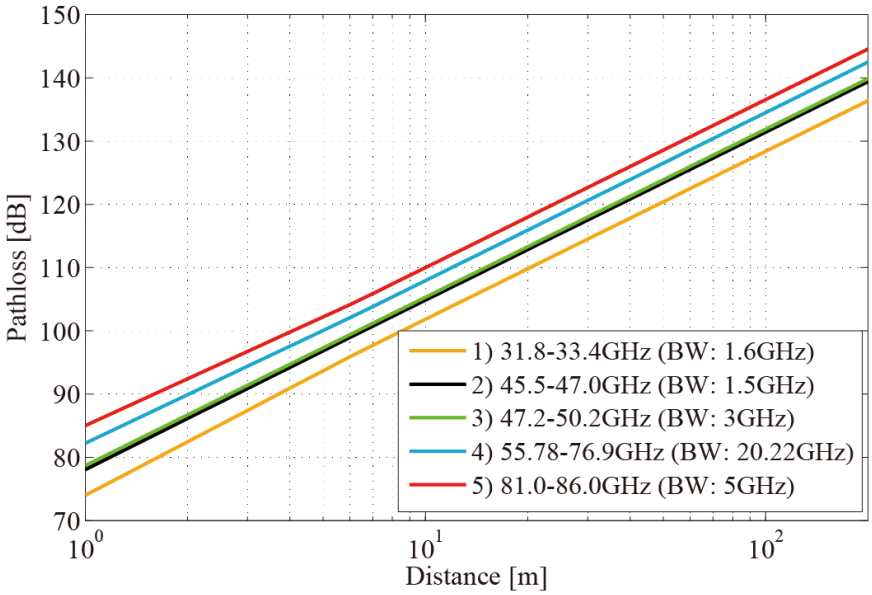

Figure 5.4 Pathloss comparison between original and interpolated model

Table 5.3 System rate gain comparison

	(1)	(2)	(3)	(4)	(5)
1000x traffic in 2020	541	582	689	1014	812
1000000x traffic in 2030	3622	3548	6667	36227	10409

Conclusion

This deliverable presented the overall view of all achievements in WP4 about radio resource management for MiWEBA architecture. Scenarios and use cases that had been studied in WP1 were revisited here to specify simulation environments including open area, street canyon, hotel lobby, and HetNet scenarios. Besides, the basics of the MiWEBA's exclusive system level simulator were described with the mm-wave channel model and massive MIMO antenna model developed in WP5, and the space-time traffic and BS power consumption models developed in WP4. Short-term and long-term radio resource management and optimizations were further developed and demonstrative evaluation results were presented. In the end, the final chapter extended the analysis to whole mm-wave frequency bands to indicate appropriate spectrum for 5G systems.

As our findings, this deliverable has shown that the proposed MiWEBA architecture with proposed short-term resource management algorithms in realistic scenarios can achieve more than 1000 times gain in system rate by installing 15 mm-wave small cell BSs per macro cell area. The protocol of location-based cell/beam discovery/selection was also developed to implement the context-based resource management. The location-based cell/beam discovery/selection is essential in particular for implementing resource optimizations and forming a self-organizing networks (SONs). Using this scheme, several optimization algorithms are developed and applied to boost energy-efficiency. As the baseline, the 1000x system rate is

achieved by our mm-wave overlay HetNet with only 2x power consumption compared to the traditional homogenous network. Implementing dynamic ON/OFF according to the dynamic traffic map can further reduce this power consumption. To further enhance the capacity, dynamic cell structuring scheme was also developed to dynamically follow the hotspot zones (using the location-based cell/beam discovery protocol) and direct idle network resources towards them.

Finally all possible bands for 5G have been investigated through the system level simulator to evaluate their performances for the future traffic requirements (1000x in 2020 and 1000000x in 2030). The evaluations have shown that among all available bands, 60GHz band with 20.22GHz bandwidth from 55.78GHz to 76.9GHz shows such a prospective capacity that makes it the most attractive band for the future 5G systems.

References

[1] K. Sakaguchi, G.K. Tran, H. Shimodaira, S. Nanba, T. Sakurai, K. Takinami, I. Siaud, E.C. Strinati, A. Capone, I. Karls, R. Arefi and T. Haustein, "Millimeter-wave evolution for 5G cellular networks," *IEICE Trans. Commun.,* vol. 98, no. 3, pp. 388-402, Mar. 2015.

[2] MiWEBA Deliverable D1.1, "Definition of scenarios and use cases," *FP7-ICT 368721/D1.1,* Dec. 2013.

[3] MiWEBA Deliverable D5.1, "Channel Modeling and Characterization," *FP7-ICT 368721/D5.1,* 2014.

[4] MiWEBA D5.2, " Highly-directional steerable mm-wave antennas development," 2015.

[5] A. Maltsev, V. Erceg, E. Perahia, C. Hansen, R. Maslennikov, A. Lomayev, A. Sevastyanov, A. Khoryaev, G. Morozov, M. Jacob, S. Priebe, T. Kürner, S. Kato, H. Sawada, K. Sato and H. Harada, "Channel Models for 60 GHz WLAN Systems," IEEE 802.11ad 09/0334r8, 2010.

[6] M. Peter, W. Keusgen and R. Felbecker, "Measurement and ray-tracing simulation of the 60 GHz indoor broadband channel: Model accuracy and parameterization," in *Antennas and Propagation, EuCAP*, Edinburgh, 2007.

[7] R. J. Weiler, M. Peter, W. Keusgen, A. Kortke and M. Wisotzki, "Millimeter-Wave Channel Sounding of Outdoor Ground Reflections," in *Radio and Wireless Symposium (RWS)*, 2015.

[8] A. Maltsev, A. Pudeyev, I. Karls, I. Bolotin, I. Morozov, R. Weiler, M. Peter and W. Keusgen, "Quasi-deterministic Approach to mmWave Channel Modeling in a Non-stationary Environment," in *IEEE GLOBECOM*, Austin, Texas, 2014.

[9] A. Maltsev, A. Pudeyev, I. Karls, I. Bolotin, I. Morozov, R. Weiler, M. Peter, W.

Keusgen, M. Danchenko and A. Kuznetsov, "Quasi-Deterministic Approach to MmWave Channel Modeling in the FP7 MiWEBA Project," in *WWRF' 33*, Guildford, GB, 2014.

[10] D. S. Baum, J. Salo, M. Milojevic, P. Kyösti and J. Hansen, "MATLAB implementation of the interim channel model for beyond-3G systems (SCME)," May 2005. [Online]. Available: http://www.tkk.fi/Units/Radio/scm/.

[11] 3GPP TR36.814 V9.0.0, "Further advancements for E-UTRA physical layer aspects".

[12] 3GPP TR36.872 V12.1.0, "Small cell enhancements for E-UTRA and E-UTRAN - Physical layer aspects".

[13] IEEE 802.11 doc. 0433r2, "PHY/MAC Complete Proposal Specification".

[14] Maltsev A., Bolotin I., Pudeyev A., Davydov A., Morozov G., "Performance evaluation of the Isolated MmWave Small Cell," in *IEEE PIMRC'2015*, Hong Kong, 2015.

[15] H. Shimodaira, G. K. Tran, K. Araki, K. Sakaguchi, S. Nanba, T. Hayashi and S. Konishi, "Cell Association Method for Multiband Heterogeneous Networks," *Personal, Indoor and Mobile Radio Communications (PIMRC Workshops), 2014 IEEE 25th International Symposium on,* Sep. 2014.

[16] MiWEBA Deliverable D4.4, "Dynamic activation & cell structuring algorithm and control protocols," 2015.

[17] "GreenTouch framework on green ICT," [Online]. Available: www.greentouch.org.

[18] "EARTH project under European Communitys Seventh Framework Programme FP7/2007-2013, grant," [Online]. Available: www.ictearth.eu.

[19] A. Maltsev, A. Sadri, A. Pudeyev, A. Davydov, I. Bolotin, G. Morozov, "Performance evaluation of the MmWave Small Cells communication system in MU-MIMO mode," in *EuCNC'2015*, Paris, France, 2015.

[20] 3. T. V.11.1.0, "Coordinated Multi-Point Operation for LTE Physical Layer Aspects: Release-11," 2011.

[21] I. Bolotin, A. Maltsev, A. Pudeyev, G.Morozov, A.Davydov, G. Tran, H. Shimodaira, "Performance Evaluation of Interference Mitigation Techniques in the Overlaying MmWave Small Cell Network," in *IEEE CSCN'2015*, Tokyo, Japan, 2015.

[22] MiWEBA Deliverable D4.3, "Dynamic resource optimization algorithm and control protocols," 2015.

[23] G. Morozov and A. Davydov, "CS/CB CoMP Scheme with Semi-static Data Traffic," in *IEEE 24th International Symposium on Personal, Indoor and Mobile Radio Communications: Fundamentals and PHY*, 2013.

[24] A. Maltsev, A. Sadri, A. Pudeyev, I. Bolotin, A. Davydov, G. Morozov, R. Weiler, "Partially Adaptive Arrays application for MU-MIMO mode in a MmWave Small Cells," in *IEEE PIMRC'2015*, Hong Kong, 2015.

[25] Federal Communications Commission, "Report and Order FCC 13-112," 2013.

[26] "METIS Website," [Online]. Available: https://www.metis2020.com/.

[27] METIS Deliverable D5.1, "Intermediate description of the spectrum needs and usage principles," Aug. 2013.

[28] "MiWaveS Website," [Online]. Available: http://www.MiWaveS.eu/.

[29] "METIS II introduction," [Online]. Available: https://5g-ppp.eu/metis-ii/.

[30] "mmMAGIC introduction," [Online]. Available: https://5g-ppp.eu/mmmagic/.

[31] NTT DOCOMO, INC., "DOCOMO's 5G Outdoor Trial Achieves 4.5Gbps Ultra-high-speed Transmission – Aiming at 5G launch by Tokyo 2020 Olympic and Paralympic Games –," Mar 2015. [Online].

[32] M. Mueck, W. Jiang, G. Sun, H. Cao, E. Dutkiewicz and S. Choi, "Novel Spectrum Usage Paradigms for 5G," *IEEE ComSoc, TCCN, White Paper,* Nov 2014.

[33] T. S. Rappaport, S. Sun, R. Mayzus, H. Zhao, Y. Azar, K. Wang, G. N. Wong, J. K. Schulz, M. Samimi and F. Gutierrez, "Millimeter Wave Mobile Communications for 5G Cellular: It Will," *IEEE Access,* vol. 1, pp. 335-349, 2013.

[34] M. R. Akdeniz, Y. Liu, M. Samimi, S. Sun, S. Rangan, T. S. Rappaport and E. Erkip, "Millimeter Wave Channel Modeling and Cellular Capacity Evaluation," Dec 2013. [Online]. Available: http://arxiv.org/abs/1312.4921v3.

[35] R. J. Weiler, M. Peter, W. Keusgen, H. Shimodaira, G. K. Tran and K. Sakaguchi, "Outdoor Millimeter-wave Access for Heterogeneous Networks – Path Loss and System Performance," *Proc. of IEEE PIMRC 2014,* Sep 2014.

[36] A. Haniz, G. K. Tran, R. Iwata, K. Sakaguchi, J. Takada, D. Hayashi, T. Yamaguchi and S. Arata, "Propagation Channel Interpolation for Localization of Illegal Radios," *IEICE Trans. Commun.,* Vols. E98-B, no. 12, Dec 2015.

[37] A. Maltsev, A. Pudeyev, I. Karls, I. Bolotin, I. Morozov, R. Weiler, M. Peter and W. Keusgen, "Quasi-deterministic Approach to mmWave Channel Modeling in a Non-stationary Environment," in *IEEE GLOBECOM*, Austin, Texas, 2104.

[38] A. Maltsev, A. Pudeyev, I. Karls, I. Bolotin, I. Morozov, R. Weiler, M. Peter, W. Keusgen, M. Danchenko and A. Kuznetsov, "Quasi-Deterministic Approach

to MmWave Channel Modeling in the FP7 MiWEBA Project," in *WWRF' 33*, Guildford, GB, 2104.